INFORMATION TO USERS

This manuscript has been reproduced from the microfilm master. UMI films the text directly from the original or copy submitted. Thus, some thesis and dissertation copies are in typewriter face, while others may be from any type of computer printer.

The quality of this reproduction is dependent upon the quality of the copy submitted. Broken or indistinct print, colored or poor quality illustrations and photographs, print bleedthrough, substandard margins, and improper alignment can adversely affect reproduction.

In the unlikely event that the author did not send UMI a complete manuscript and there are missing pages, these will be noted. Also, if unauthorized copyright material had to be removed, a note will indicate the deletion.

Oversize materials (e.g., maps, drawings, charts) are reproduced by sectioning the original, beginning at the upper left-hand corner and continuing from left to right in equal sections with small overlaps. Each original is also photographed in one exposure and is included in reduced form at the back of the book.

Photographs included in the original manuscript have been reproduced xerographically in this copy. Higher quality 6" x 9" black and white photographic prints are available for any photographs or illustrations appearing in this copy for an additional charge. Contact UMI directly to order.

UMI

A Bell & Howell Information Company
300 North Zeeb Road, Ann Arbor MI 48106-1346 USA
313/761-4700 800/521-0600

Université d'Ottawa · University of Ottawa

Equalization Algorithms for ADSL DMT System

By

Yang Xu

A thesis submitted to
the School of Graduate Studies and Research
University of Ottawa
In partial fulfillment of the requirements
For the degree of

Master of Applied Science in Electrical Engineering

Ottawa-Carleton Institute for Electrical Engineering
School of Information Technology and Engineering
Faculty of Engineering
University of Ottawa
Ottawa, Ontario, Canada

November 1998

Abstract

Discrete Multitone can achieve high capacity over Asymmetric Digital Subscriber Lines by dividing the transmission band into a number of subchannels and thus partially compensating for the nonideal channel response. Performance improvements can be obtained by judiciously designing a time domain equalizer, a frequency domain equalizer, and by suitable selection of a cyclic prefix. The transceiver front-end filter selection is also very important. In this thesis, we discuss the time domain equalizer design algorithms and the filter selection. The system performance with different filters is analyzed based on computer simulations. We then theoretically analyze the effects of the remaining distortion on the system performance and verify the results by simulations. We propose an optimized frequency domain equalizer for discrete multitone systems. Our simulation results show that the achievable bit rate over a given loop length is significantly increased with the new frequency domain equalizer design.

Acknowledgment

First of all, I would like to thank my thesis supervisor, Dr. Abbas Yongaçoglu, for his constant support and encouragement during the course of my M.A.Sc program.

Thanks to Dr. Alberto Ginesi and Christian Bourget of Nortel, who provided the excellent assistance and inspiring discussions during my thesis research.

Thanks also go to Department of Electrical Engineering of University of Ottawa who provided me with the financial support during my M.A.Sc program.

I would like to thank my colleagues, Liang Zhang, Yongjun Zhang, for many helpful discussions we had on the subject matter of this work.

Special thanks to my parents who always support me in the world and encourage me to get over all the difficulties.

Contents

Chapter 6

List of Figures

List of Tables

Glossary

ADC or A/D	Analog to Digital Converter
ADSL	Asymmetric Digital Subscriber Line
CP	Cyclic Prefix
CSA	Carrier Serving Area
DMT	Discrete MultiTone
DS	Downstream
DSL	Digital Subscriber Line
FDEQ	Frequency Domain Equalizer
FEXT	Far-End Crosstalk
FFT	Fast Fourier Transform
HDSL	High bit-rate Digital Subscriber Line
ICI	Inter-Channel-Interference
IFFT	Inverse Fast Fourier Transform
ISCI	Inter-Symbol-Inter-Channel-Interference
ISDN	Integrated Services Digital Network
ISI	Inter-Symbol-Interference

MLSE	Maximum Likelihood Sequence Estimation
MMSE	Minimum Mean Square Error
NEXT	Near-End Crosstalk
OFDM	Orthogonal Frequency Division Multiplexing
PSD	Power Spectral Density
SNR	Signal to Noise Ratio
SSNR	Shortening Signal to Noise Ratio
TDEQ	Time Domain EQualizer
TIR	Target Impulse Response
UEC	Unit Energy Constraint
US	Upstream
UTC	Unit Tap Constraint
UTP	Unshielded Twisted Pairs
VA	Viterbi Algorithm

List of Symbols

$\mathbf{b}$	Vector of TIR coefficients
$\tilde{\mathbf{b}}$	Delayed target impulse response
b_A	The aggregate number of bits per DMT symbol
b_k	Number of bits carried by *k*th subchannel
$\mathrm{CP}_{duration}$	CP duration in one DMT symbol
$d_{RX\,k}$	Received constellation distance on *k*th subchannel
$d_{TX\,k}$	Transmitted constellation distance on *k*th subchannel
e_k	Error between TIR and TDEQ branches
$f_{Nyquist}$	Nyquist frequency
f_{samp}	Sampling frequency
f_{symb}	DMT symbol rate
f_{tx}	Symbol rate at the transmitter
G^n	Equalized channel frequency response
g^n	Equalized channel impulse response
$H(f)$	Channel frequency response
$\lvert H(f)\rvert^2$	Channel power spectral density
$h(t)$	Channel impulse response
K_{FEXT}	FEXT coupling coefficient
K_{NEXT}	NEXT coupling coefficient
L_k	Number of constellation elements on *k*th subchannel
M	Number of subchannels
N_{FFT}	FFT/IFFT size

N_b+1	TIR length
N_f	TDEQ length
N_h+1	Length of channle impulse response in TDEQ design
P_{Interf}^{l}	Total interference power output of the *l*th bin at the FDEQ
P_{SIG}^{l}	Output signal power of the *l*th bin at the FDEQ
P_{TX}	Total Transmit power
Pe_k	Probability of symbol error on *k*th subchannel
P_k	Transmitted power on *k*th subchannel
SNR_k	Signal to noise ration on the *k*th subchannel
T	DMT symbol duration
T_{data}	Information data duration in one DMT symbol
$\mathbf{w}$	Vector of TDEQ coefficients
w_{FDEQ}	FDEQ coefficients
$\widetilde{x}_k$	Transmitted symbol sequence
Y^l	Output of the *l*th bin at the demodulator
Y_{ICI}^{n}	ICI at the *n*th output bin of the demodulator
$Y_{ISCI\_next}^{n}$	ISCI to the next symbol at the *n*th output bin of the demodulator
$Y_{ISCI\_pre}^{n}$	ISCI to the previous symbol at the *n*th output bin of the demodulator
$Y_{ISI\_next}^{l}$	ISI to the next symbol at the *l*th output bin of the demodulator
$Y_{ISI\_pre}^{l}$	ISI to the previous symbol at the *l*th output bin of the demodulator

Y_{SIG}^{l}	Desired signal at the *l*th output bin of the demodulator
Y_{SYM}^{l}	Hermitian symbol at the *l*th output bin of the demodulator
Z^{l}	Output of the *l*th bin at the FDEQ
Δ	Delay value in TDEQ design
Δf	Subchannel bandwidth
$\Phi_{nn}(f)$	Power spectral density of additive gaussian noise
Γ	SNR gap for bit allocation
γ	Target SNR requirement for DMT bit allocation
σ_k	Gaussian noise variance at *k*th subchannel

Chapter 1

Introduction

1.1 ADSL System

The ever increasing demand for high-speed transmission for multimedia applications has to be met using existing as well as new telecommunication facilities. The existing loop plant is dominated by copper facilities, and there are nearly one billion copper telephone lines now [1]. Currently, the wired facilities connect telephones, fax machines, and computers at slow speeds — 28.8 kbps for modems, 128 kbps for Integrated Services Digital Network (ISDN). The recent years have brought the introduction of new Digital Subscriber Line (DSL) techniques for high-speed transmission over the existing loop plant.

The transmission characteristics vary from loop to loop because of gauge changes and bridged taps of the loops [2]. Although the variations are not important for analog voice service, they have to be compensated when high-speed transmission is desired. DSL technology uses adaptive digital filtering techniques to automatically adjust equalizers and echo cancellers according to particular characteristics of the loop being used and the changes due to environment effects. High bit-rate Digital Subscriber Line (HDSL) is using two pairs to provide 1.5 Mbps service over Carrier Serving Area (CSA) loops, which have lengths within 12 kft with 24-gauge and 9 kft with 26-gauge.

Asymmetric Digital Subscriber Line (ADSL) technology is developed to solve the range and resource requirement problems the HDSL suffered. Essentially, ADSL is a pair of modems on each end of a twisted pair that transforms ordinary phone lines into high-

speed digital lines for fast Internet access. The ADSL is intended to provide up to 8 Mbps downstream service from the network to the customers and as much as 1 Mbps for the upstream from the subscriber to the central office. With this asymmetrical architecture, the ADSL eliminates the interference caused by self near-end crosstalk (NEXT) which is generated due to the coupling of the transmission on different pairs in the same cable. As shown in Figure 1.1, the HDSL is a full duplex system and the received signal is subject to self-NEXT. Because the transmission rate of upstream is much lower than the transmission rate of downstream, the ADSL significantly reduces the self-NEXT. Thus, only far-end crosstalk (FEXT) is considered in ADSL.

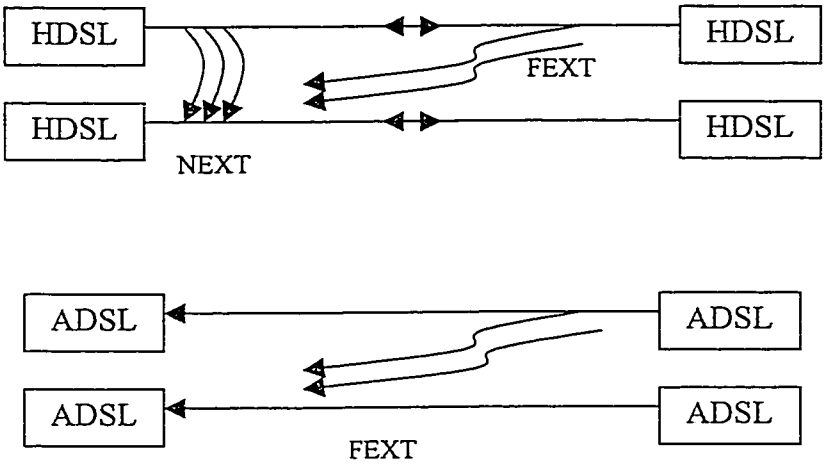

Figure 1.1 Crosstalk comparison of ADSL and HDSL

There are two basic modulation approaches in ADSL. One approach employs a single carrier technique named Carrierless Amplitude and Phase (CAP) modulation. The second and more popular approach uses multicarriers. In ADSL literature, the multicarrier technique is usually called Discrete MultiTone (DMT). DMT is the basis of ANSI Standard T1.413.

Multitone modulation methods divide the total bandwidth into a large number of small subchannels, each of which uses for example QAM modulation. If the bandwidth is made narrow enough, the original distorted channel will have an ideal impulse response in each subchannel. To maximize the reliable data rate over bandlimited channels, an optimized frequency division allocation of energy and bits is performed at the system startup. ADSL DMT technology uses only the tones with acceptable received signal level, and assigns bits to the usable tones according to the measured signal to noise ratio (SNR) on each tone. Thus the tones with more SNR carry more bits. It has been proved that the aggregate bit rate is approximately maximized if the bit and power distribution ensure equal error rates in all the subchannels [3].

In reality, the bandwidth can not be divided into subchannels with zero bandwidth, so that the amplitude response and phase-shift are not fixed at each frequency as illustrated in Figure 1.2. The slope of the magnitude response on the tone is the largest distortion and dominates the performance of a DMT design [4]. This causes interference between the tones. This problem can be solved by using a cyclic prefix (CP). If the cyclic prefix is longer than the channel impulse response, no interference occurs. However, for practical reasons, the CP is generally not as long as the channel impulse response. Therefore, a time domain equalizer (TDEQ) is employed to shorten the channel impulse response into the length of CP. Two TDEQ design methods are discussed in this work which are based on unit energy constraint (UEC) and unit tap constraint (UTC). The TDEQ is adaptive and significantly improves the system performance.

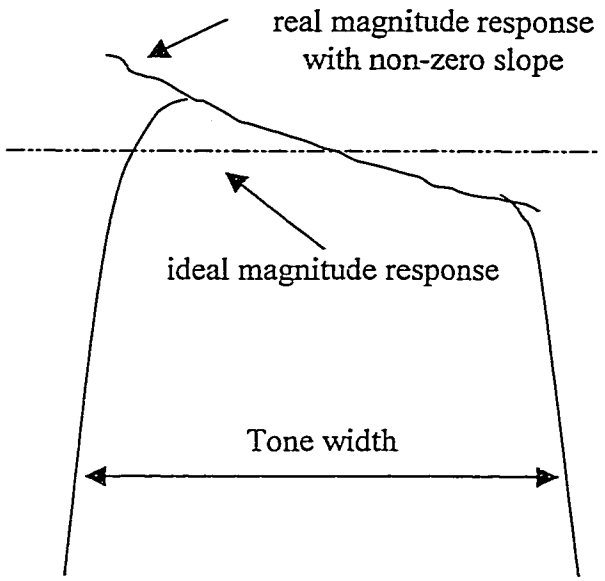

Figure 1.2 Illustration of magnitude response of one tone

Although TDEQ and CP are used to eliminate the interference caused by the non-ideal channel response, the objective can not be totally achieved. In practice, some interference still remains, which is because the shortened effective channel impulse response is not completely confined inside the CP, and decreases the system performance. We will examine the effects of the residual interference on the performance of the system through both theoretical analysis and computer simulations in the following chapters.

1.2 Thesis Organization

The remainder of this thesis is organized as follows. In Chapter 2, an overview of the multicarrier techniques and the FFT-DMT system is presented. The physical channel model and impairment environment is also discussed in Chapter 2. In Chapter 3, we analyze the time domain equalization (TDEQ) design algorithms. Two TDEQ design

constraints, which are unit energy constraint and unit tap constraint, are discussed in details. Chapter 4 gives the computer simulation results based on the design algorithms of the equalizer discussed in Chapter 3. The system performance of different filter prototypes employed at the transceiver front-end is also examined in Chapter 4. Three analog IIR filters are considered. They are Butterworth, Chebyshev-I and elliptic filters. Two digital FIR filters are also discussed. In Chapter 5, the effects of the Inter-Symbol-Interference (ISI), Inter-Channel-Interference (ICI), and Inter-Symbol-inter-Channel-interference (ISCI) on the system performance are discussed and the simulation results are presented. Conclusions are made in Chapter 6.

1.3 Contributions

The contributions of this works are:

1) Two time domain equalization design methods, which are unit energy constraint and unit tap constraint, are compared through computer simulations.
2) The design of the transceiver front-end is discussed. Several IIR and FIR filter prototypes are considered as the transceiver front-end and the system performance is simulated.
3) The effects of the ISI, ICI, and ISCI on the system transmission rate are analyzed through theory and computer simulation on the subchannel-by-subchannel basis.
4) A new frequency domain equalizer design algorithm for DMT system is given.

Chapter 2

ADSL DMT System

In this chapter first an overview of multicarrier modulation technique is given. Next, FFT-DMT system block diagram and the transmission procedure are presented. The ADSL channel and impairments are discussed. The bit allocation algorithm is one of the kernel concepts of the DMT system and the algorithm we used in our simulation is also given in this chapter.

2.1 Multicarrier Modulation System

Before we emphasize our focus on a particular multicarrier system, it is worth to discuss the general principles of the multicarrier modulation technology.

In [8], it is shown that a nonideal linear channel introduces inter-symbol-interference (ISI), which degrades system performance compared with the ideal channel. A more complex receiver is needed in order to reduce the system degradation if the span of the ISI increases. This high complexity receiver is not preferred in practice because a desired communication system must efficiently use the available channel bandwidth within the transmitter power and receiver complexity constraints. Therefore, an equalizer is required for fixed symbol rate single carrier systems, where the time dispersion of the channel is generally much greater than the symbol rate and ISI results from the nonideal frequency response of the channel. Clearly, an equalizer can not handle ISI easily when the impulse response of the channel is very long.

A multicarrier system can be used to design a bandwidth efficient communication system for the nonideal channel. The approach is to divide the available bandwidth into a number of subchannels and each subchannel is nearly ideal as shown in Figure 2.1.

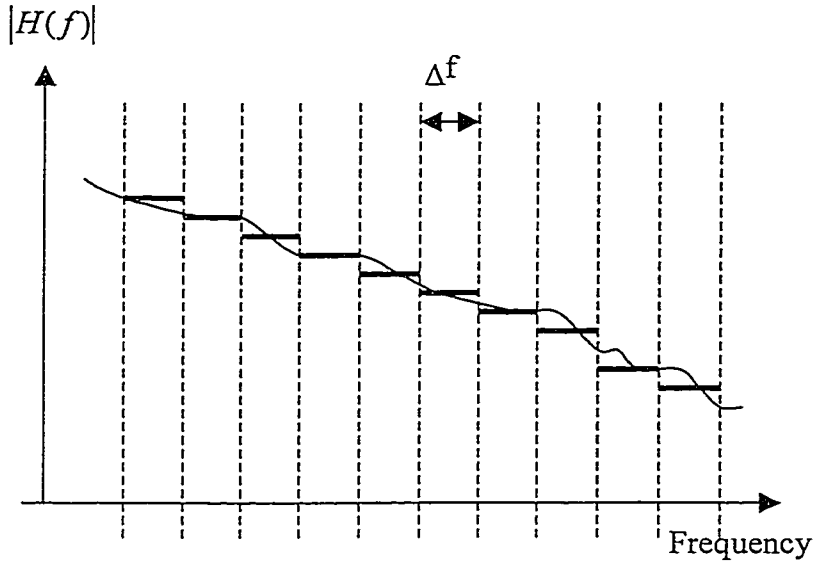

Figure 2.1. Channel frequency response division for multicarrier modulation

If we select the bandwidth of the subchannel, Δf, small enough, the characteristic of each subchannel will be close to an ideal channel. That is the channel magnitude response is approximately constant within each subchannel. The transmitted signal power is distributed subject to the frequency response of the channel under the available average transmitter power constraint. We suppose that the frequency response of a nonideal, band-limited channel is denoted by $H(f)$, and the power spectral density (PSD) of the additive gaussian noise (AWGN) is $\Phi_{nn}(f)$. We also define that the channel signal to noise ratio (SNR) is $|H(f)|^2 / \Phi_{nn}(f)$. Proakis shows in [8] that for AWGN channels, the signal power should be high when the channel SNR is high and low when the channel SNR is low as illustrated in Figure 2.2. This is called the water-filling interpretation of the optimum power distribution as a function of frequency.

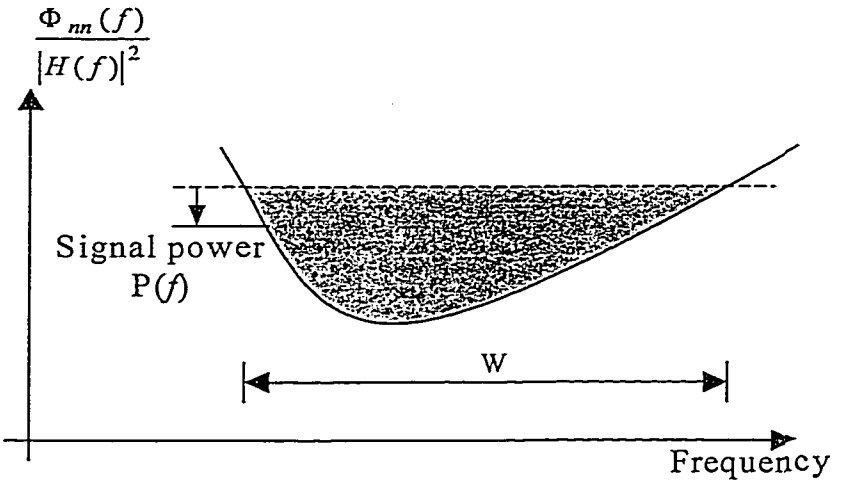

Figure 2.2. The optimum water pouring spectrum

If the available channel bandwidth is divided into subchannels of relatively narrow width, the multicarrier modulation could yield transmission rates close to capacity; and no equalization is necessary because the ISI is negligible.

2.2 FFT-DMT System

The Orthogonal Frequency Division Multiplexing (OFDM) [19] is used to implement the multicarrier modulation. That is to say the bandwidth of each subchannel, Δf, is chosen to be the inverse of the symbol duration, i.e. $\Delta f = 1/T$. Thus the carriers of each subchannel are orthogonal to each other. With the coherent demodulation, there is no contribution at a subchannel from other tones.

FFT-DMT multicarrier is a digital implementation of OFDM [20]. It employs an Inverse Fast Fourier Transform and Fast Fourier Transform (IFFT/FFT) to synthesize the signal at the transmitter and to demodulate the received signal at the receiver [8]. The system block diagram is shown in Figure 2.3 [14].

The incoming bits are first distributed optimally across all the subchannels by a serial-to-parallel buffer. The encoder maps the bits assigned to each subchannel to a complex symbol representing the QAM signal. Each subchannel has a distinct QAM constellation but operates at the same symbol rate. We denote the complex signal on the kth subchannel by X_k, and apply an N_{FFT} point IFFT on the information symbol to modulate the carriers. To ensure a real valued sequence at the output of the IFFT, we impose a Hermitian symmetry condition on the signal and generate N_{FFT} information symbols $\widetilde{X}_k$ as:

$$\widetilde{X}_k = \begin{cases} X_k, & 1 \le k \le N_{FFT}/2 - 1 \\ X^*_{N_{FFT}-k}, & N_{FFT}/2 + 1 \le k \le N_{FFT} - 1 \end{cases} \tag{2-1}$$

and $\widetilde{X}_0 = \mathrm{Re}(X_0), \widetilde{X}_{N_{FFT}/2} = \mathrm{Im}(X_0)$. Thus the N_{FFT} point IFFT yields a real valued sequence:

$$x_k = \frac{1}{N_{FFT}} \sum_{i=0}^{N_{FFT}-1} \widetilde{X}_i e^{j2\pi ik/N_{FFT}}, \qquad k = 0, 1, \cdots, N_{FFT} - 1 \tag{2-2}$$

Then a cyclic prefix with length v will be added to x_k by the algorithm as:

$$x_k = \begin{cases} x_k, & 0 \le k \le N_{FFT} - 1 \\ x_{N_{FFT}+k}, & -v \le k \le -1 \end{cases} \tag{2-3}$$

We will give more details about CP in the following chapters. These samples are fed to a channel with impulse response $h(f)$ through transmission filters and noise is added.

At the receiver, the received signal is passed through a time domain equalizer, and then the CP is removed. After an N_{FFT} point FFT, the signal can then be decoded and the output bit stream is formed.

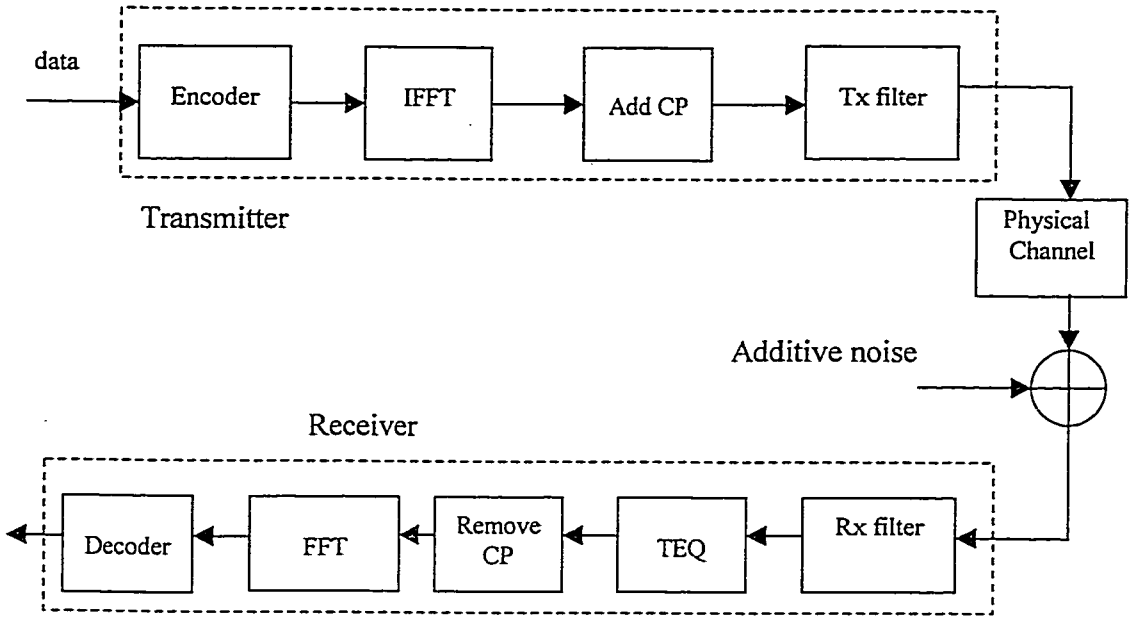

Figure 2.3 FFT-DMT block diagram

2.3 Physical Channel and Impairments in the ADSL System

2.3.1 UTP Loops

ADSL provides unidirectional high data rate service which refers to a high data rate in one direction only while HDSL is bidirectional and will only be offered for the restricted set of loops within the carrier serving area (CSA). The CSA is a subset of the subscriber loops which consists of mainly 24-gauge and 26-gauge twisted pairs. The maximum length of the loops in CSA is limited to 12 kft and 9 kft for the 24- and 26-gauge respectively. ADSL service is not restricted inside the CSA. To distinguish ADSL from HDSL service, we list several key characteristics of ADSL environment as follows:

i. All loops are non-loaded. Loaded refers to the loop that contains loading coils to equalize the 3 kHz voice frequency band.

ii. All loops consist of 26 gauge or coarser cables, either used alone or in combination with other gauge cables.

iii. The maximum allowable loop length, including bridged taps, is 18 kft.

The frequency response of the twisted pair loop can be calculated from the loop length and the propagation constant which is a function of the frequency and can be determined from the cable primary constants.

The example of the impulse response of a ADSL loop is shown in Figure 2.4 and its frequency and phase responses are shown in Figure 2.5. The ADSL loop selected is 9 kft long with 26-gauge. The coefficients of the loop is sampled at a sampling frequency of 4.416 MHz. The Nyquist frequency in Figure 2.5 is 2.208 MHz.

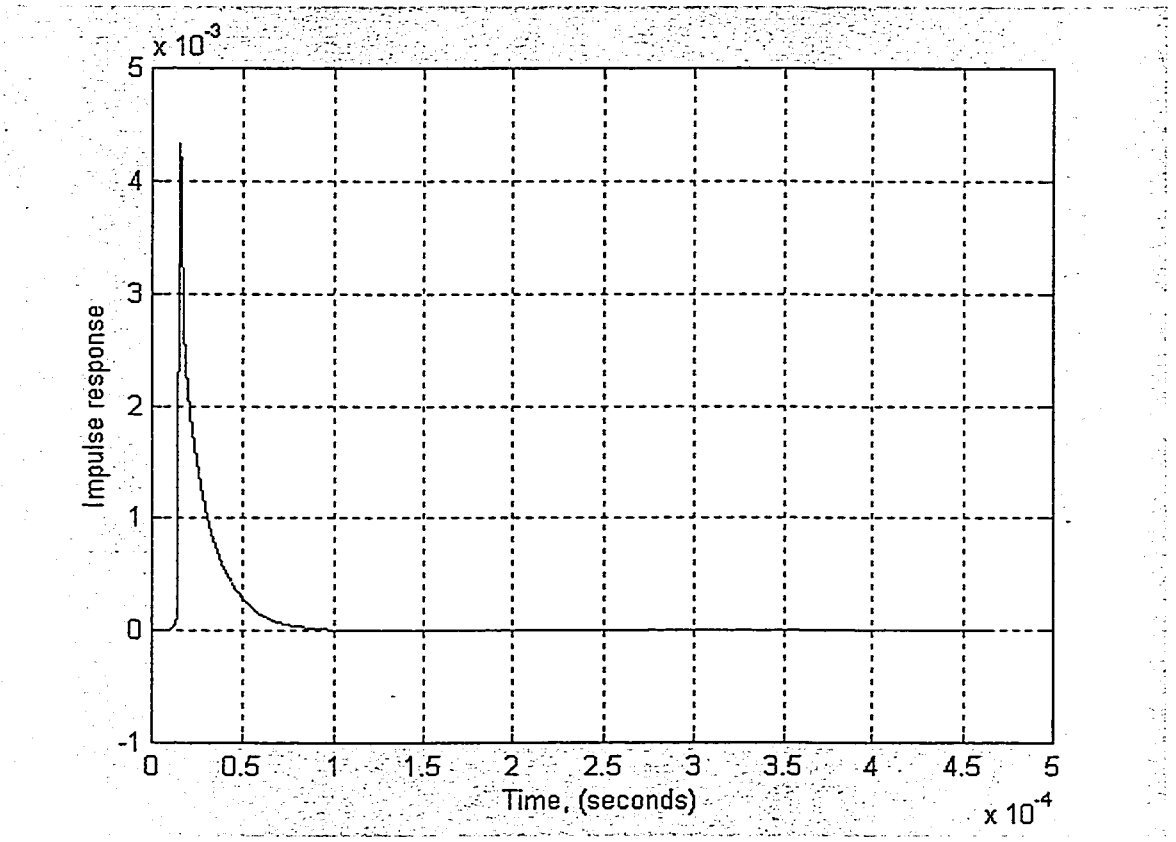

Figure 2.4 Impulse response example of an ADSL loop

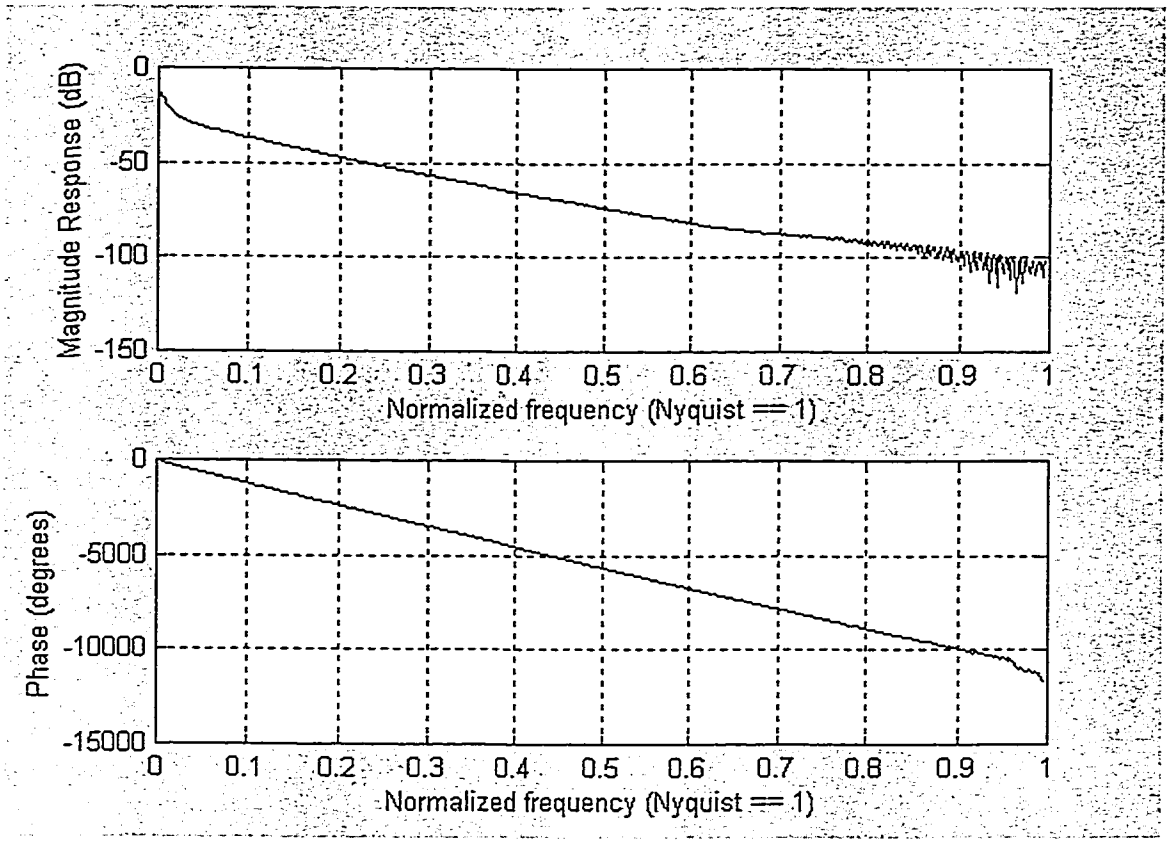

Figure 2.5 Normalized magnitude and phase response of an ADSL loop

The phase response in Figure 2.5 is very close to linear. However, it is necessary to model both the magnitude and the phase response. It is very important to model even very small amounts of phase distortion [48].

So far, we showed the physical channel of ADSL system. The system performance heavily depends on the impairments. The main impairments are:

- Intersymbol interference (ISI)
- Crosstalk
- AWGN
- Impulsive noise

2.3.2 Additive White Gaussian Noise (AWGN), Echo and Electronics Noise

Additive White Gaussian Noise (AWGN) represents a combination of echo noise and various electronic noises. Echo noise results from the combination of imperfect hybrids and gauge changes on the line as well as signals reflected from bridged taps. The residual echo after echo cancellation can be assumed to be additive white Gaussian noise. The electronics noise includes the quantization noise in analog-to-digital converters (ADC) and thermal noise in the analog portion of the transmitter and receiver.

2.3.3 FEXT and NEXT

Crosstalk is an important type of interference in DMT systems. It is caused by coupling of transmission systems over different twisted pairs which share the same cable. There are two kinds of crosstalk, one is Far End CrossTalk (FEXT), and the other one is Near End CrossTalk (NEXT). FEXT results from the transmission in the same direction carried by adjacent twisted pairs, so it is an impairment due to remote transmitters. NEXT results from transmission in different directions along adjacent twisted pairs in the same cable. Figure 2.6 shows the generation of FEXT and NEXT. Commonly, FEXT and NEXT are frequency dependent and thus modeled as colored Gaussian process.

The phenomenon of crosstalk is well studied and understood in the literature [5] [6] [7]. Generally, NEXT should have more damage on the system than FEXT because FEXT is attenuated by the channel propagation loss. However, in the ADSL environment, data is transmitted almost unidirectionally. The downstream transmission rate is much faster than the rate of upstream, so that the NEXT is significantly reduced. It is also possible to further minimize the impact of NEXT by using non-overlapping bands for the transmission of the upstream and downstream. Hence, there will be no NEXT term due to other ADSL services in the same wire bundle. The absence of NEXT significantly improves the data transport capability of the channel. However, there will be a significant amount of spill-over NEXT from bi-directional baseband services in the

same wire bundle due to nonideal filtering [7]. Then this NEXT term can be modeled with the following transfer function:

$$|H_{NEXT}(f)|^2 = K_{NEXT} f^{3/2} \tag{2-4}$$

where K_{NEXT} is the coupling coefficient determined through empirical measurement and f is frequency in Hz.

FEXT also exists in the ADSL environment, although it has much smaller power compared to NEXT. FEXT can be modeled with a coupling transfer function of the form:

$$|H_{FEXT}(d,f)|^2 = K_{FEXT} d |H(f)|^2 f^2 \tag{2-5}$$

Where $|H(f)|^2$ is the channel power spectral density function, d is the length of the cable in kft, f is frequency in Hz, and K_{FEXT} is the coupling coefficient determined through empirical measurements.

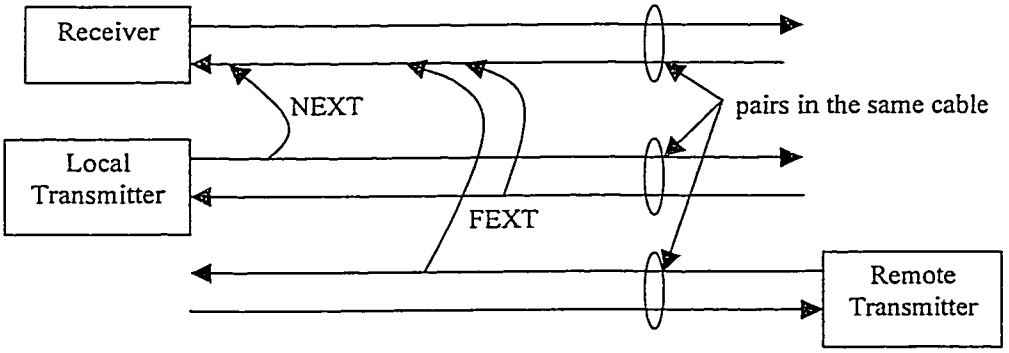

Figure 2.6 FEXT and NEXT crosstalk

2.3.4 Impulse Noise

In UTP environments, a variety of man-made equipment and environmental disturbances such as signaling circuits, transmission and switching gear, electrostatic discharges, lightning surges can be possible impulse noise sources. The occurrence of the impulse events is widely discussed in the literature. Impulse noise has been proved to be one of the major limiting factors in the transceiver's achievable performance and has been analyzed in the literature [23]–[29].

In this thesis, in designing and evaluating time domain equalizers, we did not take into account the impact of impulse noise and this subject will not be covered.

2.4 Bit Allocation and Spectrum Shaping

A multitone modulation scheme optimizes the power spectrum over more than one frequency band while a single tone modulation scheme is restricted to concentrating the transmitted power in one frequency band. As mentioned in the previous sections, the basic idea of DMT system is to use an optimized frequency division allocation of power and bits to maximize the data rate over bandlimited communication channels. With an optimized power distribution according to the characteristics of each subchannel, a DMT system can achieve much higher capacity than a single carrier system.

As indicated in [8], [11], and [13], it is best to optimize both the spectrum and the bit allocation of a DMT system in order to achieve the maximum system capacity within the available bandwidth and power constraints. In [11], it is indicated that a non-optimized spectrum results in a significant performance degradation compared with an optimized spectrum. The "water pouring" solution is well known to yield the optimal solution. In the rest of this section, we will mathematically compute the spectrum optimization and bit allocation using the method derived from the "water pouring" solution.

After the ADSL DMT system is initialized, each usable subchannel is assigned a QAM signal. We assume that a rectangular (or cross) QAM constellation is used as described in [10] and the average energy per symbol equals E. The minimum distance between adjacent constellation points is $2*a$.

If a L_k -ary QAM symbol is assigned to the kth subchannel, then the number of bits, b_k, carried by this QAM signal can be defined as:

$$b_k = \log_2 L_k \tag{2-6}$$

and the aggregate number of bits per symbol, b_A, is given by

$$b_A = \sum_{k \in M} b_k = \sum_{k \in M} \log_2 L_k \tag{2-7}$$

where M is the set of all used subchannels. Then the overall bit rate, R_b, is given by:

$$R_b = b_A \frac{f_{samp}}{N} = b_A / T \tag{2-8}$$

where f_{samp} is the sampling frequency , N is the number of samples per symbol and T is the DMT symbol duration.

According to [8] [9], the probability of symbol error for QAM signaling with even values of b_k is given by:

$$Pe_k = 4\left(\frac{\sqrt{L_k}-1}{\sqrt{L_k}}\right) Q\left(\frac{d_{RX\,k}}{2\sigma_k}\right) \tag{2-9}$$

where σ_k is the standard deviation of the in-band Gaussian noise of subchannel k, the Q-function is defined in [8] as:

$$Q(x) = \frac{1}{\sqrt{2\pi}} \int_x^{\infty} e^{-y^2/2} dy \tag{2-10}$$

and $d_{RX\,k}$ in equation (2-9) is the minimum distance between adjacent constellation points of the received symbol at kth subchannel and can be approximated by:

$$d_{RX\,k} \approx |H(f_k)| d_{TX\,k} \tag{2-11}$$

where $H(f_k)$ is the channel frequency response at the center frequency of tone k and $d_{TX\,k}$ is the transmitted constellation distance of the kth subchannel which can be expressed as $d_{TX\,k} = 2 * a$.

The value of a is related to the average symbol energy E for even number of bits and is given by [10]:

$$a^2 = \frac{3E}{2} / (2^n - 1) \tag{2-12}$$

The error probability and the average energy/symbol for odd values of b_k can also be approximated by (2-9) and (2-12).

We assume that each subchannel has the same probability of symbol error. We need to satisfy the value of the equation below to be a constant:

$$\gamma = \left(\frac{d_{RX\,k}}{2\sigma_k}\right)^2 \tag{2-13}$$

γ is usually referred to as the required SNR. For a symbol error rate (SER) of 1e-7, we need to keep γ to be 14.5 dB.

The transmitted power (normalized to the characteristic impedance of the line and the symbol period), P_k, on the kth subchannel is given by:

$$P_k = \frac{L_k - 1}{6} d_{TX\,k}^2 \tag{2-14}$$

and the normalized total transmit power is given by:

$$P_{TX} = \sum_{k \in M} P_k \tag{2-15}$$

We can solve (2-14) for L_k by combining above expressions (2-12) (2-13) and (2-14), and the result is given as:

$$L_k = 1 + \frac{3P_k|H(f_k)|^2}{2\sigma_k^2\gamma} \tag{2-16}$$

The optimum bit allocation and spectrum shape maximize the data capacity of the loop under the specified power constraint as in [11]. We can formulate this as a Lagrange optimization problem with Lagrangian, $L(*)$, as:

$$L(P_k) = \sum_{k\in M} \log_2(1 + \frac{3P_k|H(f_k)|^2}{2\sigma_k^2\gamma}) - \lambda \sum_{k\in M} P_k \tag{2-17}$$

Setting the derivative of (2-17) to be zero, we can solve the optimal values of P_k:

$$P_k = P_0 - \frac{\sigma_k^2\gamma}{3|H(f_k)|^2} \tag{2-18}$$

where P_0 is a constant. The power distribution in (2-18) is corresponding to the infinite granularity of the bit allocation and is identical to "water pouring" solution as in [8].

By defining the SNR gap $\Gamma = \gamma/3$, which represents the distance between the performance of a QAM signaling scheme and capacity over a memoryless channel [21] [22], the SNR of the *k*th subchannel is given by:

$$SNR_k = \frac{P_k|H(f_k)|^2}{2\sigma_k^2} \tag{2-19}$$

we can simplify (2-16) and calculate the maximum number of bits on this subchannel by:

$$b_k = \log_2(1 + \frac{SNR_k}{\Gamma}) \tag{2-20}$$

The above solution for the optimum bit allocation is not practical for its infinite bit granularity. In this thesis, we use unit bit granularity for the bit allocation that is to say

we assign an integral number of bits to each subchannel. The bit allocation can be calculated using the iterative process as described in [12].

An example of the bit allocation algorithm discussed above is shown in Figure 2.7. The ADSL loop we used in this example is 15 kft long with 26 gauge. The additive white Gaussian noise (AWGN) with power spectrum density (PSD) of –140 dBm is the only noise source. The PSD of the signal is –40 dBm. The transmission simulated is downstream. The tone number 64, whose center frequency is 276 kHz, is reserved for pilot and no data is transmitted on this tone. The power distribution corresponding to the bit allocation example is shown in Figure 2.8. Because we use unit bit granularity, the subchannel power distribution shows a "saw-tooth" behavior as plotted in Figure 2.8. However, the difference between the maximum and the minimum values of signal PSD is small and within 5 dBm/Hz in the example we showed.

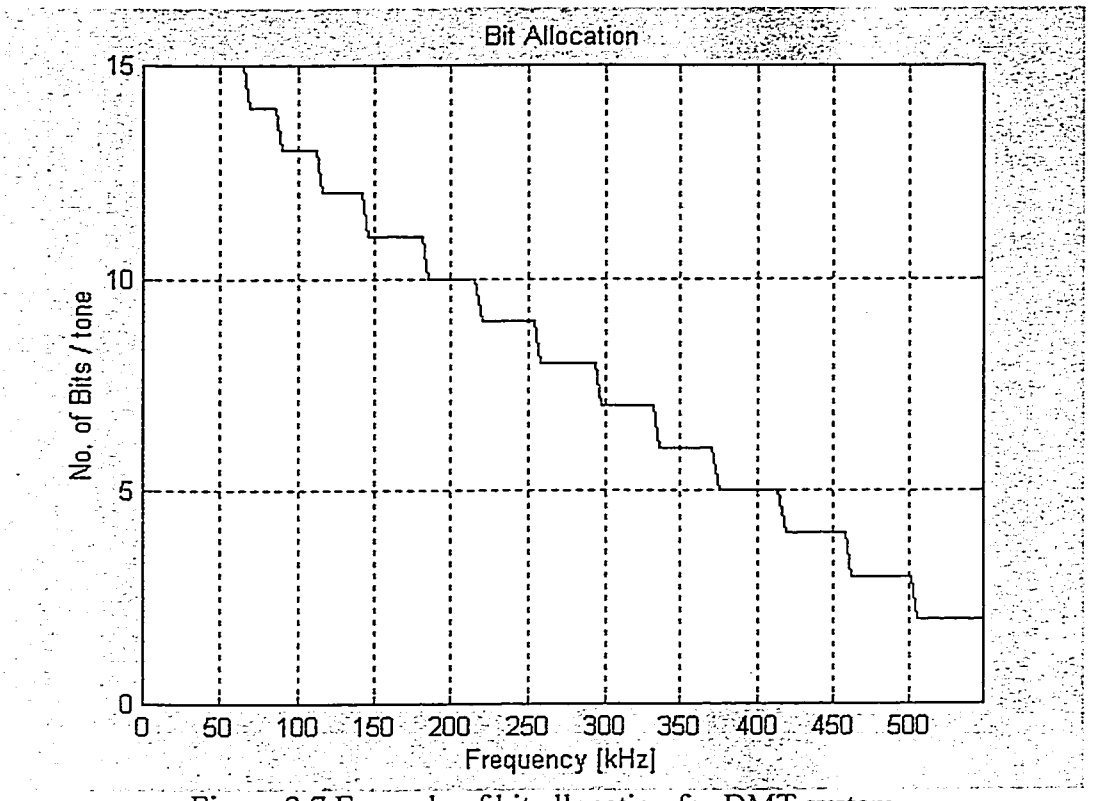

Figure 2.7 Example of bit allocation for DMT system

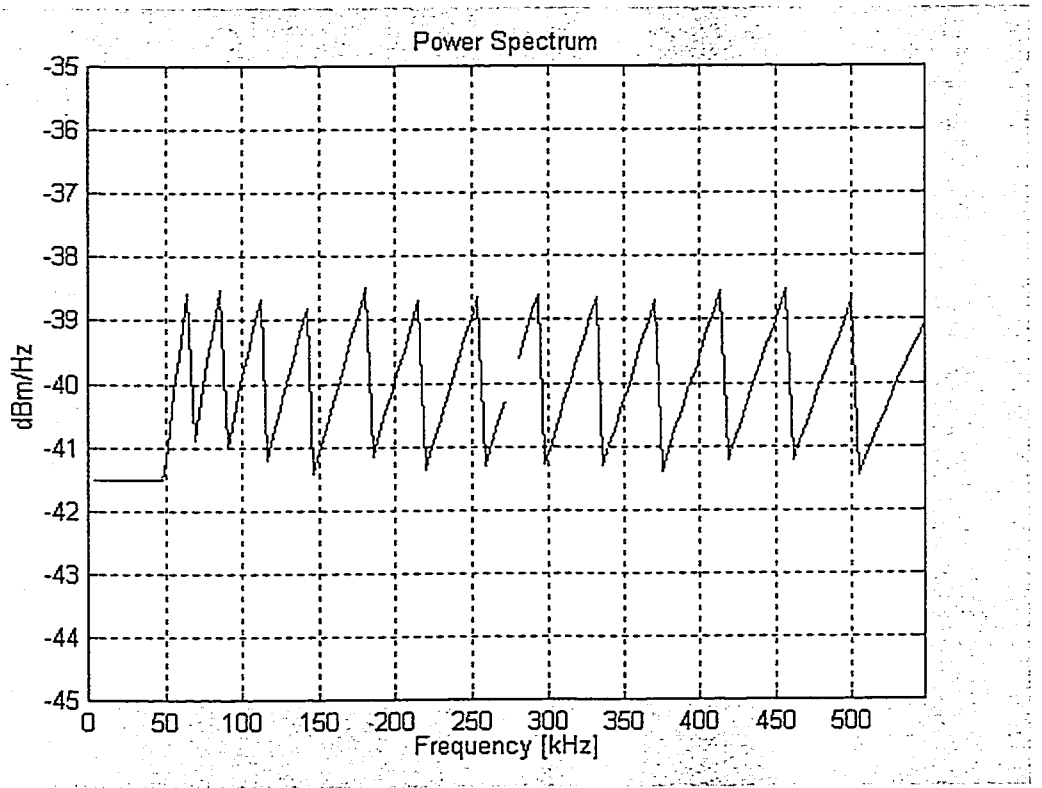

Figure 2.8 Example of optimized power spectral density for DMT system

2.5 Echo Cancellation

When full-duplex transmission is used over the twisted pair, two signals traveling simultaneously in opposite directions in the same frequency band generate echo. Generally, a highly complex echo canceller must be employed in order to eliminate the echo [15], [16], [17], [18]. The complexity of the echo cancellers rises quickly with the increases in the number of tones. To keep the system implementation complexity at a low level, an alternative is to use non-overlapping frequency bands for the upstream and downstream transmissions. Ideally, no echo occurs when the two bands are totally separated. Thus, we assume that such a frequency division is applied and we will not further consider echo cancellation technique in this work.

2.6 Transceiver Front-end

Filters are used at the transceiver front-end to separate the frequency bands for upstream (US) and downstream (DS). We examined several filter prototypes in our simulation. They are Butterworth, Chebyshev type I, and elliptic filter for analog IIR design. For digital FIR design, we select Kaiser window and Parks-McClellan algorithm. More details of these filter design is given in appendix I. We will show the effects of employing different filter types at the transceiver front-end on the system performance through simulation results in Chapter 4.

Chapter 3

Equalization for FFT-DMT

Equalization is a very important part of the FFT-DMT system. It significantly improves the system performance. In this chapter, we first introduce the requirement of the Time Domain EQualizer (TDEQ) in DMT system. Next, the structure of the equalizer in DMT system based on the Minimum-Mean-Square-Error (MMSE) criterion is given. We will concentrate on two constraints of MMSE-TDEQ design, which are unit tap constraint and unit energy constraint. The theoretical deduction of the settings of these equalization algorithms will also be given in this chapter.

3.1 Introduction

The high-performance Viterbi Algorithm (VA) is of considerable interest for data transmission in the presence of severe intersymbol interference and additive Gaussian noise. However, it usually is not practical because its computational complexity increases exponentially with the duration of the channel impulse response. So we need to find a way to reduce the length of channel impulse response.

The problem can be solved by combining equalization with this maximum likelihood sequence estimation (MLSE). The function of equalizer is to shorten the length of the channel impulse response to a much shorter duration, which usually is called cyclic prefix (CP). The cyclic prefix is added at the transmitter and discarded at the receiver in order to minimize the ISI introduced by non-ideal channel impulse response.

The CP is a guard period to prevent inter-symbol-interference (ISI) between successive symbols and inter-channel-interference (ICI) between different subchannels. Adding a blank space can solve the ISI problems, but the transmission may still suffer from ICI. This is because that the orthogonality between subcarriers can not be maintained in a distorted channel. We can use a cyclic extension of the original DMT symbol to solve this problem. The CP is generated by simply taking the last v samples of the original N sample symbol and added to the beginning of the original symbol, as shown in Figure 3.1 [31].

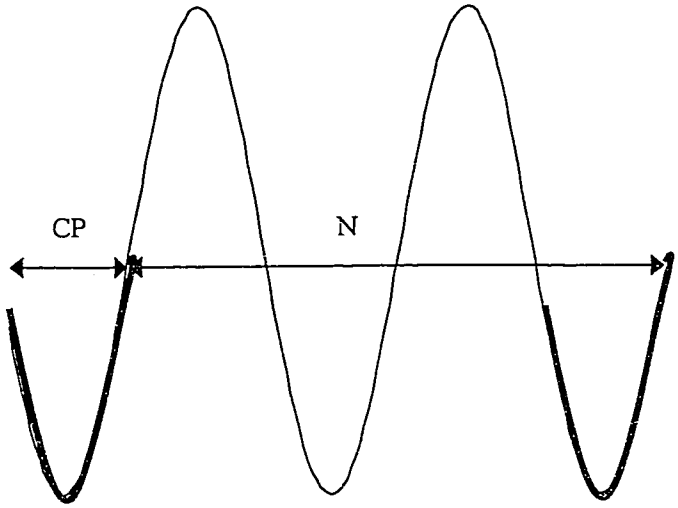

Figure 3.1. Cyclic prefix illustration

When the cyclic prefix is longer than the impulse response of the channel, the convolution of the signal and the channel will have a cyclical behavior, as illustrated in Figure 3.2, and therefore satisfies the orthogonality requirement. More details can be found in [19][46]. The length of CP, v, is determined by the length of the channel impulse response. At the receiver the CP is removed and the remaining N samples are then demodulated. If the length of the channel impulse response is equal to or less than v, the CP can successfully eliminate ISI and ICI. However, there is a problem by using this CP -- the transmission efficiency is reduced by a factor of $CP/(CP+N)$. In order to keep the

transmission efficiency high, it would be ideal by either using a large N or making v as small as possible. Because increasing N may introduce several other problems such as increasing the computational complexity and the end-to-end delay, it is quite important to use a small v. However, v is related to the length of the channel impulse response which varies from channel to channel and is typically not under the control of the designer.

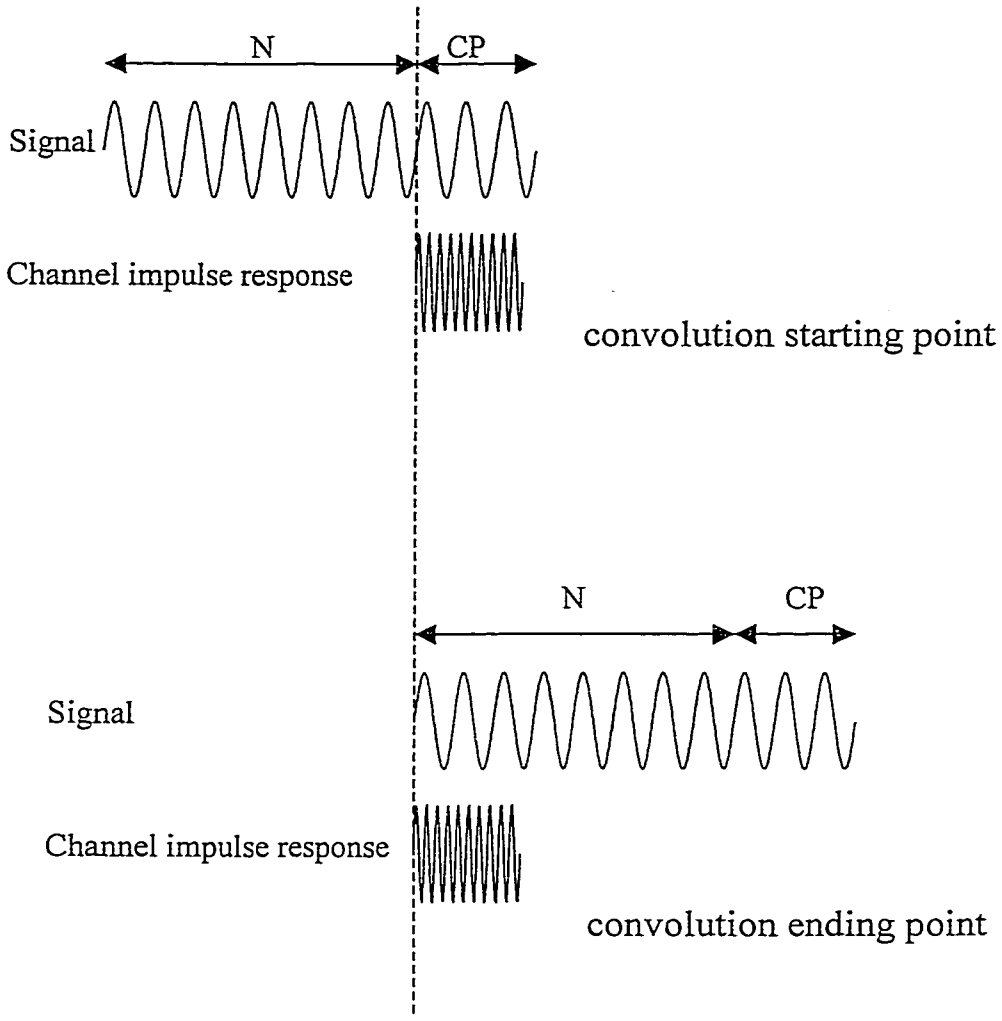

Figure 3.2 CP functional illustration

To shorten the channel impulse response, a time domain equalizer (TDEQ) can be used right after the analog-to-digital (AD) converter at the receiver. The basic purpose of

using this TDEQ in the system is to shorten the duration of the channel impulse response. The function of the TDEQ is illustrated in Figure 3.3. We can see that the original channel impulse response is much shortened by the TDEQ. This ensures the use of a small ν can successfully reduce the ISI while keeping a high transmission efficiency. Then the effective channel after equalization is the convolution of transmit filters, physical channel, receive filters and this TDEQ. It is desirable to make this effective channel impulse response to be equal or less than the CP.

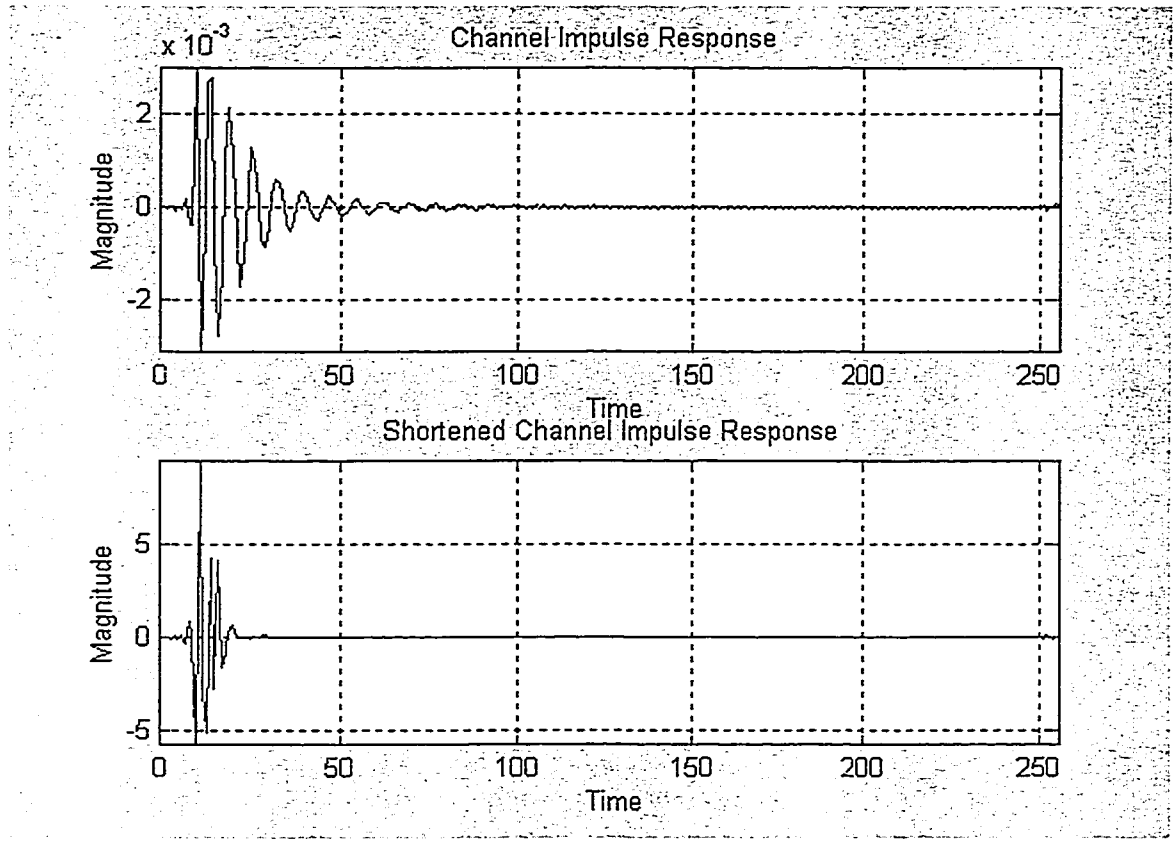

Figure 3.3 TDEQ Function Illustration

Many criteria were considered for designing the reduced length target impulse response (TIR) that results from the equalized original channel impulse response. Qureshi and Newhall truncated the original channel impulse response to get the desired one in [36]. Messerschmitt presented a monicity constraint on the TIR and used the whitened-matched-filter as the equalizer structure [37]. However, an infinite-length equalizer was

used in the literature mentioned above. This is an ideal assumption but not practical since a finite number of filter taps is required for practical implementation. Some practical realizable equalizer design algorithms will be discussed in the following sections.

3.2 Equalizer Structure

In most practical situations, the channel response is not known. Thus adaptation of the equalizer during system startup is essential when data is transmitted over an unknown channel. The coefficients of the adaptive TDEQ can be adjusted recursively. Non-recursive adaptive equalization can be obtained based on channel estimates. In this thesis, the channel impulse response is assumed to be be given.

The block diagram of a linear time domain equalizer is shown as in Figure 3.4. The channel impulse response is assumed to be linear, time invariant and has $N_h + 1$ taps denoted as $\{h_0, h_1, \cdots, h_{N_h}\}$. $\{\mathbf{x_k}\}$ is the input data sequence, $\{\mathbf{n_k}\}$ is the additive Gaussian noise sequence with variance σ_n^2, and $\{\mathbf{y_k}\}$ is the channel output sequence. It is also assumed that the input data sequence and the noise sequence are uncorrelated with each other. It also needs to be mentioned that the noise sequence is colored due to crosstalk in typical high-speed subscriber loop [32]. We need to calculate the optimum TDEQ and TIR settings according to these parameters.

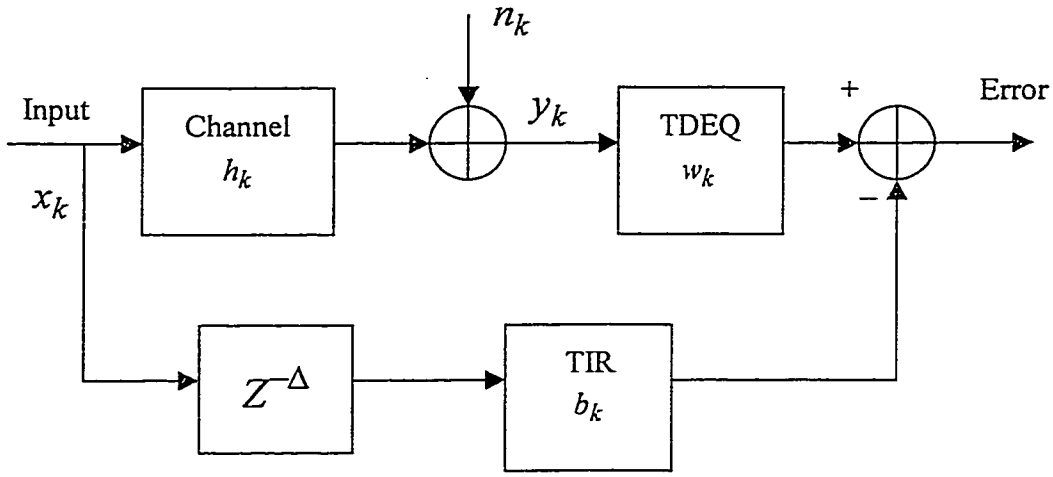

Figure 3.4 Block diagram of the time domain equalizer

From Figure 3.4, we can write the input/output relationship for the discrete time equivalent channel as:

$$y_k = \sum_m h_m x_{k-m} + n_k \tag{3-1}$$

Using (3-1) and only looking at N_f successive samples of y_k, we can write the input/output relation in a matrix form as:

$$\mathbf{y_k} = \mathbf{H}\mathbf{x_k} + \mathbf{n_k} \tag{3-2}$$

where we define the input, output, noise and channel matrix as following:

$$\mathbf{x_k} = \begin{bmatrix} x_k \\ x_{k-1} \\ \vdots \\ x_{k-N_f-N_h+1} \end{bmatrix}, \qquad \mathbf{n_k} = \begin{bmatrix} n_k \\ n_{k-1} \\ \vdots \\ n_{k-N_f+1} \end{bmatrix},$$

$$\mathbf{y_k} = \begin{bmatrix} y_k \\ y_{k-1} \\ \vdots \\ y_{k-N_f+1} \end{bmatrix},$$

and

$$\mathbf{H}=\begin{bmatrix} h_0 & h_1 & \cdots & h_{N_h} & 0 & \cdots & 0 \\ 0 & h_0 & h_1 & \cdots & h_{N_h} & 0 & \cdots \\ \vdots & \vdots & \ddots & \ddots & \ddots & \ddots & \vdots \\ 0 & \cdots & 0 & h_0 & h_1 & \cdots & h_{N_h} \end{bmatrix}$$

Unlike the TIR case in [33], the TIR here is restricted to be causal. That is the TIR, b_i, should satisfy $b_i = 0$ for $i \leq 0$. Therefore, a relative delay Δ between the TDEQ and the TIR is introduced [34]. Thus, if the estimated sequence $\{\hat{x}_k\}$ at the output is delayed by Δ time units, the input to threshold device at time k is $\hat{x}_{k-\Delta}$, which is the optimal estimate of $x_{k-\Delta}$ given the channel outputs $\{y_k, y_{k-1}, \cdots\}$ and past decisions $\{x_{k-\Delta-1}, x_{k-\Delta-2}, \ldots\}$. Thus the delay can be interpreted as the decision delay inherent in a causal realization of TIR. This delay is not associated with any delay in the threshold device itself.

As it is shown in Figure 3.4, there are two symbol-spaced filters. One is the Time Domain Equalizer (TDEQ), $\mathbf{w} = [w_0 w_1 \cdots w_{N_f-1}]^{\mathrm{T}}$, which consists of N_f taps and $[\,]^{\mathrm{T}}$ denotes the transpose operation of matrix. The other one is the Target Impulse Response (TIR), $\mathbf{b} = [b_0 b_1 \cdots b_{N_b}]^{\mathrm{T}}$, which consists of $N_b + 1$ taps. This TIR is the ideal truncated effective channel impulse response with acceptable duration. Its length, $N_b + 1$, is equal or less than CP+1. The TDEQ is designed to force the overall impulse response to approximate this TIR [33]. However, TDEQ can not ideally truncate the channel impulse response to TIR. In any application of prefiltering to approximate TIR, the TIR itself and the TDEQ should be carefully chosen in order to minimize the error because of noise and the difference between the FIR and the actual impulse response that is achieved.

From Figure 3.4, the error between the two branches can be expressed as:

$$e_k = \tilde{\mathbf{b}}^{\mathrm{T}}\mathbf{x}_k - \mathbf{w}^{\mathrm{T}}\mathbf{y}_k \tag{3-3}$$

where

$$\tilde{\mathbf{b}}^{\mathrm{T}} = \left[\mathbf{0}_{1\times\Delta}\ b_0\ b_1 \cdots b_{N_b}\ \mathbf{0}_{1\times S}\right] = \left[\mathbf{0}_{1\times\Delta}\ \mathbf{b}^{\mathrm{T}}\ \mathbf{0}_{1\times S}\right]$$

is the delayed target impulse response, and $S = N_f + N_h - \Delta - N_b - 1$, the input sequence and output sequence are defined as in (3-2).

Then, the mean square error can be expressed as:

$$\begin{aligned} \mathrm{MSE} &= \mathrm{E}\left[|e_k|^2\right] \\ &= \mathrm{E}\left[\left(\tilde{\mathbf{b}}^{\mathrm{T}}\mathbf{x}_k - \mathbf{w}^{\mathrm{T}}\mathbf{y}_k\right)\bullet\left(\tilde{\mathbf{b}}^{\mathrm{T}}\mathbf{x}_k - \mathbf{w}^{\mathrm{T}}\mathbf{y}_k\right)^*\right] \\ &= \tilde{\mathbf{b}}^{\mathrm{T}}\mathrm{R}_{xx}\tilde{\mathbf{b}} - \tilde{\mathbf{b}}^{\mathrm{T}}\mathrm{R}_{xy}\mathrm{w} - \mathrm{w}^{\mathrm{T}}\mathrm{R}_{yx}\tilde{\mathbf{b}} + \mathrm{w}^{\mathrm{T}}\mathrm{R}_{yy}\mathrm{w} \end{aligned} \tag{3-4}$$

The orthogonality principle states that the optimal error sequence is uncorrelated with the observed data, which is $\mathrm{E}\left\{e_k\mathbf{y}_k^*\right\}$, the $(\,)^*$ operation indicates the complex conjugate transpose. Therefore, we have

$$\tilde{\mathbf{b}}^{\mathrm{T}}\mathrm{R}_{xy} = \mathrm{w}^{\mathrm{T}}\mathrm{R}_{yy} \tag{3-5}$$

Combining equations (3-4) and (3-5), we get the Minimum Mean Square Error (MMSE) as:

$$\mathrm{MMSE} = \tilde{\mathbf{b}}^{\mathrm{T}}\mathrm{R}_{x|y}\mathrm{b} \tag{3-6}$$

where

$$\mathrm{R}_{x|y} = \mathrm{R}_{xx} - \mathrm{R}_{xy}\mathrm{R}_{yy}^{-1}\mathrm{R}_{yx} \tag{3-7}$$

in equation (3-7), the $N_f + N_h$ dimensional input correlation matrix is defined as:

$$\mathbf{R}_{xx} = \mathbf{E}\left[\mathbf{x}_k\mathbf{x}_k^*\right] \tag{3-8}$$

the N_f dimensional noise correlation matrix is defined as:

$$\mathbf{R}_{nn} = \mathbf{E}\left[\mathbf{n}_k\mathbf{n}_k^*\right] \tag{3-9}$$

the input-output cross-correlation matrix is defined as:

$$R_{xy} = R_{yx}^{*} = E\left[\mathbf{x}_k \mathbf{y}_k^{*}\right] = R_{xx} H^{T} \tag{3-10}$$

and the N_f dimensional output auto-correlation matrix is defined as:

$$R_{yy} = E\left[\mathbf{y}_k \mathbf{y}_k^{*}\right] = H R_{xx} H^{T} + R_{nn} \tag{3-11}$$

Since we assume the input data are independent, the input correlation matrix can be simplified to an identity matrix I. We also can find that R_{yy} is Toeplitz. Its inverse operation can be done through using an efficient algorithm that is Levinson's algorithm. Then the operation complexity is proportional to N_f.

If a desired TIR is chosen, a time domain equalizer will be derived to force the overall channel impulse response to this TIR within a minimum mean square error. If we have a desired CP, and we equalize the length of the target impulse response to the length of CP, the TIR will be optimized in terms of MMSE. Then the coefficients of TDEQ will be calculated in a straightforward manner.

There are many solutions of **b** and **w** for equation (3-6) to minimize the MSE value. To avoid the trivial case of no MSE which corresponds to no transmission, and to obtain unique value of **b** and **w**, we need apply further constraints on the equation.

For convenience, we define another matrix R_Δ from $R_{x|y}$ as:

$$R_\Delta = [0_{(N_b+1)\times\Delta} \quad I_{N_b+1} \quad 0_{(N_b+1)\times S}]\, R_{x|y} \begin{bmatrix} 0_{\Delta\times(N_b+1)} \\ I_{N_b+1} \\ 0_{S\times(N_b+1)} \end{bmatrix} \tag{3-12}$$

From the definition, we can see that R_Δ is a sub-block picked up from $R_{x|y}$ as shown below:

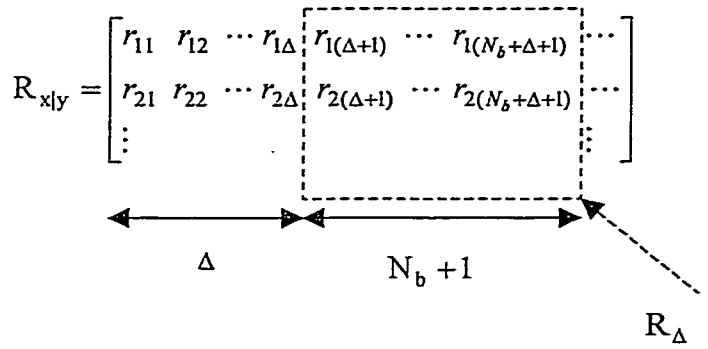

The delay value, Δ, determines the position of the sub-block and the length of the TIR determines its size.

3.2.1 Unit Energy Constraint (UEC)

We can impose a Unit Energy Constraint (UEC) [33] on the TIR which forces the energy of **b** to be unity i.e.

$$b^* b = 1 \tag{3-13}$$

Since MMSE is always equal or greater than zero, it is a positive definite quadratic form in **b** which depends only upon **b** and the channel characteristics. This MMSE can be minimized by choosing **b** to be the eigenvector corresponding to the minimum eigenvalue of R_Δ. Then the coefficients of TDEQ can be calculated in straightforward manner from equation (3-5) by matrix inversion.

3.2.2 Unit Tap Constraint (UTC)

We can also apply a Unit Tap Constraint (UTC) [34] [39] on the TIR which sets one of the TIR coefficients to be unity i.e.:

$$b^* e_l = 1 \tag{3-14}$$

where e_l is the unit column vector with unity in the lth position. We need to find the optimum index for the unit element position in e_l that achieves the minimum mean square error for UTC:

$$\mathrm{MMSE}^{\mathrm{UTC}} = \frac{1}{R_{\Delta}^{-1}(l,l)} \tag{3-15}$$

and this index can be estimated by:

$$l_{opt} = \arg\max_{0 \le l \le N_b} \left\{ R_{\Delta}^{-1}(l,l) \right\} \tag{3-16}$$

Therefore, the optimum solution for the TIR coefficients will be:

$$b = \frac{R_{\Delta}^{-1} e_{l_{opt}}}{R_{\Delta}^{-1}(l_{opt}, l_{opt})} \tag{3-17}$$

The optimum equalizer settings are determined from (3-5):

$$w = R_{yy}^{-1} R_{yx} b \tag{3-18}$$

It is useful to indicate that by selecting $l = 1$ the above solution is equal to the Decision Feedback Equalizer (DFE) solution [35] [41].

An example of the TIR under UEC and UTC is shown in Figure 3.5. The TIR length is 17. The TIR under UEC has unit energy, so that the absolute values of its coefficients are all less than unity. For the TDEQ design under UTC, we showed two TIR settings with unity at the first and last tap, respectively.

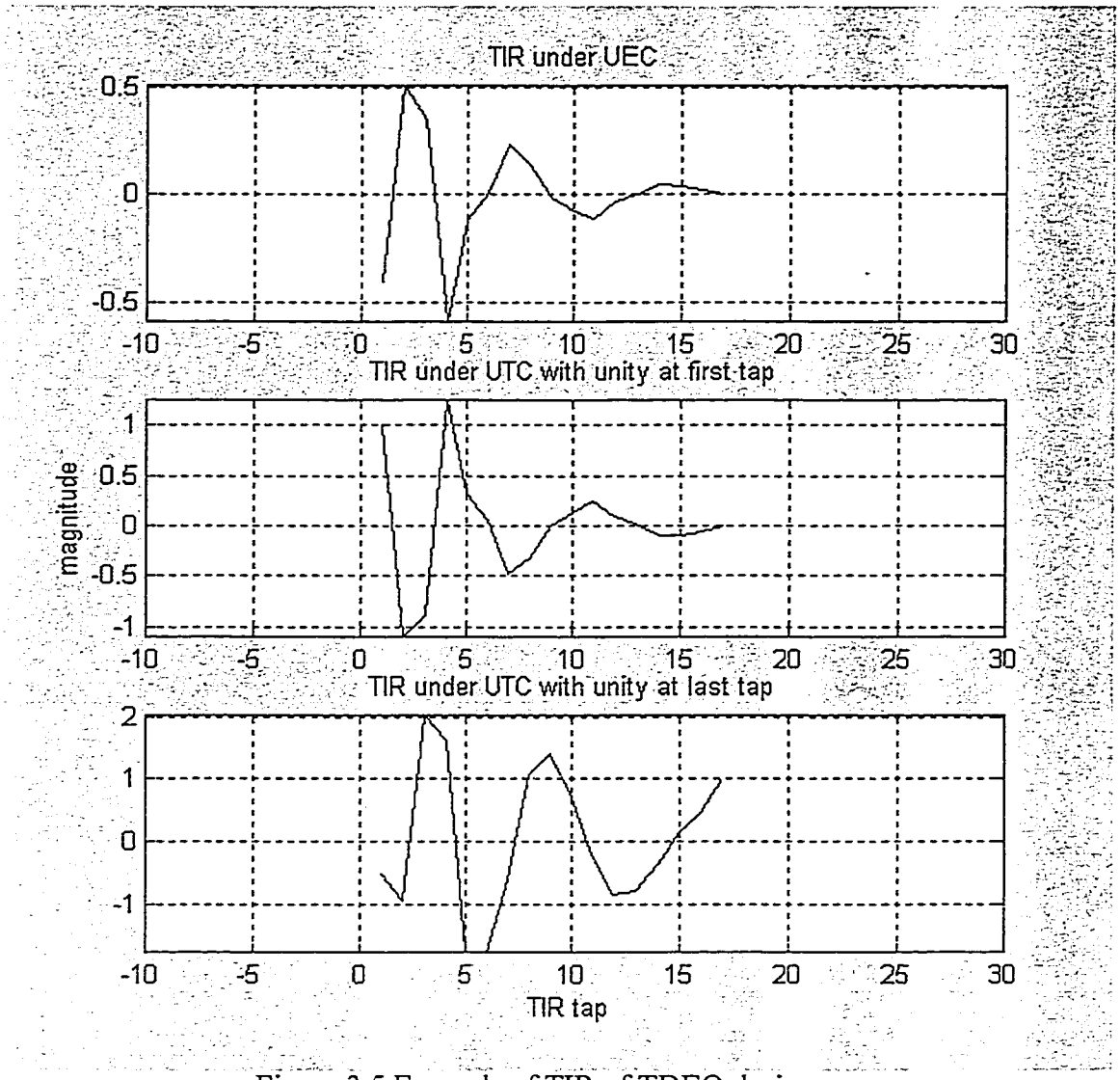

Figure 3.5 Example of TIR of TDEQ design

3.2.3 UEC and UTC Comparison

These two constraints applied on the equalizer design have their own properties. UTC formulates the MSE as a quadratic form in the TIR coefficients. This offers more geometrical insight into the problem. It has been proved in [34] that the TDEQ design under UEC results in a lower MSE than that of the UTC. The MMSE of UTC equals to

the MMSE of UEC if and only if all the eigenvalues of R_Δ are equal. This is as to say that the channel is memoryless and the input data and noise processes are white.

The MMSE is only one of the parameters to evaluate the TDEQ performance. We also need to apply the derived TDEQ in the system and measure the system throughput to compare the two design constraints. We do this by using simulations, and the results are presented in chapter 4.

3.2.4 Fast Computation Algorithm

There are several methods to train the TDEQ settings during the startup of the system [38] [39]. These methods require either intense computation such as matrix inversion or significant amount of iterations and time before the algorithm reaches convergence. Therefore, these methods are not suitable for the applications which are sensitive to the complexity costs or convergence time. The slow convergence motivates study of non-iterative methods to compute the optimum equalizer settings for practical situations.

Lee and Cioffi have proposed the non-recursive fast computation for both decision feedback equalizer (DFE) and the linear TDEQ designs in [40] [32]. The results for the TDEQ design are briefly summarized below. The target impulse response is given by:

$$b_k = \frac{1}{M}\sum_{i=0}^{M-1}\overline{B}_i e^{J2\pi ik/M}, \qquad k = 0,1,\cdots N-1 \tag{3-19}$$

where l is the index for the unit element, M is the TDEQ length, N is the TIR length, and $\overline{B}_i$ is defined as:

$$\overline{B}_i = \frac{1}{k'}(SNR_i + 1)e^{-J2\pi il/M}, \qquad i = 0,1,\cdots M \tag{3-20}$$

in (3-20) the SNR_i is defined as the signal to noise ratio on the ith channel, and k' is a scaling constant to make the lth element of the target response b_k equal to 1, that is $b_l = 1$.

The TDEQ coefficients are given by:

$$w_k = \frac{1}{M} \sum_{i=0}^{M-1} W_i e^{J2\pi ik/M}, \qquad k = 0,1,\cdots M-1 \tag{3-21}$$

where W_i is defined by:

$$W_i = \frac{\varepsilon M H_i^* p_{\Delta,i} B_i}{\varepsilon M |H_i|^2 + |\tilde{N}|^2} \tag{3-22}$$

in (3-22), ε is the signal power of the input data sequence, H_i is the ith element of M-point FFT of channel impulse response, $\tilde{N}_i$ is the ith element of the FFT of additive noise sequence, B_i is the ith M-point FFT element of TIR coefficients, Δ is delay value, and $p_{\Delta,i} = e^{-J2\pi\Delta i/M}$.

The fast algorithm approximates the Toeplitz matrices in the calculations of the TDEQ coefficients as described above by the circulant matrices. The direct matrix inversion can be avoided. The equalizer coefficients can be computed using only the FFT and the IFFT. Since FFT/IFFT pair is employed by the modulation and demodulation in DMT system, the equalizer coefficients can be computed by sharing the same FFT/IFFT pair without costing additional hardware. The simulation results presented in the literature shows that the SNR difference between the fast computational algorithm and exact solution is within a few tenth dB level which is acceptable.

Chapter 4

Simulation Results and Analysis

The time domain equalizer design algorithms have been theoretically analyzed in chapter 3, and different constraints have been described. In this chapter, we will apply the equalizers to the DMT system and show the effects of different TDEQ designs on the system performance through computer simulations. In this chapter, first some common simulation parameters will be given according to the ADSL-DMT standard. Next, simulation results of the TDEQ performance will be shown. In addition to the TDEQ design, the filter design at the transceiver front-end will also be considered. Different filter prototypes will be examined. The system performance of these filter prototypes combined with TDEQ designs will be shown and the best filter types for our system will be chosen based on the simulation results.

4.1 Simulation Parameters

4.1.1 Spectrum, Tone and Cyclic Prefix

In selecting the system parameters, some basic rules should be followed to achieve the best performance. One of them is that the symbol duration should be chosen as long as possible in order to reduce the inter-symbol-interference introduced by the non-ideal channel impulse response. As the ratio of the symbol duration to the channel impulse response duration increases, the level of the inter-symbol-interference decreases. Actually, in high-speed data transmission, this can not be satisfied. A cyclic prefix is then used to

expand the symbol duration. However, the CP is discarded at the receiver, and it is not decoded. Hence, the CP duration must also be selected carefully in order to maintain high transmission efficiency, which has been discussed in chapter 3.

For the downstream, the total usable bandwidth is up to 1104 kHz according to the ADSL DMT standard. In the standard, the ADSL DMT symbol rate, $f_{symb} = 4\text{kHz}$, the carrier separation, $\Delta f = 4.3125\text{kHz}$. Then the information data duration, $T_{data} = 1/\Delta f = 231.9\mu s$. The whole spectrum is divided into 256 subchannels which implies that the size of the FFT/IFFT can be calculated as:

$$\mathrm{N_{FFT}} = 2 \times \mathrm{M} = 512$$

where M is the number of subchannels. The sampling frequency is calculated as:

$$f_{samp} = 2 \times \mathrm{M} \times \Delta f = 2208\ \text{kHz}$$

The Nyquist frequency is half of the sampling frequency, and can be calculated as:

$$f_{Nyquist} = 1104\text{kHz}$$

The last 32 samples from the original data symbol are picked out and repeated as the cyclic prefix. The duration of CP at above sampling frequency is:

$$\mathrm{CP}_{duration} = 32 \times \left(1/f_{samp}\right) = 14.5\,\mu s$$

So, the total transmitted symbol duration is:

$$\text{total symbol duration} = T_{data} + CP_{duration} = 231.9 + 14.5 = 246.4\ \mu\text{s}$$

and the transmission efficiency is:

$$\text{Transmission efficiency} = T_{data} / \left(T_{data} + CP_{duration}\right) = 94.1\%$$

which is a tolerable efficiency with 5.9% transmission efficiency reduction due to CP.

ADSL uses the superframe structure as shown in Figure 4.1. Each superframe is composed of 68 ADSL data frames, which are encoded and modulated into DMT symbols, followed by a synchronization symbol, which carries no data. The application of this

synchronization symbol permits recovery of the frame boundary after micro-interruptions that might otherwise force retraining. With this superframe structure, the actual transmitted symbol rate is:

$$f_{tx} = 69/68 \times f_{symb} = 4.059kHz$$

From the user data perspective, the DMT symbol rate is still 4 kHz. And we have the following relationship:

$$\Delta f = f_{tx} * (2M + CP)/(2M)$$

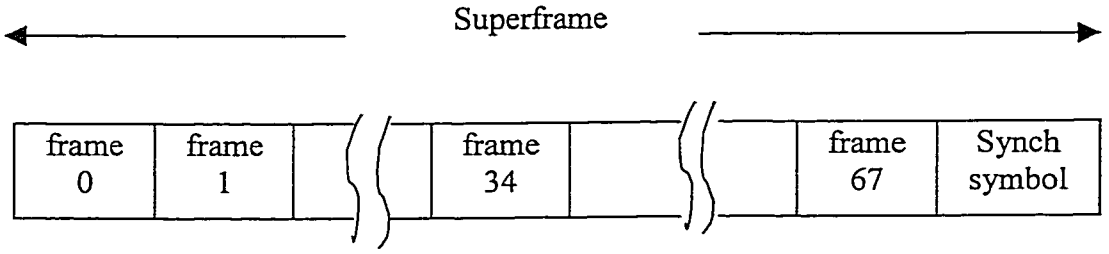

Figure 4.1 ADSL Superframe structure for downstream

The calculation of these parameters for upstream is similar as that of the downstream. We will briefly go through it. For the upstream, the available bandwidth is up to 138 kHz. There are 32 subchannels inside this bandwidth. A FFT/IFFT pair with size 64 is used as the modulator/demodulator. Upstream has the same symbol duration and same subchannel bandwidth as the downstream. The sampling frequency will be $f_{samp} = 2 \times M \times \Delta f = 276\,kHz$ and $f_{Nyquist} = 138kHz$. Upstream and downstream also share the same CP duration. Therefore, there are 4 samples in the CP. The transmission efficiency is also 94.1%.

The power spectral density (PSD) of the transmitted signal is specified in [5]. For downstream (DS), the average PSD within the used passband shall be no greater then –40 dBm/Hz. The passband ripple shall be no greater than +3.5 dB, and the maximum PSD is –36.5 dBm/Hz. For upstream (US), the average PSD within the used passband shall be no

greater than –38 dBm/Hz. The passband ripple shall be no greater then +3.5 dB and the maximum PSD of –34.5 dBm/Hz applies across the whole band. More details of the spectral response for the transmitted signal can be found in [5].

Pilot subcarrier is used in both DS and US for synchronization. The pilot carriers reserved for DS and US are 275 kHz and 69 kHz, respectively.

Above are the standard parameters. At our simulations, we use only half of the total available bandwidth for downstream to meet our project requirements. This spectrum usage is called unlimited-lite. The parameters for US, DS and DS lite are summarized in table 4.1. All the simulation results shown in this chapter are for the downstream with the spectral usage of unlimited-lite.

Table 4.1: Parameters for spectrum usage of DS and US

PARAMETERS	US	DS	DS Lite
Number of carriers (M)	32	256	128
Cyclic prefix (samples)	4	32	16
Sampling Frequency(f_{samp})	276 kHz	2208 kHz	1104 kHz
Carrier Spacing ($\Delta f = f_{samp}/2M$)	4.3125 kHz	4.3125 kHz	4.3125 kHz
Symbol Rate (f_{symbol})	4 kHz	4 kHz	4 kHz
Pilot Tone Frequency	69 kHz	276 kHz	276 kHz
Tx PSD	-38 dBm/Hz	-40 dBm/Hz	-40 dBm/Hz

We select 9kft 26 AWG asynchronous digital subscriber loop (ADSL) as our physical channel model in our simulations throughout this thesis, unless indicated otherwise. The loop coefficients are sampled at a sampling rate of 4.4MHz, which is different than the transmission symbol sampling rate.

4.1.2 System Performance Measures

It is important to choose the proper parameters to evaluate the system performance. In this section, we will define two parameters. One is the shortening signal to noise ratio. The other measure is the maximum achievable bit transmission rate.

Shortening Signal to Noise Ratio (SSNR)

The first question to be answered for the TDEQ design is: how well the TDEQ squeezes the long response of the whole effective channel into exactly the length of the TIR? Generally, the impulse response is not shortened perfectly. Some energy lies outside the largest CP+1 consecutive samples of the shortened channel impulse response. Shortening Signal to Noise Ratio (SSNR) is defined in [47] as the ratio of the energy in the largest consecutive CP+1 samples to the energy in the remaining samples as one of the measures of performance of TDEQ. The values of SSNR present the result of the shortening operation by the TDEQ. Theoretically, the higher the SSNR value, the better the TDEQ design.

Maximum Achievable Bit Rate

The objective of using a TDEQ in DMT system is to transmit information at a high rate. So we also simulate the final transmission bit rate we can achieve by using the

proposed model. The bit allocation is implemented by using the algorithm described in chapter 2. To avoid using a huge QAM constellation, we limit the maximum number of bits assignable to a subchannel to be 15, which is suggested in standard. The bit allocation starts from 2 because this is the smallest QAM constellation.

4.1.3 TIR and TDEQ Length

The selection of the TIR length is quite simple. As we select the DS-Lite as the spectrum usage for our simulation, the TIR length will be chosen as $CP+1=17$ according to Table 4.1. Ideally, the CP should be long enough to eliminate the intersymbol interference and interchannel interference while keeping transmission redundancy at a minimum.

We plotted the variation of the SSNR performance with TDEQ length, N_f, in Figure 4.2 and Figure 4.3. In Figure 4.2, we did not use any filter at the transceiver front-end. In Figure 4.3, we employed a Butterworth filter as the transceiver front-end. Both of the TDEQ designs are under UEC. We examined the TDEQ design with many different delay values, and the two figures shown were generated using the nearly optimum values.

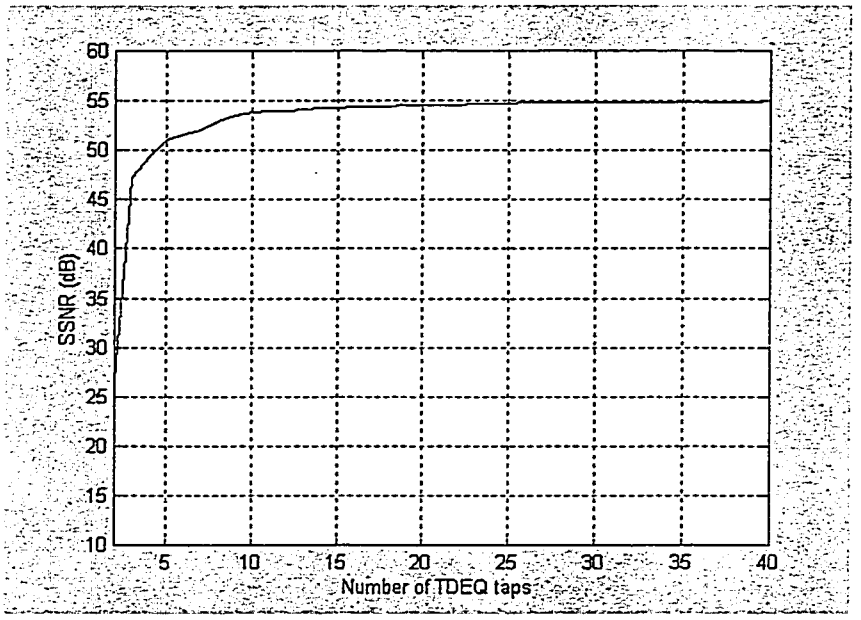

Figure 4.2: Variation of the SSNR performance with TDEQ length using no transceiver front-end

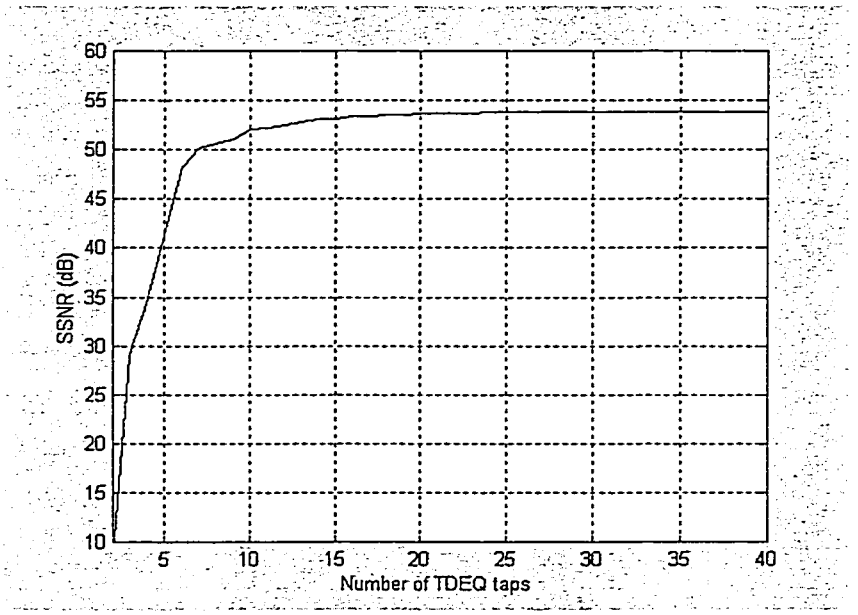

Figure 4.3: Variation of the SSNR performance with TDEQ length using Butterworth filter as the transceiver front-end

We can see that for channels that have a long impulse response (such as the loop considered in this thesis), using a short TDEQ length would lead to a poor performance. Figure 4.2 and Figure 4.3 also show that with an increasing TDEQ length, the SSNR is also increasing until it reaches an almost constant level. Further increases in TDEQ length do

not have any significant improvement on SSNR. We have obtained similar results by investigating the SSNR performance for different transceiver front-ends under both the UEC and the UTC. Therefore, a 10-tap TDEQ structure will be used throughout the simulation for the downstream to achieve a high performance with low complexity. Both of Figure 4.2 and Figure 4.3 show that a TDEQ with 10 taps can shorten the channel

4.1.4 Filter Description

As analyzed in the previous section, the transmission is taking place in two directions along the UTP, the downstream (DS) and upstream (US). Thus interference between DS and US may occur. To eliminate this interference, a complex echo canceller should be used in the system. Generally, this echo canceller is very computationally complex. To avoid increasing the system complexity introduced by this echo canceller, separate bandwidth is assigned to upstream and downstream. Because the upstream and the downstream occupy only their own frequency band, we can assume that there is no interference between them. Therefore, the problem becomes an issue of choosing the proper filters and applying them at the transceiver front-end.

Three analog IIR filters and two linear phase digital FIR filters are selected to be simulated as the transceiver front-end. The analog IIR filters are Butterworth, Chebyshev-I, and elliptic filters. The two digital FIR filters are implemented using Parks-McClellan algorithm (equiripple) and Kaiser window. These filters are built to meet particular system requirements at the transceiver front-end.

To meet the different channel high frequency and low frequency properties, the lowpass and highpass filters are generated separately for the analog IIR filter. Thus the order requirements appear to be asymmetric. The convolution is used to simulate the overall impulse response of the bandpass filter.

We only simulate the downstream at this time. The desired filter has a passband from 100 kHz to 500 kHz. The stopband starts 40 kHz away on either side of the cutoff frequencies. The maximum permissible passband loss is 1 dB and at least 20 dB attenuation is required in the stopband.

To meet the same system filter requirements, different types of filters require different orders. The resulting responses of different filters are different although they are designed to meet the same requirements. The results of filter designs will be shown later in this chapter.

4.2 Performance of the Time Domain Equalizer

In this section, we will compare the system performance in terms of SSNR and transmission bit rate under the UEC and the UTC for the TDEQ design. To concentrate only on the equalizer design, we assume that no transceiver front-end filters are used at this time.

Before comparing the two TDEQ design algorithms, we investigate the effect of using a long CP instead of TDEQ to reduce the distortion caused by the channel. In Figure 4.4, we plotted the system performance with varying the CP length. We can see that the transmission rate increases when CP length increases until it approaches the overall channel impulse response duration. We also see that a relatively long CP has to be used to ensure a high-speed transmission. When a CP with 120 samples is used, we can achieve a high transmission rate with the cost of a significant transmission efficiency reduction by a factor of 31.9%. In reality, the reduction is not acceptable. It is necessary to employ a TDEQ to shorten the channel impulse response so that a relative short CP can successfully reduce the inter-symbol-interference.

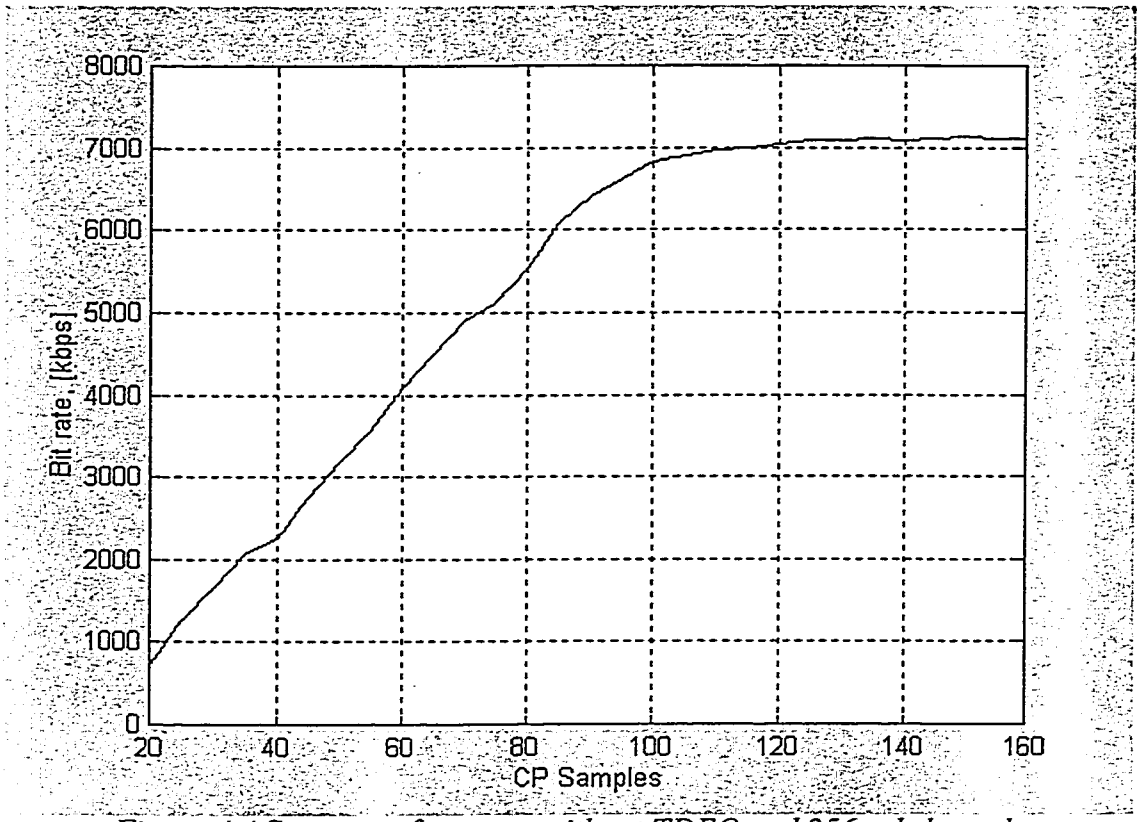

Figure 4.4 System performance without TDEQ and 256 subchannels

In Figure 4.5, we plotted the variation of the SSNR values with delay under both the UEC and the UTC with TIR and TDEQ coefficients calculated as indicated in chapter 3. We also plotted the achievable bit rate performance in Figure 4.6 with different TDEQ designs. In our simulation, we changed the index of the TIR unit element under the UTC to examine its effect on the system performance.

We can see from Figure 4.5 that the effect of the delay on the SSNR is significant under both the UEC and the UTC. An improper delay value selection could result in an enormous performance degradation. However, there is typically a range of delay values for which the SSNR performance is near optimum. Under the UTC, the effect of the selection of the unit element index is not very critical as long as the delay value is inside the near optimum range. The index only slightly changes the SSNR performance. As shown in chapter 3, the SSNR under the UEC is always higher than its value under the UTC no matter what the selection of the unit element index is.

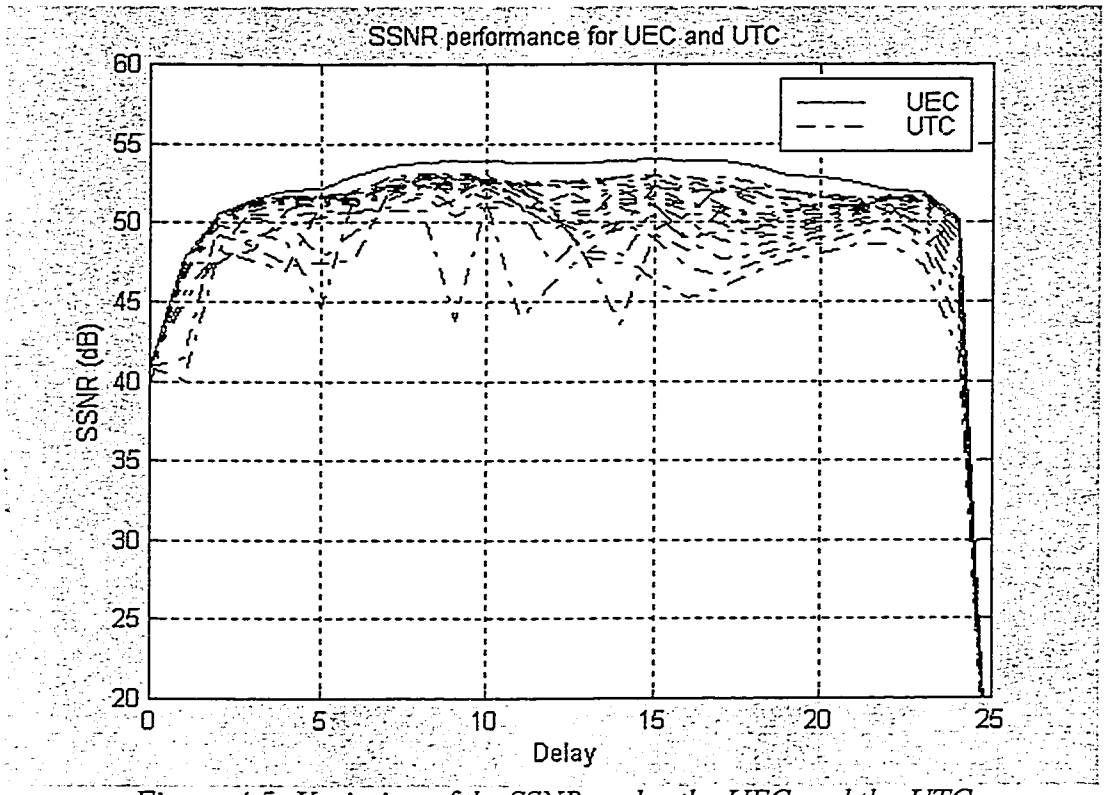

Figure 4.5: Variation of the SSNR under the UEC and the UTC

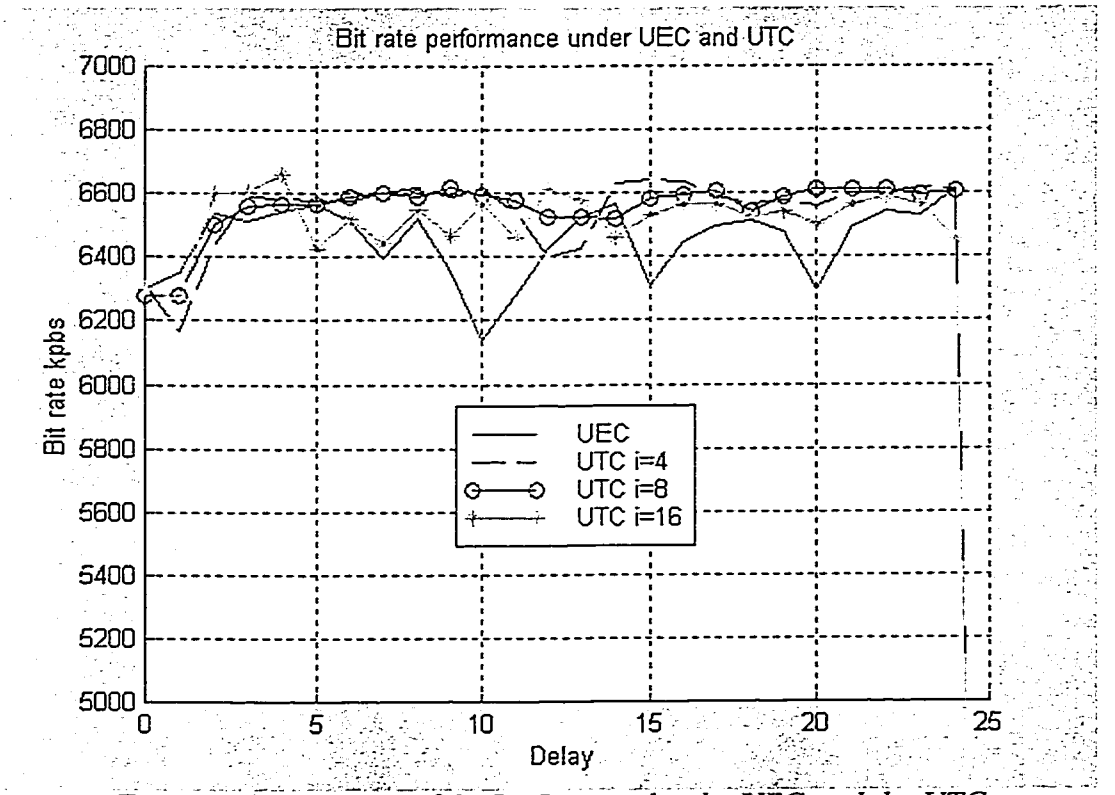

Figure 4.6: Variation of the Bit Rate under the UEC and the UTC

Similar to the case regarding the effect of TDEQ design on SSNR, delay also plays an important role on the achievable bit rate performance. There is a range of delay values inside which the bit rate performance is near optimum. A delay value selection outside this range may result in a significant bit rate degradation. The choice of the index under the UTC is not very important inside the range either. However, the achievable bit rate under the UEC is not always better than its value under the UTC which is different than the case of SSNR. We only plotted index value of 4, 8 and 16 in Figure 4.6 and that is sufficient to show the conclusion. We also can see that the difference between the two constraints is not very big in the achievable bit rate. Thus either of the constraints can be used.

Generally, we can achieve a high transmission rate when the SSNR value is high for a particular delay value. As shown in Figure 4.5, 4.6 and Table 4.2, 4.3, the near-optimum delay values for the SSNR and the bit rate are around the same range. However, a higher SSNR value does not guarantee a higher transmission rate. As mentioned above, the SSNR value under the UEC is always higher than its value under UTC but the bit rate under UEC is not always higher than its value under UTC for the entire range of delay values.

Table 4.2: Best SSNR and corresponding delay value under both constraints

Constraint		Best SSNR (dB)	Best delay (samples)
UEC		53.98	15
UTC With Index (i)	i=0	53.09	9
	i=1	53.04	8
	i=2	52.92	8
	i=3	52.83	8
	i=4	52.94	15
	i=5	52.93	14
	i=6	52.87	14
	i=7	52.72	10
	i=8	52.71	9
	i=9	52.71	8
	i=10	52.50	10
	i=11	52.51	10
	i=12	52.54	10
	i=13	52.32	7
	i=14	52.10	10
	i=15	51.71	8
	i=16	51.36	10

Table 4.3: Best achievable bit rate and corresponding delay value under both constraints

Constraint		Best bit rate (kbps)	Best delay (samples)
UEC		6612	24
UTC With Index (i)	i=4	6640	15
	i=8	6616	9
	i=16	6660	4

4.3 Performance of Different Transceiver Front-end Filters

4.3.1 Comparison of Different Filters

The filters at the transceiver front-end are designed to meet the same system requirement as described in section 5.1.2, but the actual responses are different according to different filter prototypes. We will show the actual responses of different filter prototypes in this section in both time domain and frequency domain. We will also compare the complexity to implement each filter prototype.

As shown in Figure 4.7 to 4.11, each of the five filter types has its own response to achieve the same filtering requirement. We summarized the orders requirement of different filters to satisfy the system requirement in table 4.4. It is obvious that there is great difference of the complexity for realizing different filters.

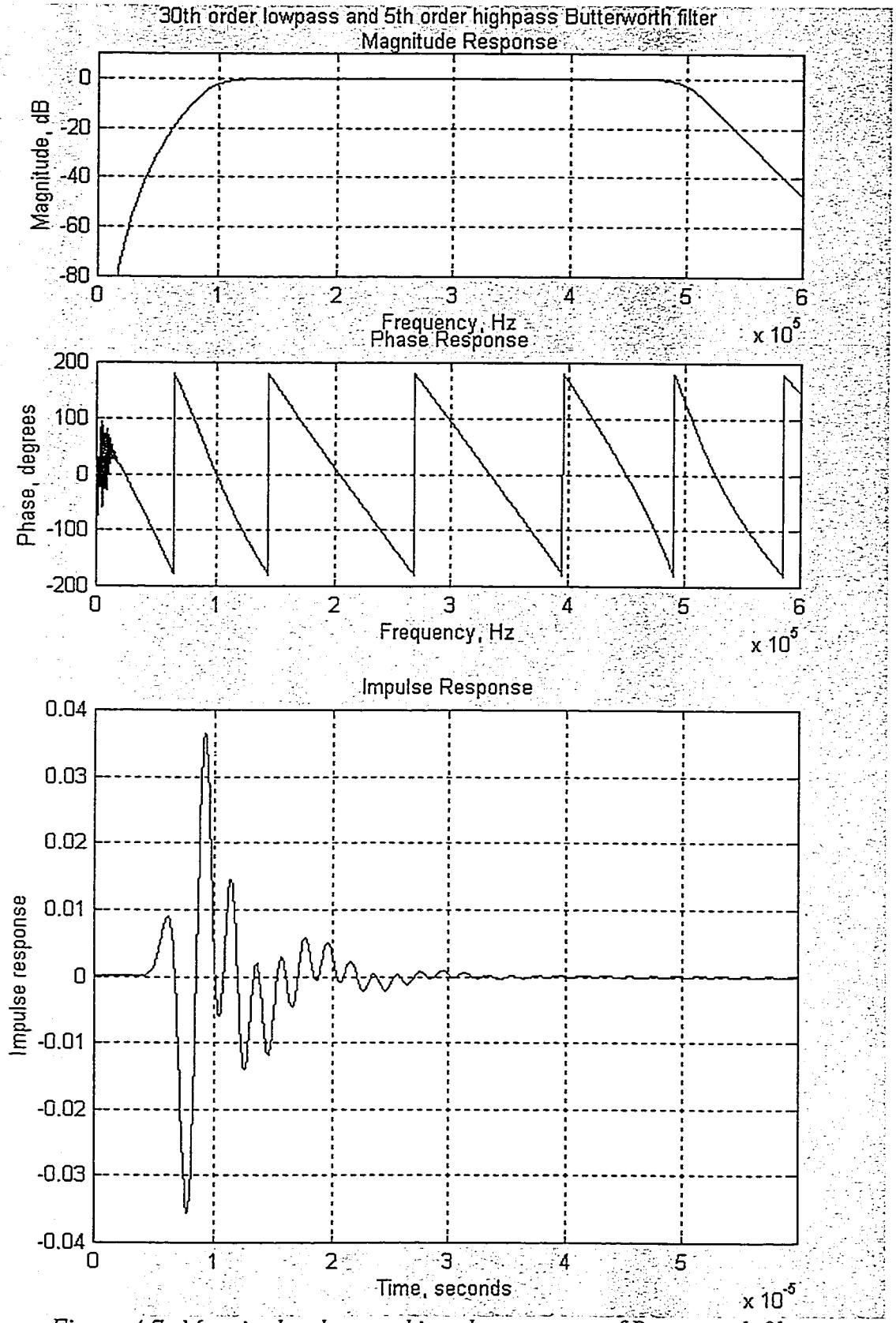

Figure 4.7: Magnitude, phase and impulse response of Butterworth filter

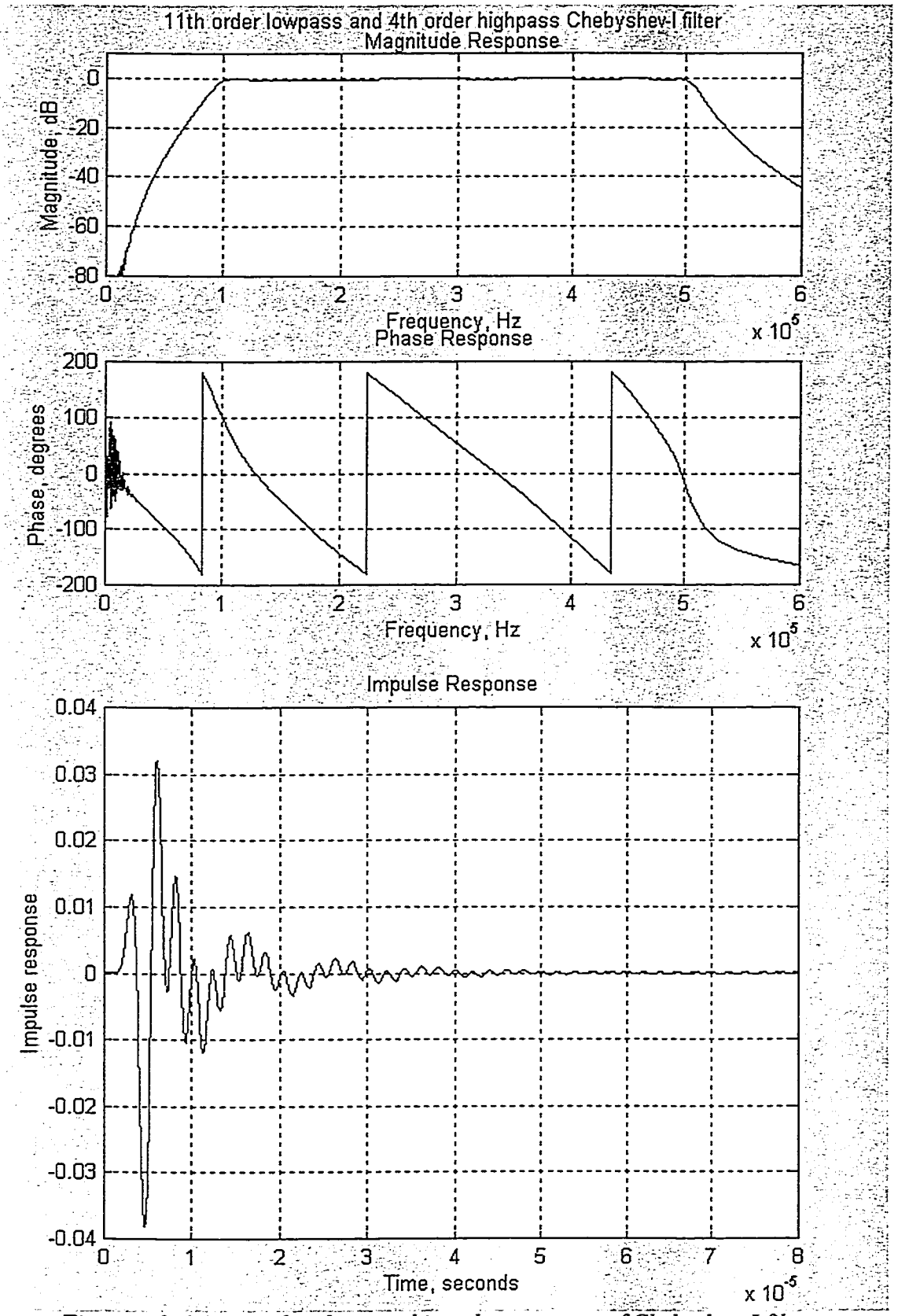

Figure 4.8: Magnitude, phase and impulse response of Chebyshev-I filter

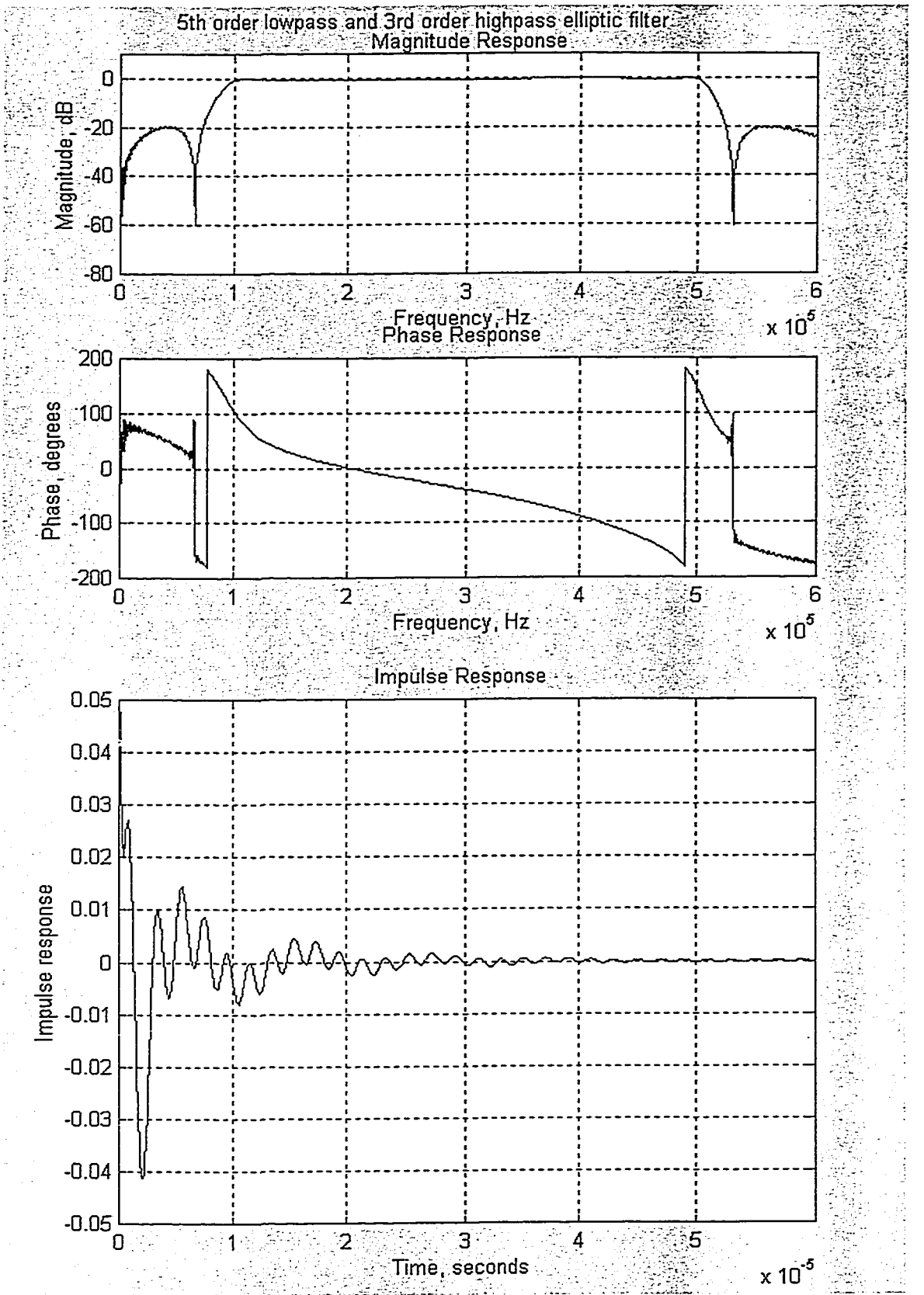

Figure 4.9: Magnitude, phase and impulse response of elliptic filter

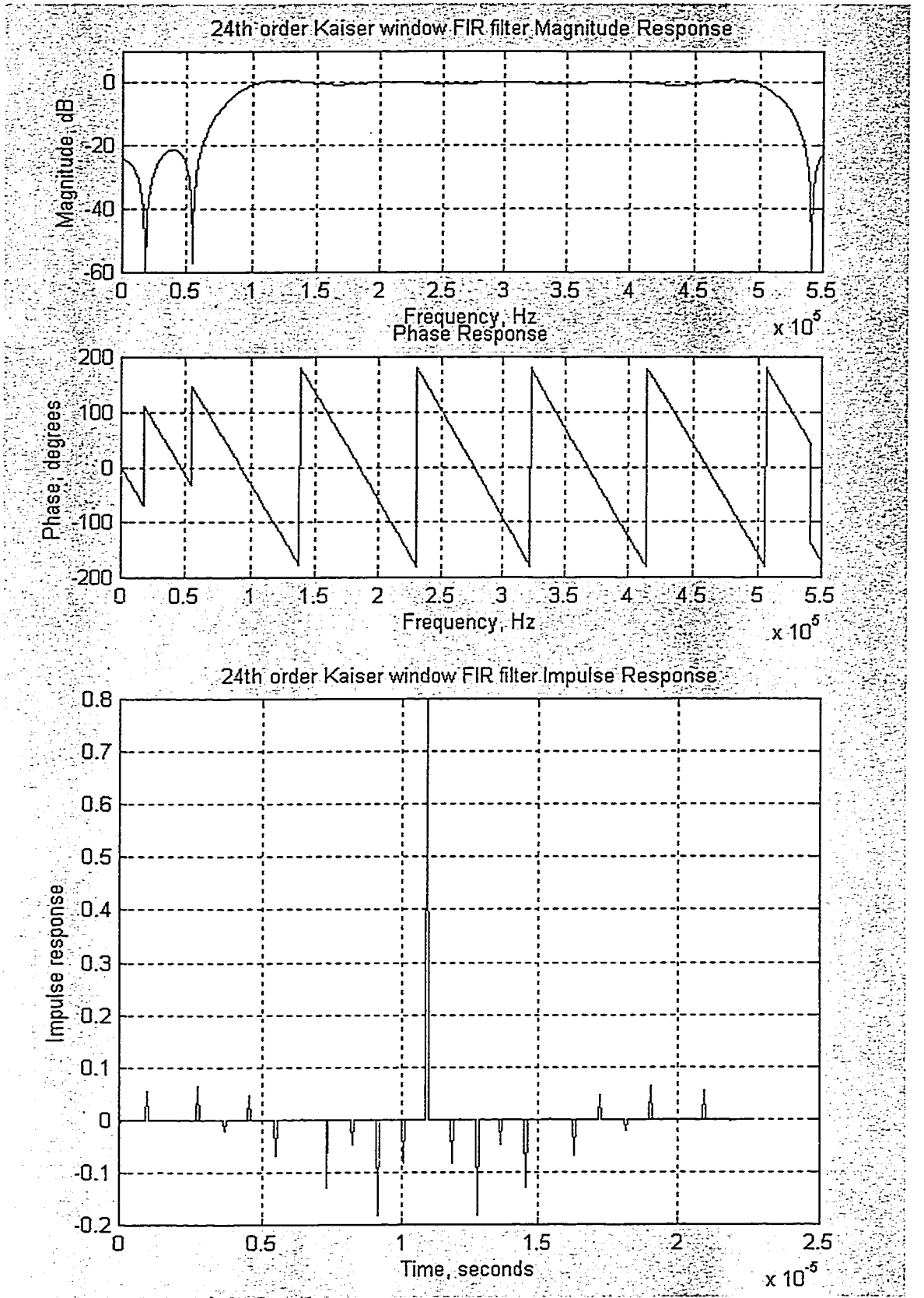

Figure 4.10: Magnitude, phase and impulse response of Kaiser window filter

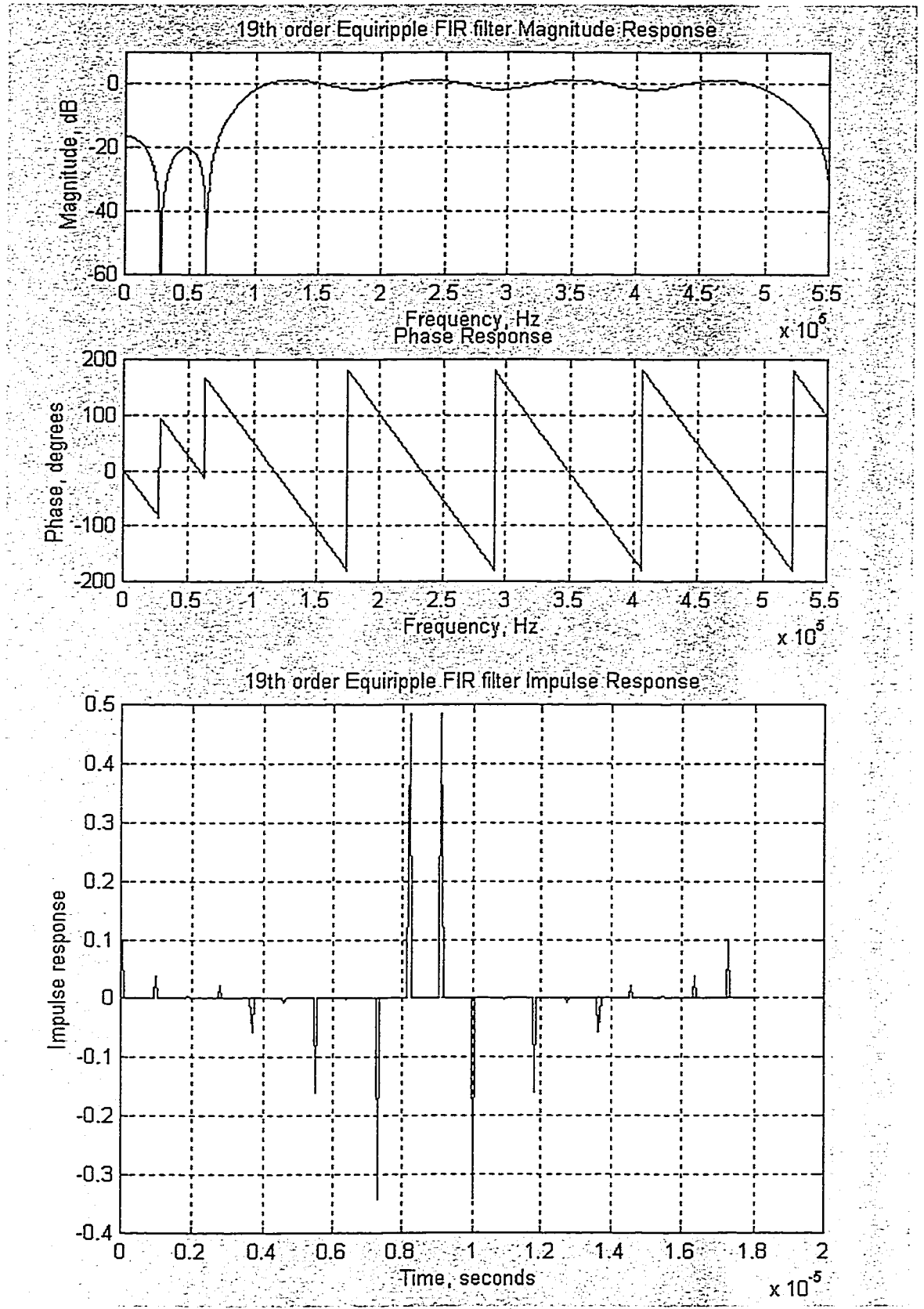

Figure 4.11: Magnitude, phase and impulse response of Equiripple filter

The magnitude response of the Butterworth filter is maximally flat over in the passband and monotonic over the transmit and stop band. But Butterworth filter sacrifices its rolloff steepness for this monotonic passband behavior. Therefore, in order to meet the same transition bandwidth, the Butterworth filter needs higher filter order than Chebyshev or elliptic filters. In case the smoothness is not required, other filters can be used to avoid increasing the complexity [42].

Chebyshev type I filter minimizes the absolute difference between the ideal and actual frequency response over the entire passband by incorporating an equiripple in the passband. Its stopband response is maximally flat. The transition from passband to stopband of Chebyshev-I filter is faster than that of the Butterworth filter. As shown in Table 4.4, the Butterworth filter requires much high orders.

Elliptic filter offers steeper rolloff characteristics than Butterworth or Chebyshev filter in the cost of equiripple in both the passband and stopband as shown in Figure 4.9. Generally, elliptic filter meets given performance specifications with a lower order than other filter types.

Table 4.4: Filter orders for different filter prototypes

Filter type	Filter order	
	Low pass filter	High pass filter
Butterworth	30	5
Chebyshev-I	11	4
Elliptic	5	3
Kaiser window	24	
Equiripple	19	

The two bandpass digital FIR filters are directly generated by the signal processing tool box of MATLAB®. Both of them have linear-phase. The equiripple filter minimizes the maximum error between the desired frequency response and the actual frequency response and exhibits an equiripple behavior in the frequency response.

So far, we generated the transceiver front-end based on different filter prototypes, and we compared their design complexity in terms of the required filter orders to satisfy the same filtering requirements. We only considered the filter itself and did not apply it to the system. We will show the effects of the filter design on the system in the following sections.

4.3.2 System Performance

We performed computer simulations to examine the effects of different filter types in the system combining with TDEQ design. The results are summarized in the following plots and tables.

Table 4.5: System SSNR performance with different filter prototypes

	SSNR (dB)	
FILTERS	**UEC**	**UTC**
Butterworth	53.66	53.20
Chebyshev-I	41.08	40.22
Elliptic	53.70	52.45
Equiripple	21.22	21.08
Kaiser	26.11	25.18

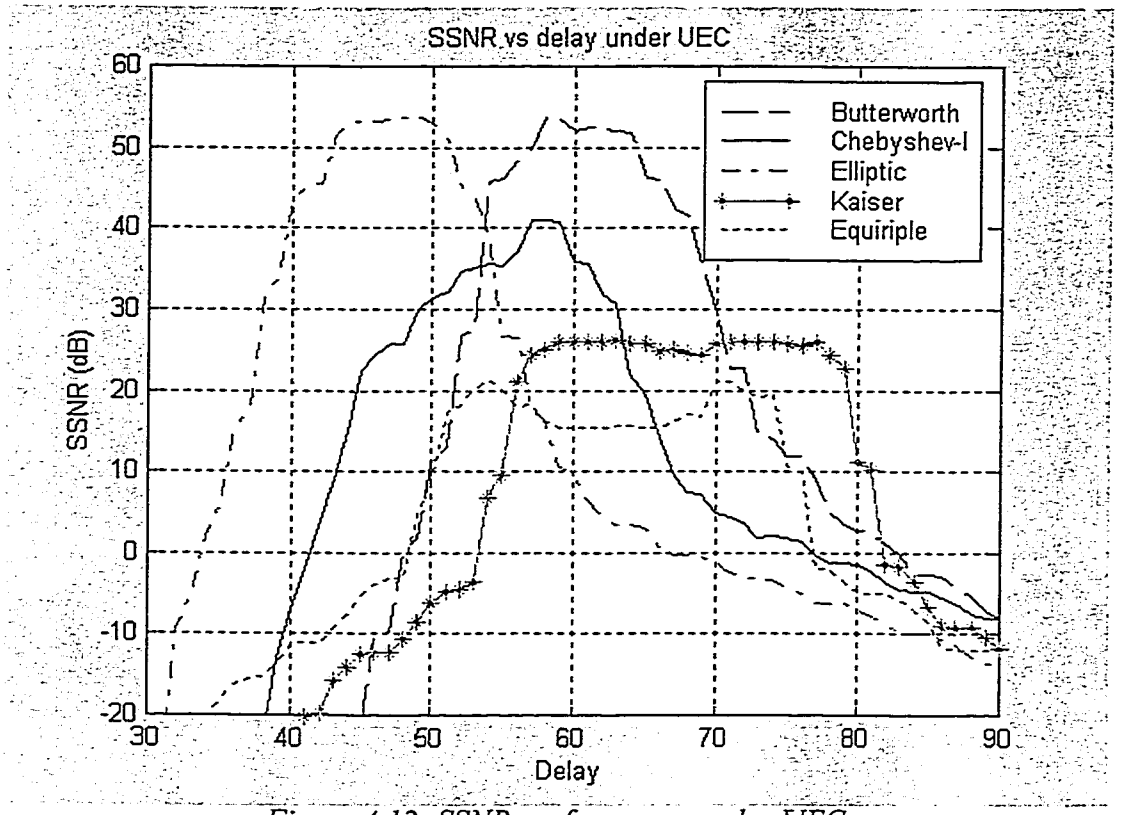

Figure 4.12: SSNR performance under UEC

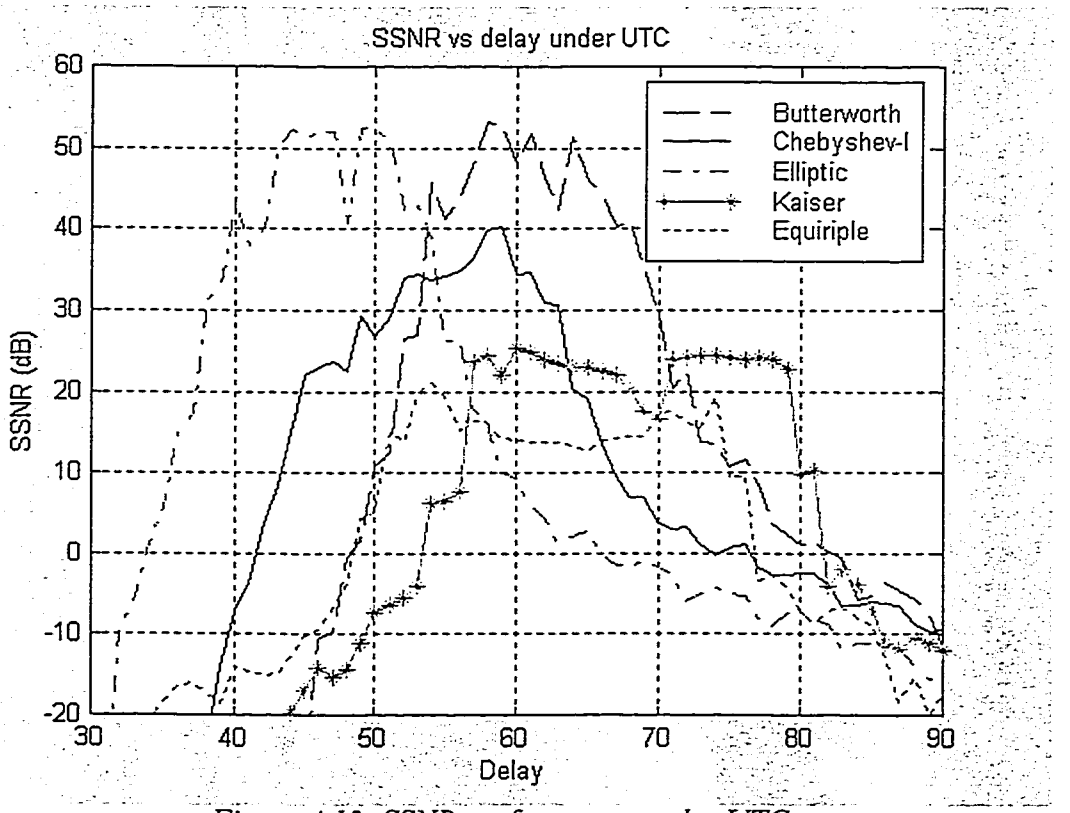

Figure 4.13: SSNR performance under UTC

Table 4.6: System bit rate performance with different filter prototypes

	Bit rate (kbps)	
FILTERS	**UEC**	**UTC**
Butterworth	5340	5416
Chebyshev-I	4468	4236
Elliptic	5408	5372
Equiripple	2396	2488
Kaiser	3208	3064

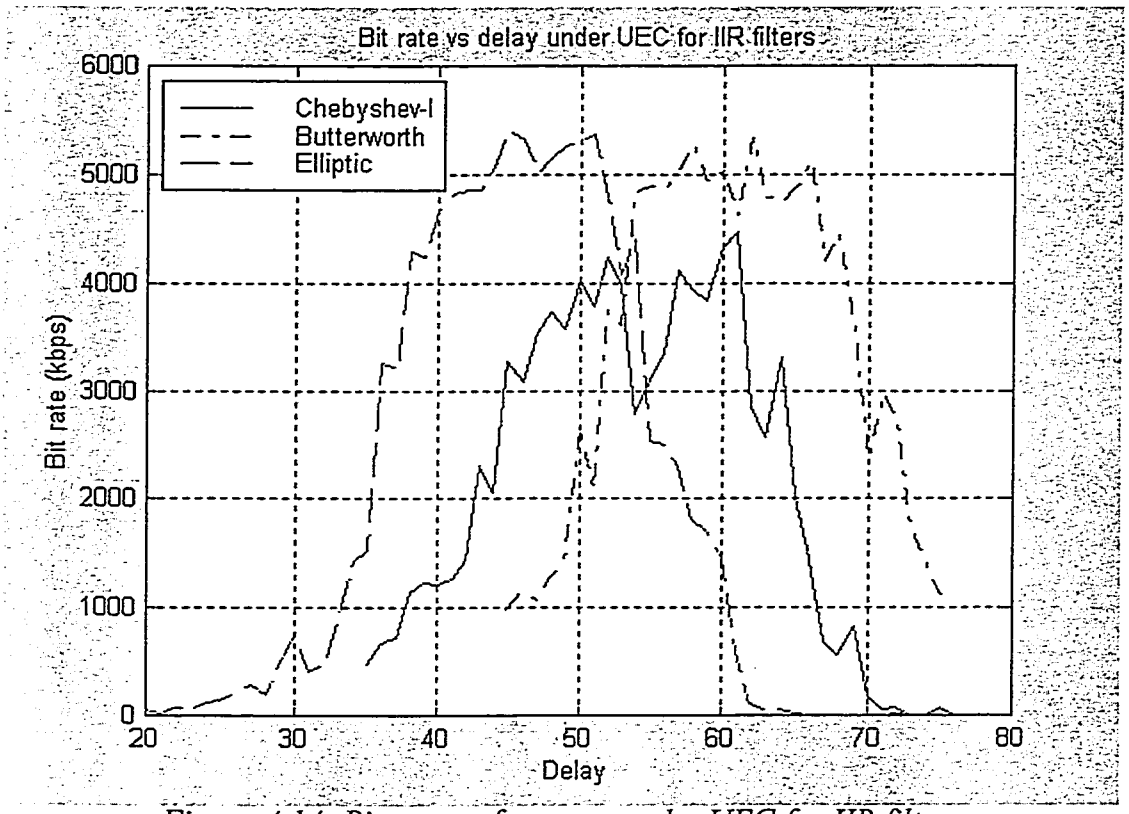

Figure 4.14: Bit rate performance under UEC for IIR filters

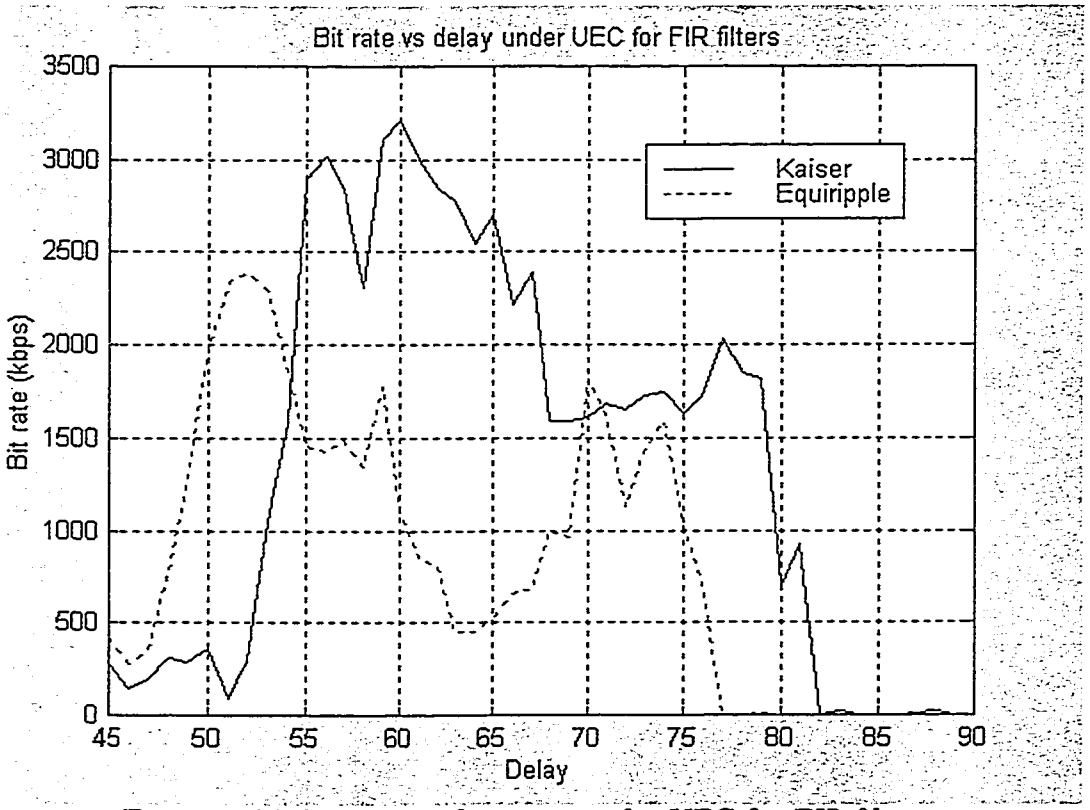

Figure 4.15: Bit rate performance under UEC for FIR filters

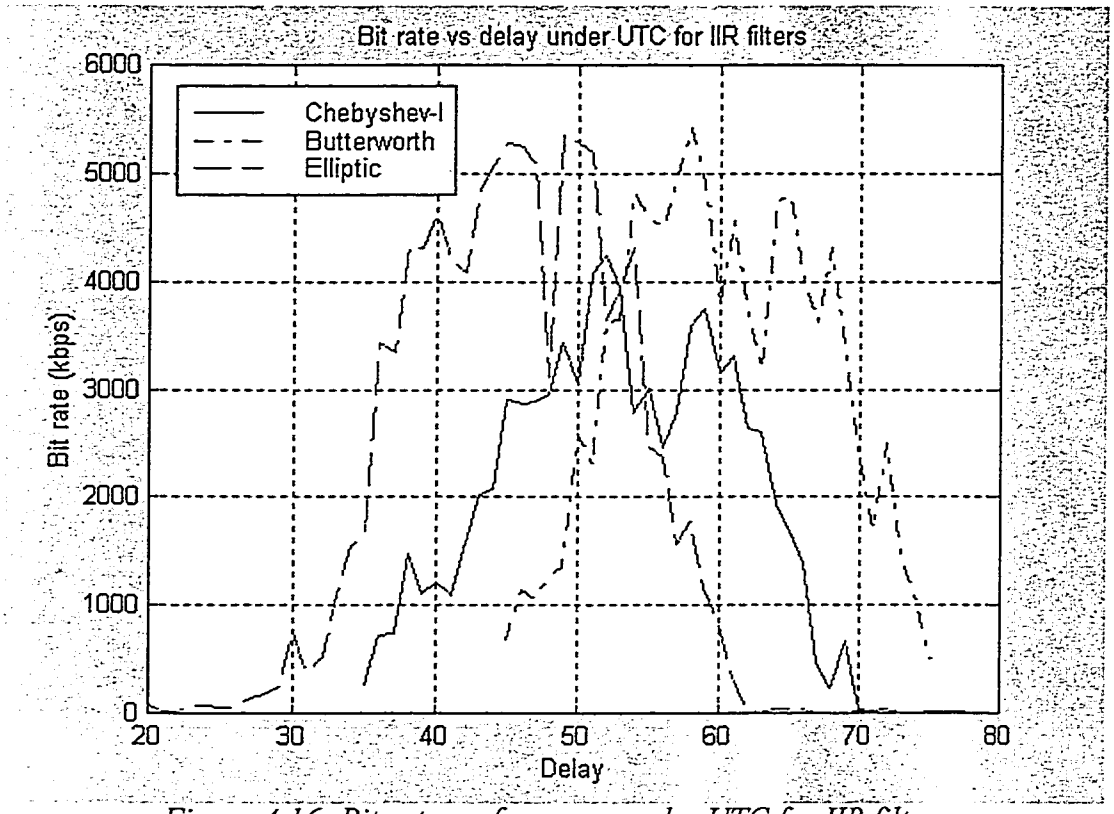

Figure 4.16: Bit rate performance under UTC for IIR filters

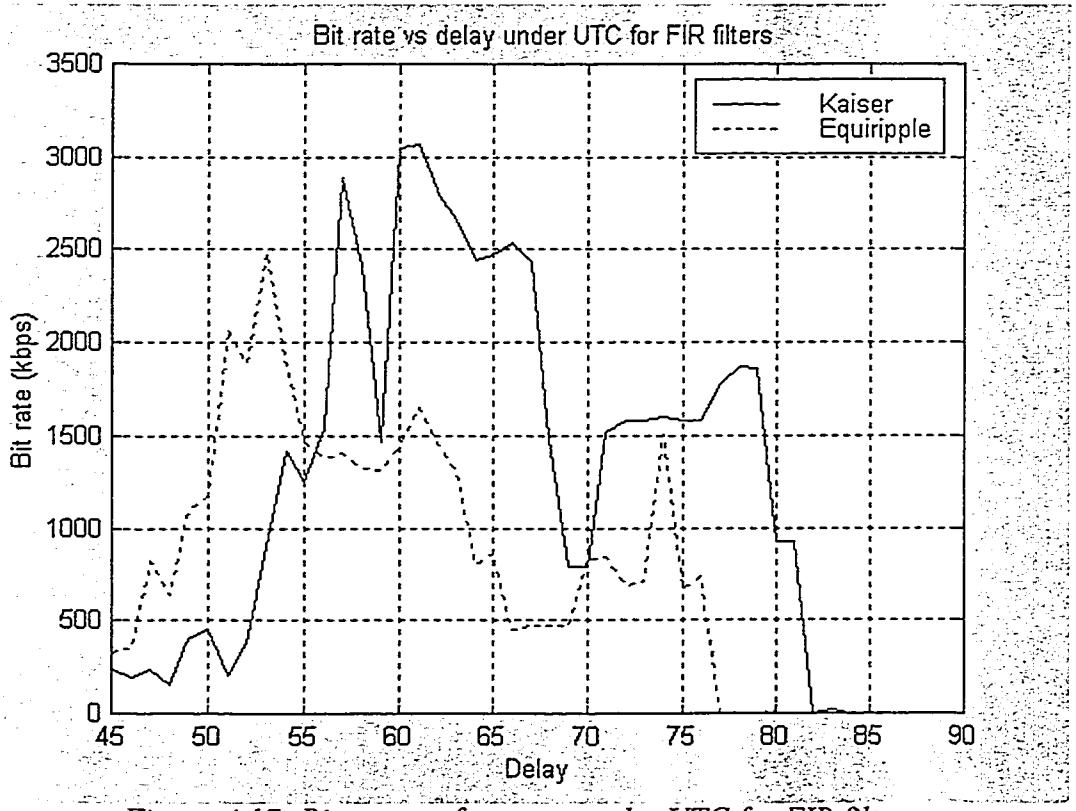

Figure 4.17: Bit rate performance under UTC for FIR filters

As expected, the effects of the filters are different according to their characteristics. Generally, the longer the impulse response of the filter, the worse is the performance. This is because with a longer impulse response of the filter, it is harder for the TDEQ to squeeze the overall channel impulse response within the length of CP.

From the previous section, we can see that the Chebyshev-I filter has the longest impulse response compared to Butterworth and elliptic filters. It can be found in Table 4.5, 4.6 and Figure 4.12, 4.13, 4.14, 4.16 that the system has the worst performance in terms of both SSNR and bit rate with the Chebyshev-I filter as the transceiver front-end. Butterworth and elliptic filters have similar performance. From the performance point of view, either Butterworth or elliptic filter can be chosen as the transceiver front-end that achieves a high performance.

The simulation results show that a high bit rate can be achieved with a TDEQ design and a proper filter selection. Bit rates over 5Mbps can be used for the data transmission with the Butterworth or elliptic filter as the transceiver front-end.

Same as in the cases with no front-end filters employed, the delay value for the TDEQ design can be selected from a range of values that all result in near-optimum performance. There are not many differences between the performance of the two TDEQ design algorithms.

The performance of the two digital FIR filters is much lower than that of the analog IIR filters as shown in Table 4.5, 4.6 and Figure 4.12 to 4.17. The analog filter implementation requires less memory and has lower computational complexity. Since there are no performance advantages of FIR over IIR, we can say that an IIR filter is preferable for our system.

4.4 Conclusions

In this chapter, we presented the computer simulation results of the system performance. The TDEQ design and the effects of transceiver front-end filters have been investigated. System performance has been analyzed in terms of the SSNR and the achievable bit rate. The observations can be summarized as follows.

TDEQ design

Two practical realizable constraints, which are UEC and UTC, for the MMSE-TDEQ design are considered in our simulations. There is a very important parameter for TDEQ design under both UEC and UTC, which is defined as the relative delay between TIR and the shortened channel resulted by TDEQ as described in Chapter 3. A proper delay value is very important for the TDEQ design to achieve a high system performance. An inappropriate delay value selection may result in a significant performance degradation as shown in Figure 4.5, Figure 4.6 and Figure 4.12 to Figure 4.17. Fortunately, the proper delay value is not a unique value. There is a range from which we can select the delay values for the TDEQ design which all result in a near-optimum performance. This is also shown in the figures listed above.

For SSNR performance, the TDEQ design under the UEC always gives better result than the design under the UTC for the same TDEQ length, TIR length and delay value. This has also been shown in the literature [34]. However, this conclusion is not always true for the system achievable bit rate. In Figure 4.6, we can see that for some of the delay values, the achievable bit rates using UTC-TDEQ design are better than those values using UEC-TDEQ design. However, the difference is very small compared with the achievable bit rate. We can make the conclusion that either UEC or UTC can be employ for our TDEQ design in order to achieve a high system performance.

An extra parameter is used only for UTC-TDEQ design, which is the index of the unit element in the TIR. In Figure 4.5 and Figure 4.6, it is shown that the effects of the index selection is not very critical for the UTC-TDEQ design as long as the delay value is inside its near optimum range.

Transceiver front-end

Several filter prototypes as the transceiver front-end have been tested in our simulations. There is a great difference among different filter types in terms of the system performance and the filter complexity to satisfy the system requirements.

Butterworth sacrifices the steepness of its transition band for the flat passband behavior. For the same filter order, the transition band of Butterworth filter is wider than the transition band of Chebyshev-I or elliptic filter. Therefore, the complexity of the Butterworth filter is higher to satisfy the same filter requirement compared with the other two analog IIR filters. This is clearly shown in Figure 4.7, 4.8, 4.9 and in Table 4.4.

From the system performance point of view, using either Butterworth or elliptic filter results in high transmission rate, which is over 5 Mbps, and both are higher than using Chebyshev-I filter as the transceiver front-end. Thus either Butterworth or elliptic filter can be selected to achieve a high transmission rate.

The two digital FIR filter design algorithms are examined in Figure 4.15, Figure 4.17 and Table 4.6 for their bit rate performance. The system achievable bit rates are much lower compared with using the analog IIR filters as the transceiver front-end. Since the analog filter also has the implementational advantage that it requires less memory and lower computational complexity, we can conclude that the analog IIR filters are more suitable for our system than the digital FIR filters.

Chapter 5

Interference of the DMT System

If the shortened overall channel impulse response is not limited inside the length of the CP, which is the situation in most of the practical systems, the interference between symbols and different carriers occurs. In this chapter, we will first analyze the interference caused by the non-ideal overall impulse response of the channel for the DMT system, and then examine the effects of the interference on the system performance in terms of the achievable bit rate. The interference introduced by improper frequency domain equalizer design is also analyzed in this chapter.

5.1 Introduction

The ADSL channel is far from an ideal channel which has a constant amplitude response over the entire bandwidth and the phase response is a linear function of the frequency [43]. An ADSL channel distorts the transmitted signal in amplitude and phase. As a result of these distortions caused by the nonideal channel frequency response, a succession of pulses transmitted through the channel at rates comparable to the limited channel bandwidth are smeared to the point that they are no longer distinguishable as well-defined pulses at the receiving terminal. Instead, they overlap and thus, intersymbol interference occurs.

Multitone modulation can be used to transmit reliably the highest possible data rates over channels with intersymbol interference. As mentioned in the previous chapters, the cyclic prefix is employed to preserve the orthogonality between the carriers. If the length of the cyclic prefix is equal or longer than the largest delay of the channel, the orthogonality will be ensured. In this case, the intersymbol interference and interchannel interference are eliminated [46].

However, in most of the ADSL transmission cases, the channel impulse response is longer than the cyclic prefix. Thus, the interference arises. The signal presenting in the current DMT symbol from previous DMT symbols cause the intersymbol interference (ISI). The insufficient length of the cyclic prefix can not ensure the orthogonality of the subcarriers anymore. Therefore, the inter-channel-interference (ICI) occurs. And as a combination, the transmission also suffers from inter-symbol-inter-channel (ISCI).

The effects of the interference are discussed in literature [44] [45]. In this chapter, we will analyze its effects on the data transmission rate combining with TDEQ design.

5.2 Interference between Subchannels

A simplified DMT model is shown in Figure 5.1. The difference between this system and the block diagram we showed in Figure 2.3 is that we add a frequency domain equalizer (FDEQ) after the demodulator. This FDEQ consists of N_{FFT} complex 1-tap filters. Then, each output sample of the FFT is multiplied by a complex coefficient [50]. We assume that the equalized overall channel impulse response is g^n. Then, the tap settings for the FDEQ, w_{FDEQ}, can be expressed as [49]:

$$w_{FDEQ}^n = (G^n)^{-1} \quad n = 0, 1, \cdots, N_{FFT} - 1 \tag{5-1}$$

where G^n is the FFT of g^n and can be expressed as:

$$G^n = \sum_{k=0}^{N_{FFT}-1} g^n e^{-j2\pi kn/N_{FFT}} \qquad n = 0, 1, \cdots, N_{FFT}-1 \qquad (5\text{-}2)$$

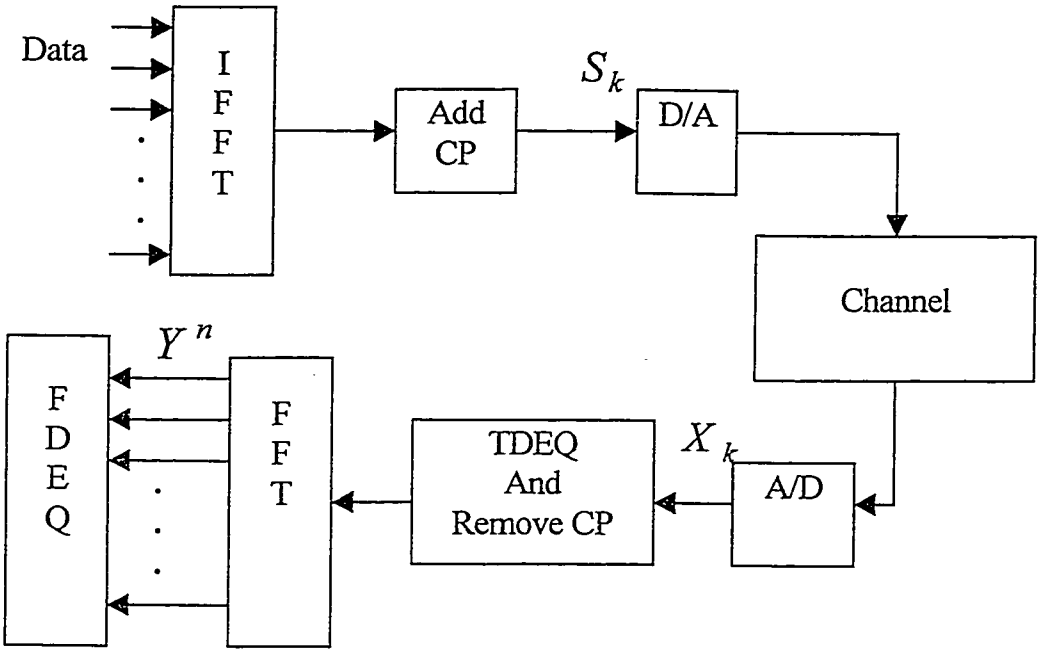

Figure 5.1. Simplified DMT system model

We will calculate the interference level analytically on a subchannel-by-subchannel basis in this section, and then we will examine the effects of the interference on the bit allocation in the following sections.

For convenience, we re-write the expression of the modulated real-valued symbol sequence as given in Chapter 2 at the transmitter as:

$$\tilde{x}_k = \frac{1}{N_{FFT}} \sum_{i=0}^{N_{FFT}-1} C^i e^{j2\pi ik/N_{FFT}}, \quad k = 0, 1, \cdots, N_{FFT}\text{-}1 \qquad (5\text{-}3)$$

After added CP, this symbol sequence is passed through the D/A and transmitted into the channel. There are $N_{FFT}/2$ subchannels in this DMT system. We select the ith tone as

the probe tone and only transmit data on this particular subchannel. Then the energy we received on the other tones will be the interference contributed by tone *l*. With no transmission on the other tones, the cyclically prefixed transmitted symbol sequence of transmission only on *l*th subchannel can be expressed in time domain as:

$$S_k = \frac{1}{N_{FFT}}(C^l e^{j2\pi kl/N_{FFT}} + C^{l*} e^{-j2\pi kl/N_{FFT}})U_k, k = -CP, -CP+1, \cdots, N_{FFT}-1 \quad (5\text{-}4)$$

where C^l is the information symbol transmitted on the *l*th subchannel which presents the system bit assigned to this subchannel, the second part at the right hand side of the equation is the Hermitian symmetric part of the symbol transmitted on the *l*th subchannel which is employed to ensure the real-valued time sample series and is generated as described in chapter 3. U_k is a unity gain window function as shown in Figure 5.2 which confines the transmitted signal in the time interval form –CP to $N_{FFT}-1$. The cyclic prefix is already added to the original signal as described in section Chapter 3.

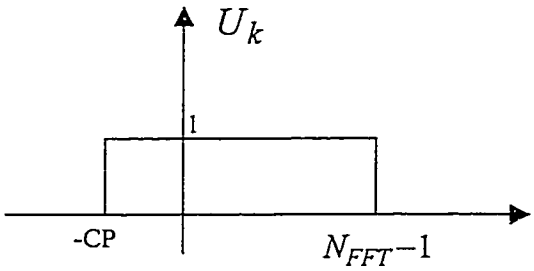

Figure 5.2 Rectangular function

We assuming that the channel has an overall impulse response g_k, which includes the transmitter filter, the physical channel, the receiver filter, and the time domain equalizer. The transmitted signal goes through this channel and the input to the demodulator is:

$$\begin{aligned} R_k &= S_k \otimes g_k \\ &= \frac{1}{N_{FFT}} \sum_{m=-CP}^{N_{FFT}-1} g_{k-m}(C^l e^{j2\pi ml/N_{FFT}} + C^{l*} e^{-j2\pi ml/N_{FFT}}) \end{aligned} \quad (5\text{-}5)$$

The demodulated symbol on the *l*th tone can be expressed as:

$$Y^l = \sum_{k=n1}^{n2} R_k e^{-j2\pi lk / N_{FFT}} \tag{5-6}$$

where the range defined by *n1* and *n2* is the desired time interval for difference symbol analysis.

It is assumed that the transmitted symbol is delayed, Δ, by the channel with a linear phase. This delay value is introduced by the TDEQ design as described in Chapter 3. The time intervals of the transmitted symbol and the received symbols are illustrated in Figure 5.3.

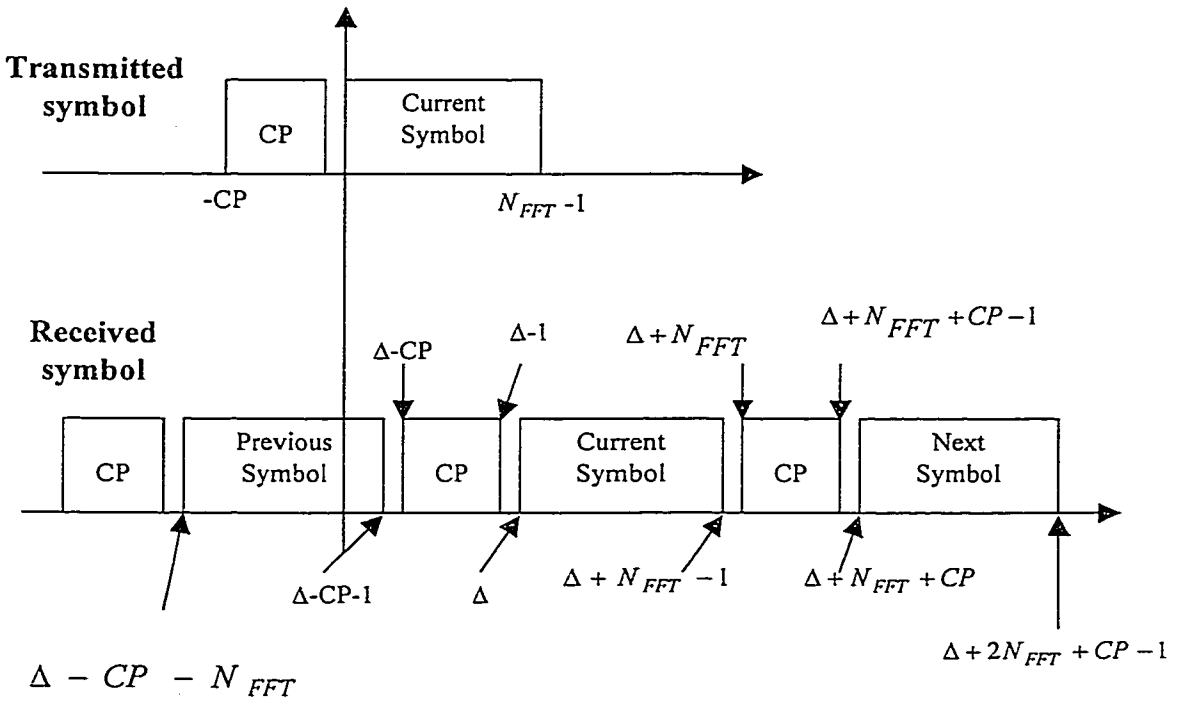

Figure 5.3 Symbol Interval Description

According to Figure 5.3, the desired signal at the output of the lth subchannel after the demodulation is:

$$\begin{aligned} Y_{SIG}^{l} &= \frac{1}{N_{FFT}} \sum_{k=\Delta}^{\Delta+N_{FFT}-1} \sum_{m=-CP}^{N_{FFT}-1} g_{k-m} C^{l} e^{j2\pi ml/N_{FFT}} e^{-j2\pi dk/N_{FFT}} \\ &= \frac{1}{N_{FFT}} C^{l} \sum_{k=\Delta}^{\Delta+N_{FFT}-1} \sum_{m=-CP}^{N_{FFT}-1} g_{k-m} e^{-j2\pi d(k-m)/N_{FFT}} \end{aligned} \tag{5-7}$$

The interference contribution to the lth channel which is caused by sending the Hermitian symmetric symbol can be written as:

$$\begin{aligned} Y_{SYM}^{l} &= \frac{1}{N_{FFT}} \sum_{k=\Delta}^{\Delta+N_{FFT}-1} \sum_{m=-CP}^{N_{FFT}-1} g_{k-m} C^{l*} e^{-j2\pi ml/N_{FFT}} e^{-j2\pi dk/N_{FFT}} \\ &= \frac{1}{N_{FFT}} C^{l*} \sum_{k=\Delta}^{\Delta+N_{FFT}-1} \sum_{m=-CP}^{N_{FFT}-1} g_{k-m} e^{-j2\pi d(m+k)/N_{FFT}} \end{aligned} \tag{5-8}$$

In case the channel impulse response is perfectly confined within the CP, we can simplify expression (5-8) as:

$$Y_{SYM}^{l} = \frac{C^{l*}}{N_{FFT}} \sum_{k=\Delta}^{\Delta+N_{FFT}-1} \left[\sum_{i=-\infty}^{\infty} g_i e^{-j2\pi il/N_{FFT}} \right] e^{-j2\pi dk/N_{FFT}} \tag{5-9}$$

Apparently, the inner summation is the FFT of the channel impulse response at the center frequency of lth tone and is independent of k. Since the outer summation is operated over a whole period of the exp(·) function, the value of (5-9) is zero. Then, we find that the Hermitian symmetric symbol has zero contribution to the desired symbol if the channel impulse response is equal or less than the length of CP.

The ISI is caused by the information symbol in the same subchannel at the different symbol interval. We assume that the interference from current symbol only extends to its

adjacent symbols because the impulse response of the channel is not very long, and we consider the previous and the next symbol separately. Therefore, the two terms of ISI can be written as:

$$Y^{l}_{ISI\_pre} = \frac{1}{N_{FFT}} \sum_{k=\Delta-CP-N_{FFT}}^{\Delta-CP-1} \sum_{m=-CP}^{N_{FFT}-1} g_{k-m}(C^{l} e^{j2\pi ml/N_{FFT}} + C^{l*} e^{-j2\pi ml/N_{FFT}}) e^{-j2\pi dk/N_{FFT}} \tag{5-10}$$

$$Y^{l}_{ISI\_next} = \frac{1}{N_{FFT}} \sum_{k=\Delta+CP+N_{FFT}}^{\Delta+2N_{FFT}+CP-1} \sum_{m=-CP}^{N_{FFT}-1} g_{k-m}(C^{l} e^{j2\pi ml/N_{FFT}} + C^{l*} e^{-j2\pi ml/N_{FFT}}) e^{-j2\pi dk/N_{FFT}} \tag{5-11}$$

The Inter-Channel-Interference (ICI) is caused by the information symbols in the other subchannels at the same symbol period. The output at the nth subchannel of the demodulator, where $n \neq l$, can be written as:

$$Y^{n}_{ICI} = \frac{1}{N_{FFT}} \sum_{k=\Delta}^{\Delta+N_{FFT}-1} \sum_{m=-CP}^{N_{FFT}-1} g_{k-m}(C^{l} e^{j2\pi ml/N_{FFT}} + C^{l*} e^{-j2\pi ml/N_{FFT}}) e^{-j2\pi nk/N_{FFT}} \tag{5-12}$$

The Inter-Symbol-Inter-Channel-Interference (ISCI) is caused by the information symbol in the other subchannel at different symbol interval. It also contains previous and next terms as ISI. At nth subchannel where $n \neq l$, the outputs can be written as:

$$Y^{n}_{ISCI\_pre} = \frac{1}{N_{FFT}} \sum_{k=\Delta-CP-N_{FFT}}^{\Delta-CP-1} \sum_{m=-CP}^{N_{FFT}-1} g_{k-m}(C^{l} e^{j2\pi ml/N_{FFT}} + C^{l*} e^{-j2\pi ml/N_{FFT}}) e^{-j2\pi nk/N_{FFT}} \tag{5-13}$$

$$Y^{n}_{ISCI\_next} = \frac{1}{N_{FFT}} \sum_{k=\Delta+CP+N_{FFT}}^{\Delta+2N_{FFT}+CP-1} \sum_{m=-CP}^{N_{FFT}-1} g_{k-m}(C^{l} e^{j2\pi ml/N_{FFT}} + C^{l*} e^{-j2\pi ml/N_{FFT}}) e^{-j2\pi nk/N_{FFT}} \tag{5-14}$$

Similar as the deduction for the Hermitian symmetric symbol, we can prove that in ideal condition where the CP is longer than the channel impulse response, the ICI, ISI, and ISCI terms disappear. Thus, the interference is totally eliminated.

At the output of the demodulator, the output consists of two parts, which are the desired signal and the combination of all the interference as calculated above. This output then passes through the FDEQ and each tone is multiplied by a complex coefficient. The output of the FDEQ on the lth tone, Z^l, can be written as:

$$\begin{aligned} Z^l &= (Y^l_{SIG} + (Y^l_{SYM} + Y^l_{ISI\_pre} + Y^l_{ISI\_next} + Y^l_{ICI} + Y^l_{ISCI\_pre} + Y^l_{SICI\_next})) * w^l_{FDEQ} \\ &= (Y^l_{SIG} + Y^l_{Interf}) * w^l_{FDEQ} \end{aligned} \quad (5\text{-}15)$$

where w^l_{FDEQ} is the FDEQ coefficient on the lth branch, and Y^l_{Interf} represents all the interference terms on lth tone.

Then the expected power of the desired signal and the distortion can be calculated by taking variance operation on Z^l in (5-15). Since the information symbols on each tone are modulated independently, the crossterms between the signal and distortion will disappear. Thus, we can come up with the following expressions for the signal power and the distortion power respectively:

$$P^l_{SIG} = (Y^l_{SIG} * w^l_{FDEQ})^2 \quad (5\text{-}16)$$

$$P^l_{Interf} = (Y^l_{Interf} * w^l_{FDEQ})^2 \quad (5\text{-}17)$$

We assume that the information symbols in each subchannel have the same energy, and the equations shown in (5-16) and (5-17) are normalized to this energy. Thus, with ideal FDEQ design, the signal power should be unity. However, the FDEQ coefficients computed in (5-1) can not satisfy this condition. We will show the effects of the FDEQ settings in the following simulation results and the modification on the FDEQ settings will be given in the following section of this chapter.

5.3 Effects of Interference Analysis

In the previous chapter, we showed the relationship between the SSNR and the bit rate. We found that SSNR is not a perfect measurement for system performance, because it does not determine the maximum bit rate that can be achieved. In this section, we will examine the effects of the interference which has been discussed in the previous section on the system performance in terms of the maximum achievable bit rate based on computer simulations.

5.3.1 Simulation Environment

A short ADSL loop with 1 kilo-feet long and 26 AWG is selected as the physical channel model. To concentrate our analysis on the effect of the ISI, ICI and ISCI only, we assume there is only AWGN and no NEXT, or FEXT.

We only use channel indices from 34 to 111 for downstream to be the available frequency bandwidth for the bit allocation calculation, so that the transceiver front-end filters with passband from 146 kHz to 480 kHz were applied to satisfy the filtering requirements. The maximum number of bits that can be assigned to each subchannel is 8, which is suggested for DMT-lite system.

The TDEQ length is 10 for the downstream, which is the same as we used in Chapter 4. UTC is selected for the TDEQ design, and the unit tap index is fixed to be 1 to simplify the comparison.

5.3.2 Simulation Results

5.3.2.1 Interference Level

We plotted the normalized interference level in Figure 5.4 including the interference caused by the Hermitian symmetric symbol and the FDEQ. The result shown in Figure 5.4 is for the downstream transmission. We select a delay value inside the near-optimum range for the TDEQ design. First, we find that our current FDEQ settings are not optimally trained. It is the biggest interference source compared to the others. At some particular carriers, the distortion contributed by the improper FDEQ settings is almost 20 dB higher than the other distortion sources. Thus, we can get some gains by optimizing the current FDEQ settings. Next, we see that the contribution of conjugate symmetric symbol is very small compared to ICI, ISI and ISCI as long as the delay for TDEQ design is inside its near-optimum range. It is more than 20 dB lower than the ICI, ISI, and ISCI. We have examined this over numerous simulations. Thus, its effects are negligible.

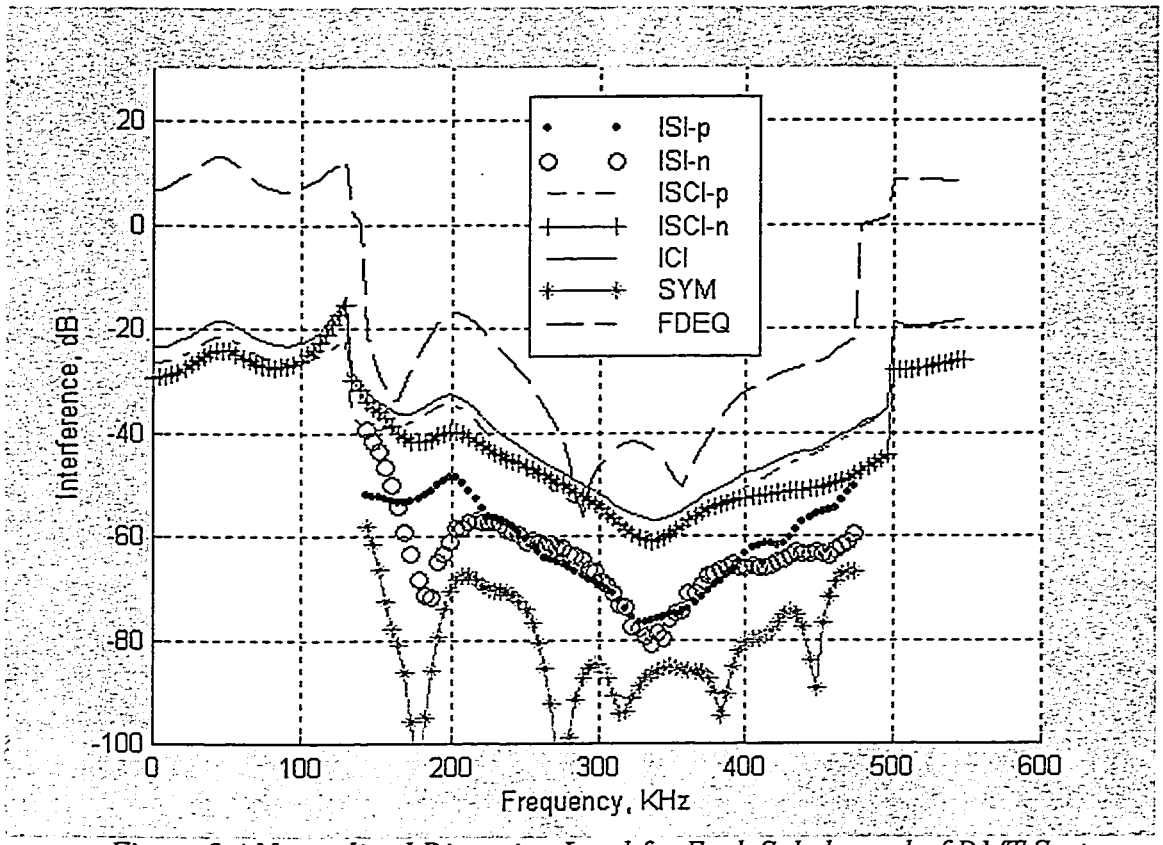

Figure 5.4 Normalized Distortion Level for Each Subchannel of DMT System

The legend used in the above figure is summarized in Table 5.1

Table 5.1 Legend list of Figure 5.4

Symbol used in Figure 5.4	Interference term
ISI-p	ISI previous
ISI-n	ISI next
ISCI-p	ISCI previous
ISCI-n	ISCI next
ICI	ICI
SYM	Hermitian symmetric symbol
FDEQ	FDEQ

5.3.2.2 Effects on Bit Allocation

To have a better understanding of the ISI, ICI, and ISCI, we simulated the relationships among them and the bit allocation. We limited the number of bits that can be carried by each carrier from 2 to 8 in the simulation. Again, the TDEQ design with variant delay values are considered.

Figures 5.5, and 5.6 present two results of the simulations for the DS transmission. The delay values for the TDEQ design is 16 and 30, respectively. The tone number 64, with central frequency 276 kHz, is reserved for pilot and no data information is carried on it. The results plotted in Figures 5.5 and 5.6 show that the bit allocation is directly related with interference level. The bit allocation has an inversely proportional relationship with the total interference level. The lower the total interference in a subcarrier, the more bits are assigned to the subchannel, thus, the higher transmission rate can be achieved. Furthermore, if the interference is lower than a value, around –40 dB in our simulation, the bit allocation reaches the max allowable bits, a further decrease in the interference will not contribute to the bit rate.

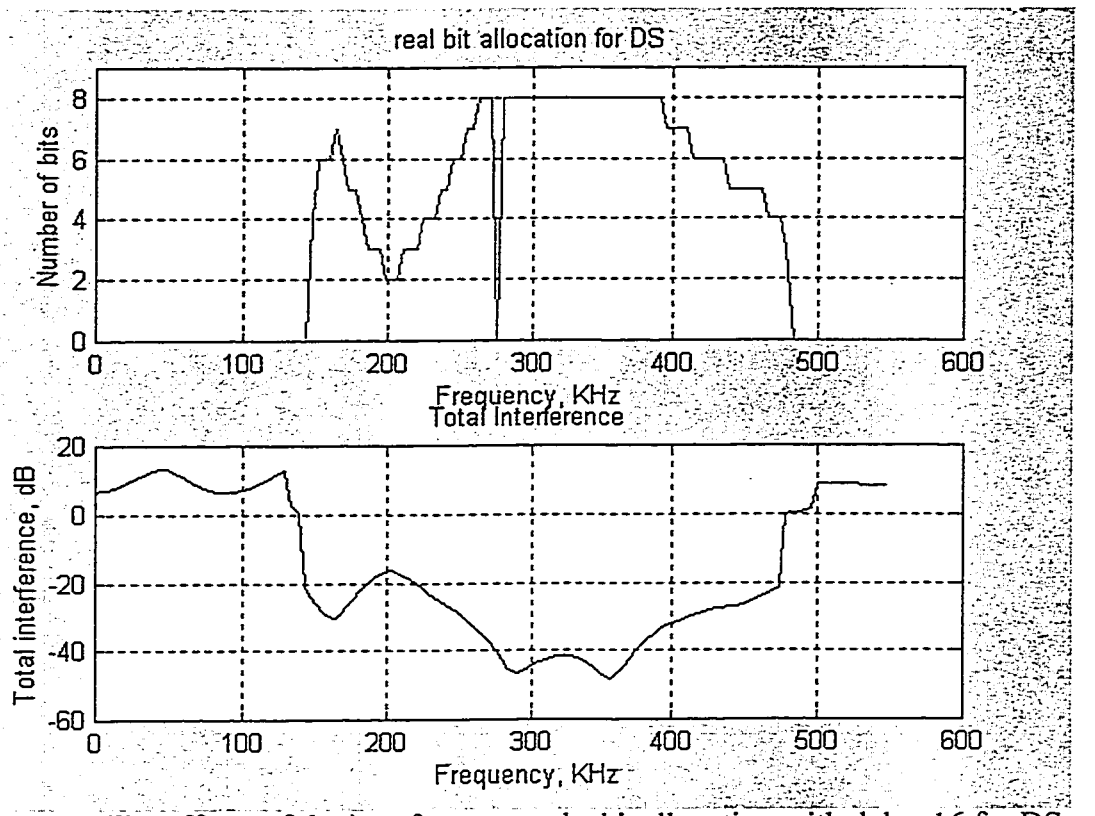

Figure 5.5 The effects of the interference on the bit allocation with delay 16 for DS

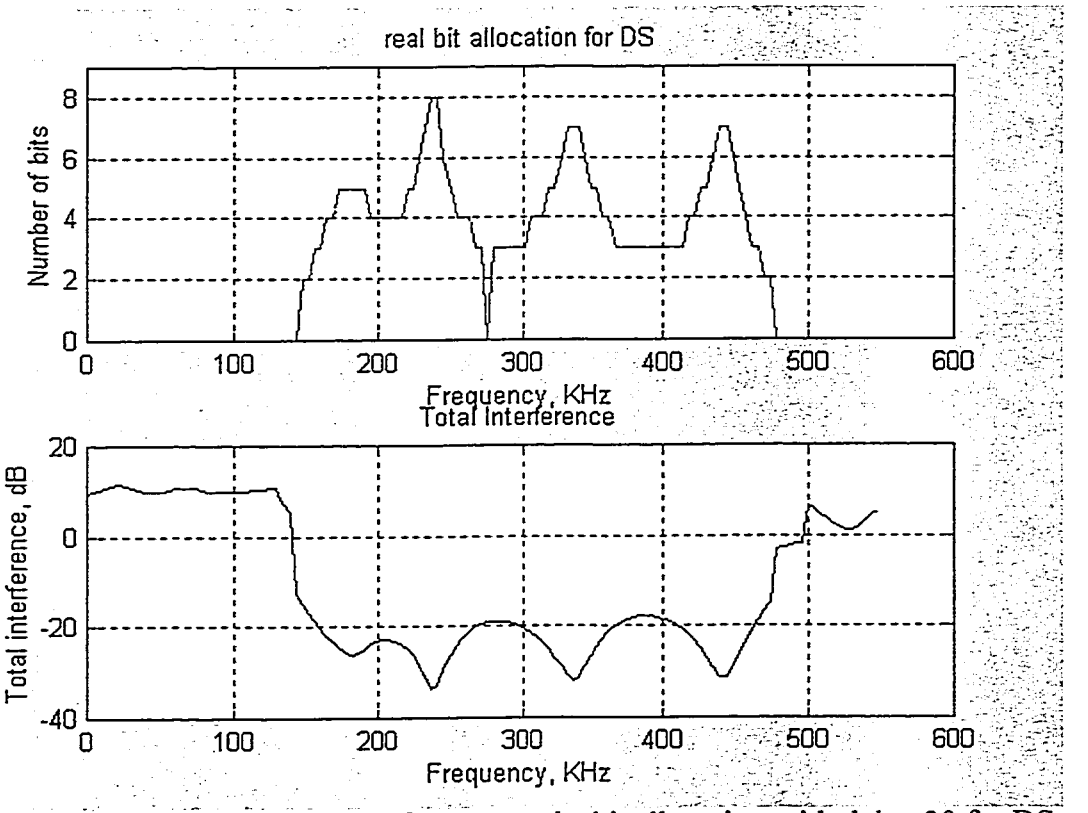

Figure 5.6 The effects of the interference on the bit allocation with delay 30 for DS

5.3.3 Optimized FDEQ Design

As shown in Figure 5.4, the current FDEQ design has the most contribution to the distortion. This is because the FDEQ design described in section 5.2 does not depend on the real received signal. The optimized FDEQ design according to the received signal will be given in this section.

We calculated the desired signal in equation (5-7). We see that the received signal calculation only depends on the difference between k and m. Thus, we can simply (5-7) as:

$$Y_{SIG}^{l} = \frac{1}{N_{FFT}} C^{l} \sum_{i=0}^{\Delta+N_{FFT}-1+CP} g_n e^{-j2\pi il/N_{FFT}} \tag{5-18}$$

The summation calculation over i is taking place in the rectangular area as shown in Figure 5.7. The diagonal lines present the values of i.

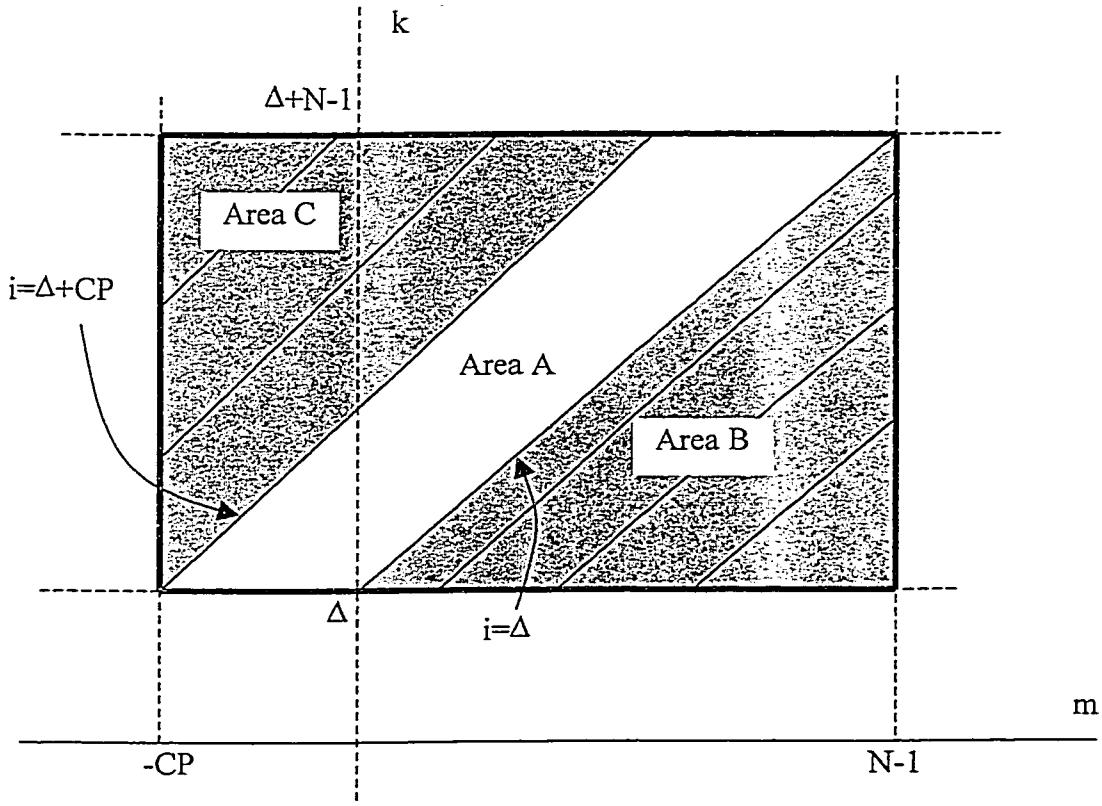

Figure 5.7 Illustration of the Signal Calculation

We further split the whole rectangle into three sub-areas as shown in Figure 5.7 and calculate them separately.

The value of i in area A is from Δ to Δ+CP, which refer to the case that the channel impulse response is completely confined within the CP. Then, we can calculate the signal in area A as:

$$Y_A^l = \frac{C^l}{N_{FFT}} \sum_{n=\Delta}^{\Delta+CP} g_m e^{-j2\pi nl / N_{FFT}} \tag{5-19}$$

The value of i in area B is from 0 to Δ-1, and the output can be written as:

$$Y_B^l = C^l \sum_{i=0}^{\Delta-1} (1 + \frac{i-\Delta}{N_{FFT}}) g_i e^{-j2\pi il / N_{FFT}} \tag{5-20}$$

The value of i in area C is from Δ+CP+1 to $\Delta + N_{FFT} + CP - 1$, and the output can be written as:

$$Y_C^l = C^l \sum_{i=\Delta+CP+1}^{\Delta+N_{FFT}+CP-1} (1 - \frac{i-\Delta-CP}{N_{FFT}}) g_i e^{-j2\pi il / N_{FFT}} \tag{5-21}$$

The equations from (5-19) to (5-21) indicate that we should employ a window function as shown in Figure 5.8 instead of using the rectangular window on the overall channel impulse response to calculate the FDEQ settings.

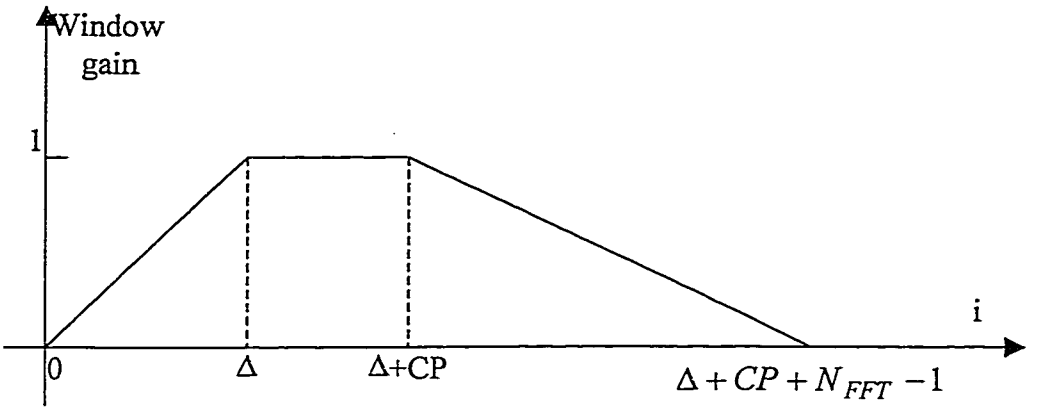

Figure 5.8 Window function for FDEQ design

We employed the optimized FDEQ under the same conditions as shown in Figure 5.6. The bit allocation result calculated using the modified FDEQ design is given in Figure 5.9. Apparently, with the optimized FDEQ design algorithm, we increased the number of bits carried by each subchannel if the subchannel is not fully loaded. The transmission rate for the optimized FDEQ design is 2316 kbps while its value is 1300 kbps for the old FDEQ design. Thus, we significantly increase the achievable bit rate by applying the window function on the overall channel impulse response for the FDEQ design. Obviously, the new FDEQ design also extends the range of the delay values which result in the near-optimum system performance.

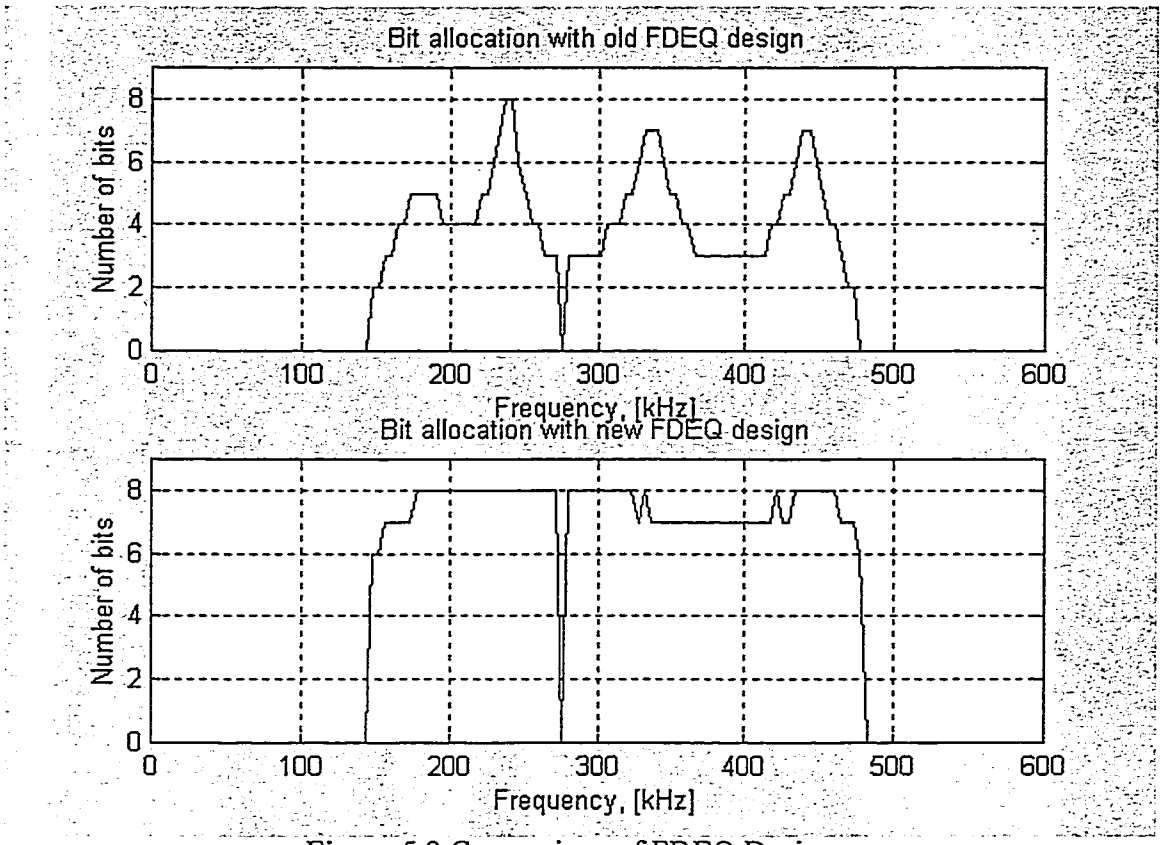

Figure 5.9 Comparison of FDEQ Designs

5.4 Conclusions

In this chapter, we examined the effects of the distortion caused by the non-ideal channel impulse response on the system achievable bit rate. We found that the system achievable bit rate is directly related with this interference level. We have found in Chapter 4 that SSNR is not a sufficient parameter to examine the TDEQ design. Thus, we can use the power of the total interference instead of SSNR to estimate our TDEQ designs without calculating the system achievable bit rate every time we change the delay value, which is impractical in real time system.

From our simulation results, we also found that the FDEQ coefficients based on the calculation suggested in [49] are not the optimum settings. Instead of using the original channel impulse response to calculate the FDEQ settings, we should apply a window function as shown in Figure 5.9. Our simulation results show that we can significantly increase the system performance.

Chapter 6

Summary and Conclusions

In this thesis, we studied various aspects of equalizer design algorithms in the DMT ADSL system. Effects of different filter types employed as the transceiver front-end are analyzed. The distortion caused by the non-ideal channel are analyzed and simulated. A new frequency domain equalizer design algorithm is derived. Summary of the results and observations are given in the following sections.

6.1 TDEQ Design

TDEQ designs under UEC and UTC by varying the delay values are compared in Figures 4.5, 4.6 and Tables 4.2, 4.3. From this investigation, we can make the following conclusions.

- An improper delay value selection for the TDEQ design results in a great system performance degradation.
- The delay values for the TDEQ design can be selected from a range that result in a near-optimum system performance.
- The position of the unit element in the target impulse response for UTC-TDEQ design is not critical as long as the delay value is inside its optimum value range.
- UEC always has better SSNR performance than UTC.

- The achievable maximum transmission rate using UEC-TDEQ is not always better than that of UTC-TDEQ, but the difference is small. Therefore, either UEC or UTC can be used as the TDEQ design method and both of them can ensure a reliable high transmission rate.

6.2 Transceiver Front-end

- The time domain and frequency domain responses of different filter types are plotted in Figures from 4.7 to 4.11. These filters are designed to satisfy the same front-end requirements. The orders are summarized in Table 4.4

  - Butterworth filter has higher complexity than the Chebyshev-I and elliptic filters.
  - Elliptic filter meets the filter requirement with the lowest order requirement.

- The performance of different filter prototypes as the transceiver front-end shown in Figures 4.12 to 4.17 and in Tables 4.5, 4.6.

  - There is a big performance difference between the different transceiver front-end filters.
  - From an achievable bit rate viewpoint, either Butterworth or elliptic filters can be employed at the front-end. And both of them ensure a high transmission rate.
  - There are no advantages of using the digital FIR filters over the analog IIR filters in terms of the achievable bit rate performance.

6.3 Interference of DMT System

In Chapter 5, we theoretically analyzed the effects of the distortions on the system performance. Although we employ CP technique to compensate for the non-ideal channel response, the system still suffers from ISI, ICI, and ISCI because the equalized channel impulse response is not completely confined within the CP. To analyze the impacts of various interference terms, we have developed analytical expressions. Based on these expressions, the simulated interference level is plotted in Figure 5.4. The conclusions from this figure are:

- Our current FDEQ design contributes the highest power to the total distortion.
- The interference due to the transmission of the Hermitian symmetric symbol has a very low level, which is negligible compared with ISI, ICI, and ISCI.

- The relationship between the bit allocation and the total distortion level is shown in Figure 5.5 and Figure 5.6.

  - The number of bits that can be carried on a tone is related to the total interference level of that tone in an inversely proportional manner.
  - If the interference power in a subchannel is lower than a particular value, around –40 dB is our case, the bits assigned to the subchannel reaches the maximum limit and further lowering the interference will not contribute to the system performance.
  - The interference power level is a better system performance measure than the SSNR.

6.4 FDEQ Design

The new FDEQ design is analyzed in section 5.3.3. The comparison of the proposed new FDEQ design with the old FDEQ design is given in Figure 5.9.

- The proposed FDEQ design algorithm improves the system performance significantly.
- Instead of using the original overall channel impulse response, we should apply a window function, as shown in Figure 5.8, on the channel impulse response to design the FDEQ for the DMT system.
- Proposed FDEQ design algorithm also extends the range of the near-optimum delay values.

Appendix I

Filter Design

To design a frequency-selective filter, the desired characteristics are specified in the frequency domain in terms of the desired magnitude and phase response of the filter. In the filter design process, we determine the coefficients of a causal FIR or IIR filter that closely approximates the desired frequency response specifications. The question of which type of filter to choose, FIR or IIR, depends on the characteristics of the problem and on the specifications of the desired frequency response [30].

In practice, FIR filters are employed in applications where there is a requirement for a linear-phase characteristic within the passband of the filter. If there is no linear-phase requirement, either an IIR or an FIR filter could be employed. If some phase distortion is either tolerable or unimportant, an IIR filter is preferable, primarily because its implementation involves fewer parameters, requires less memory and has lower computational complexity.

Ideal filters are noncausal and hence physically unrealizable for real-time system. Causality implies that the response characteristic $H(w)$ of the filter cannot be zero, except at a finite set of points in the frequency range. In addition, $H(w)$ cannot have an infinitely sharp cutoff from passband to stopband, that is, $H(w)$ cannot drop from unity to zero directly.

Although the frequency response characteristics possessed by ideal filters may be desirable, they are not absolutely necessary in most practical applications. If we relax these conditions, it is possible to realize causal filters that approximate the ideal filters as closely as we desire. In particular, it is not necessary to insist that the magnitude $|H(w)|$ be constant in the entire passband of the filter. A small amount of ripple in the passband

is usually tolerable. Similarly, it is not necessary for the filter response to be zero in the stopband. A small, nonzero value or a small amount of ripple in the stopband is also tolerable. The transition of the frequency response from passband to stopband defines the transition band or transition region of the filter as illustrated in Figure A-I.1. The band-edge frequency ω_p defines the edge of the passband, while the frequency ω_s denotes the beginning of the stopband. Thus the width of the transition band is $\omega_s - \omega_p$. The bandwidth of the filter is usually defined as the width of the passband. The ripple in the passband of the filter is denoted as δ_p and the magnitude varies between the limits $1 \pm \delta_p$. The ripple in the stopband of the filter is denoted as δ_s. So in filter design, we only need to specify the maximum tolerable passband ripple, the maximum tolerable stopband ripple and two-band edge frequencies.

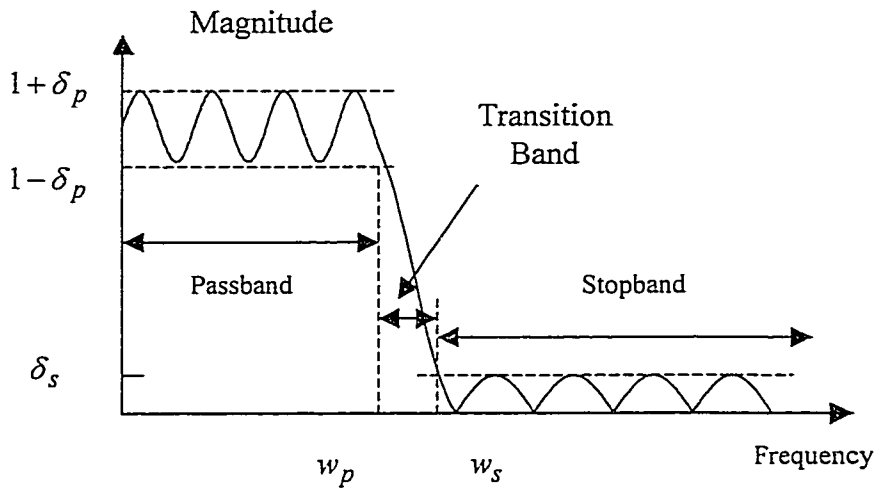

Figure A-I.1 Magnitude characteristics of physically realizable filters

Basically, IIR digital filter can easily be obtained by beginning with an analog filter and then using a mapping to transform the s-plane into the z-plane. Thus the design of a digital filter is reduced to designing an appropriate analog filter and then performing the

conversion from $h(s)$ to $h(z)$, in such a way so as to preserve as much as possible, the characteristics of the analog filter.

Analog filter design is a well-developed field and many books have been written on the subject. We briefly go through the important characteristics of commonly used analog fillers. The discussion is limited to lowpass filters and either a bandpass, or highpass filter can be converted from a lowpass prototype filter.

- Butterworth filters

Lowpass Butterworth filters are all-pole filters characterized by the magnitude—squared frequency response

$$|H(\Omega)|^2 = \frac{1}{1+(\Omega/\Omega_c)^{2N}} = \frac{1}{1+\varepsilon^2(\Omega/\Omega_p)^{2N}} \qquad \text{(A-I-1)}$$

where N is the order of the filter, Ω_c is its –3dB frequency(cutoff frequency), Ω_p is the passband edge frequency, and $1/(1+\varepsilon^2)$ is the band edge value of $|H(\Omega)|^2$.

The magnitude frequency response of the Butterworth filters is monotonic in both the passband and stopband. The order of the filter required to meet an attenuation δ_p at a specified frequency Ω_s is easily determined from (A-I-1). Thus the Butterworth filter is completely characterized by the parameters N, δ_p,ε, and the ratio Ω_s/Ω_p.

- Chebyshev filters

There are two types of Chebyshev filters. Type I Chebyshev filters are all-pole filters that exhibit equiripple behavior in the passband and a monotonic characteristic in the stopband. On the other hand, the family of type II Chebyshev filters contains both poles and zeros and exhibits a monotonic behavior in the passband and an equiripple

behavior in the stopband. The zeros of this class of filters lie on the imaginary axis in the s-plane.

The magnitude squared of the frequency response characteristic of a type I Chebyshev filter is given as

$$|H(\Omega)|^2 = \frac{1}{1+\varepsilon^2 T_N(\Omega/\Omega_p)} \tag{A-I-2}$$

A type II Chebyshev filter contains zeros as well as poles. The magnitude squared of the frequency response is given as

$$|H(\Omega)|^2 = \frac{1}{1+\varepsilon^2 [T_N^2(\Omega_s/\Omega_p)/T_N^2(\Omega_s/\Omega)]} \tag{A-I-3}$$

where ε is a parameter of the filter related to the ripple in the passband and $T_N(x)$ is the Nth order Chebyshev polynomial defined as

$$T_N(x) = \begin{cases} \cos(N\cos^{-1}x), & |x| \le 1 \\ \cosh(N\cosh^{-1}x), & |x| > 1 \end{cases} \tag{A-I-4}$$

We observe that the Chebyshev filters are characterized by the parameters N, δ_p,ε, and the ratio Ω_s/Ω_p.

In general, the Chebyshev filter meets the specifications with a fewer number of poles than the corresponding Butterworth filter. If we compare a Butterworth filter to a Chebyshev filter having the same number of poles and the same passband and stopband specifications, the Chebyshev filter will give a smaller transition bandwidth.

- Elliptic filters

Elliptic filters exhibit equiripple behavior in both the passband and the stopband. This class of filters contains both poles and zeros and is characterized by the magnitude-squared frequency response:

$$|H(\Omega)|^2 = \frac{1}{1+\varepsilon^2 U_N(\Omega/\Omega_p)} \qquad \text{(A-I-5)}$$

where $U_N(x)$ is the Jacobian elliptic function of order N, and ε is a parameter related to the passband ripple.

The filter order N, passband ripple δ_p, stopband ripple δ_S, and transition ratio Ω_S / Ω_p are needed to fully define a elliptic filter.

Elliptic filters spread the approximation error equally over the passband and the stopband. So it is the most efficient design algorithm from the viewpoint of yielding the smallest-order filter for a given set of specifications. Equivalently, we can say that for a given order and a given set of specifications, an elliptic filter has the smallest transition bandwidth.

References

[1] ADSL forum, WWW site materials. http://www.adsl.com/. Aug. 1998.

[2] David L. Waring, "The Asymmetrical Digital Subscriber Line (ADSL): A New Transport Technology for Delivering Wideband Capabilities to the Residence", pp.1979-1986, Globecom '91.

[3] John A. C. Bingham, "Multicarrier Modulation for Data Transmission: An Idea Whose Time Has Come", IEEE Commun. Mag., pp. 5-14, May 1990.

[4] J. M. Cioffi, "A Tutorial Review of DMT ADSL for Issue 2 [96-016]", ANSI T1E1.4/96-016, Jan. 22, 1996.

[5] John Bingham, Frank van der Putten, "Standards Project for Interfaces Relating to Carrier to Customer Connection of Asymmetrical Digital Subscriber Line (ADSL) Equipment", T1.413, Issue 2", Sept. 26, 1997.

[6] Jean-Jacques Werner, "The HDSL Environment", IEEE Journal on Selected Areas in Communications, Vol. 9, No. 6, pp. 785-800, Aug. 1991.

[7] Peter S. Chow, Jerry C. Tu, John M. Cioffi, " Performance Evaluation of a Multichannel Transceiver System for ADSL and VHDSL Services", IEEE Journal on Selected Areas in Communications, Vol. 9, No. 6, pp. 909-919, Aug. 1991.

[8] J. G. Proakis, "Digital Communications", New York McGraw-Hill, 1983.

[9] Irving Kalet, "The Multitone Channel", IEEE Trans. On Commun., Vol. 37, No. 2, pp.119-124, Feb. 1989.

[10] G. D. Forney Jr., et al., "Efficient Modulation for Band-Limited Channels", IEEE Journal on Selected Areas in Communications, Vol. SAC-2, pp. 632-647, Sept. 1984.

[11] M. Barton, M. L. Honig, "Optimization of Discrete Multitone to Maintain Spectrum Compatibility with Other Transmission Systems on Twisted Copper Pairs", IEEE Journal on Selected Areas in Communications, Vol. 13, NO. 9, Dec. 1995.

[12] Peter S. Chow, John M. Cioffi, John A. C. Bingham, "A Practical Discrete Multitone Transceiver Loading Algorithm for Data Transmission over Spectrally Shaped Channels", IEEE Trans. on Commun., Vol. 43, No. 2/3/4, pp.773-775, Feb. 1995.

[13] J. T. Aslanis, J. M. Cioffi, "Achievable Information Rates on Digital Subscriber Loop: Limiting Information Rates with Crosstalk Noise", IEEE Trans. On Commun., Vol. 40, No. 2, pp. 361-372, Feb. 1992.

[14] Antonio Ruiz, John M. Cioffi, Sanjay Kasturia, "Discrete Multiple Tone Modulation with Coset Coding for the Spectrally Shaped Channel", IEEE Trans. On Commun., Vol. 40, No. 6, pp. 1012-1029, June. 1992.

[15] Walter Y. Chen, James L. Dixon, and David L. Waring, "High Bit Rate Digital Subscriber Line Echo Cancellation", IEEE Journal on Selected Areas in Communications, Vol. 9, NO. 6, Aug. 1991.

[16] Minnie Ho, J. M. Cioffi, and John A. C. Bingham, "High-Speed Full-Duplex Echo Cancellation for Discrete Multitone Modulation", pp. 772-776, ICC 93.

[17] Minnie Ho, J. M. Cioffi, and John A. C. Bingham, "Discrete Multitone Echo Cancellation", IEEE Trans. on Commun., Vol. 44, No. 7, pp. 817-825, July 1996.

[18] J. M. Cioffi, and John A. C. Bingham, "A Data-Driven Multitone Echo Canceller", IEEE Trans. on Commun., Vol. 42, No. 10, pp. 2853-2869, Oct. 1994.

[19] Ove Edfors, Magnus Sandell, Jan-Jaap van de Beek, Danial Landstrom, Frank Sjoberg, "An Introduction to Orthogonal Frequency-Division Multiplexing", Research Report TULEA 1996:16, Div. of Signal Processing, Luleå University of Technology, Luleå, Sept. 1996.

[20] S. B. Weinstein, Paul M. Ebert, "Data Transmission by Frequency-Division Multiplexing Using the Discrete Fourier Transform", IEEE Trans. on Commun., Vol. Com-19, No. 5, Oct. 1971.

[21] G. D. Forney Jr., and M. V. Eyuboğlu, "Combined Equalization and Coding Using Precoding", IEEE Commun. Mag., Vol 29, No.12, pp.25-34, Dec. 1991.

[22] T. Nicholas Zogakis, James T. Aslanis Jr., and J.M. Cioffi, "A Coded and Shaped Discrete Multitone System", IEEE Trans. on Commun., Vol. 43, No. 12, Dec. 1995.

[23] J.J Werner, "Impulse Noise in the Loop Plant", Session 348.1, ICC'90.

[24] C. F. Valenti and K. Kerpez, "Analysis of Wideband Noise Measurements and Implications for Signal Processing in ADSL System", International Conference on Communications, Vol.2, pp. 826-832, 1994.

[25] Melbourne Barton, "Impulse Noise Performance of an Asymmetric Digital Subscriber Lines Passband Transmission System", IEEE Trans. On Commun., Vol. 43, No 2/3/4, Feb./Mar./Apr., 1995.

[26] P. S. Chow, J. M. Cioffi, R. K. Maxwell, "Performance of Multicarrier with DSL Impulse Noise", T1E1.4/91-195, Nov. 11, 1991.

[27] M. Ghosh, "Analysis of the Effect of Impulse Noise on Multicarrier and Single Carrier QAM systems", IEEE Trans. On Commun., Vol. 43, No 2, 1995.

[28] W. Henkel and T. Keβler, "A Wideband Impulsive Noise Survey in the German Telephone Network: Statistical Description and Modeling", AËU. Vol. 48, No. 6, May 1994.

[29] W. Henkel, T. Kessler, and H. Y. Chung, "Coded 64-CAP ADSL in an Impulse-Noise Environment—Modeling of Impulse Noise and First Simulation Results", IEEE Journal on Selected Areas in Communications, Vol. 13, No. 9, Dec. 1995.

[30] J.G. Proakis, "Digital Signal Processing", London, Prentice-Hall, 1996.

[31] A. Ginesi, and Christian Bourget, "DMT Tutorial", Nortel, Feb. 1998.

[32] I. Lee, J. S. Chow, and J. M. Cioffi, "Performance Evaluation of a Fast Computation Algorithm for the DMT in High-Speed Subscriber Loop", IEEE Trans. on Commun. Vol. 13, No. 9, Dec. 1995.

[33] D. D. Falconer, and F. R. Magee, Jr., "Adaptive Channel Memory Truncation for Maximum Likelihood Sequence Estimation", Bell System Technical Journal, Vol. 52, No. 9, pp.1541-1562, 1973.

[34] Naofal Al-Dhahir, J.M. Cioffi, "A Low-Complexity Pole-Zero MMSE Equalizer for ML Receivers", Proc. Allerton Conf. Commun., Control, Comput., pp. 623-632, Sept. 1994.

[35] J. M. Cioffi, Glen P. Dudevoir, M. Vedat Eyuboglu, and G. David Forney Jr., "Minimum Mean-Square-Error Decision Feedback Equalization and Coding — part I", IEEE Trans. on Commun., Vol. 43, No. 10, Oct. 1995.

[36] S. Qureshi, and E. Newhall, "An Adaptive Receiver for Data Transmission over Time-Dispersive Channels", IEEE Trans. on Information Theory, 19(4): 448-457, July 1973.

[37] D.Messerschmitt, "Design of a Finite Impulse Response for the Viterbi Algorithm and Dicision-Feedback Equalizer", International Conference on Commun., pp. 37D.1-37D.5, June 1974.

[38] J. Chow, J. M. Cioffi, and J. Bingham, "Equalizer Training Algorithms for Multicarrier Modulation Systems", pp. 761-765, ICC'93.

[39] J. Chow, J. M. Cioffi, "A Cost Effective Maximum Likelihood Receiver for Multicarrier Systems", pp. 948-952, ICC'92.

[40] Inkyu Lee, J.M. Cioffi, "A Fast Computation Algorithm for the Decision Feedback Equalizer", IEEE Trans. on Commun. Vol. 43, No. 11, Nov. 1995.

[41] Naofal Al-Dhahir, J. M. Cioffi, "MMSE Decision-Feedback Equalizers: Finite-Length Results", IEEE Trans. on Information Theory, Vol. 41, No. 4, July 1995.

[42] Signal Processing Toolbox for Use with MATLAB®.

[43] A. Ruiz and J. M. Cioffi, "A Frequency-domain approach to combined spectral shaping and coding", in ICC'87, Seattle, WA, June 1987, pp1711-1715.

[44] A. D. Rizos, J. G. Proakis, and T.Q. Nguyen, "Comparison of DFT and Cosine Modulated Filter Banks in Multicarrier Modulation", IEEE Globecom '94.

[45] Jorge L. Seoane, Sarah K. Wilson, and Saul Gelfand, "Analysis of Intertone and Interblock Interference in OFDM when the Length of the Cyclic Prefix is Shorter than the Length of the Impulse Response of the Channel", IEEE Globecom '92.

[46] Abraham Peled, and Antonio Ruiz, "Frequency Domain Data Transmission Using Reduced Computational Complexity Algorithms", Proc. IEEE ICASSP, pp. 964-967 1980.

[47] Peter J. W. Melsa, Richard C. Younce, and Charles E. Rohrs, "Impulse Response Shortening for discrete Multitone Transceivers", IEEE Trans. on Commun., Vol 44, No. 12, Dec 1996.

[48] Mark Hawryluck, "Evaluation of Modulation Techniques for Broadband Access over Twisted Pair", Master Thesis, Univ. of Ottawa, 1997.

[49] Jacky S. Chow, Jerry C. Tu, and John M. Cioffi, "A Discrete Multitione Transceiver System for HDSL Applications", IEEE Journal on Selected Areas in Commun., Vol. 9, No. 6, Aug. 1991.

[50] Hikmet Sari, Georges Karam, and Isaballe Jeanclaude, "Transmission Techniques for Digital Terrestrial TV Broadcasting", IEEE Commun. Mag., Feb. 1995.

IMAGE EVALUATION TEST TARGET (QA-3)

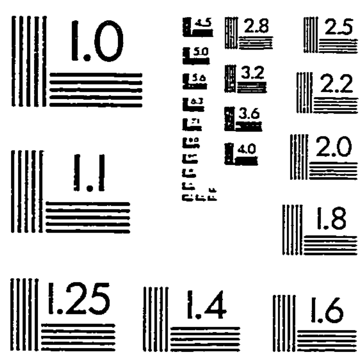

150mm

6"

APPLIED IMAGE, Inc
1653 East Main Street
Rochester, NY 14609 USA
Phone: 716/482-0300
Fax: 716/288-5989